CHALMERS

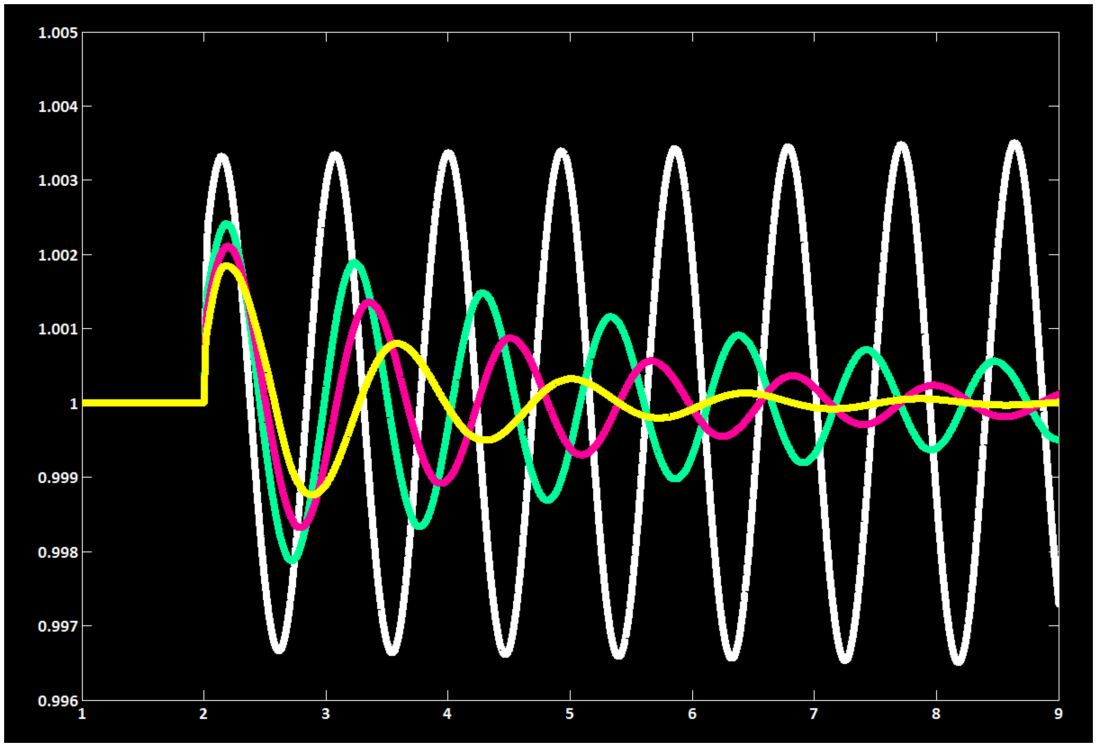

Power System Stabilizers for The Synchronous Generator

Tuning and Performance Evaluation

Master of Science Thesis

ANDREA ANGEL ZEA

Department of Energy and Environment
Division of Electric Power Engineering
CHALMERS UNIVERSITY OF TECHNOLOGY
Göteborg, Sweden 2013

Power System Stabilizers for The Synchronous Generator

Tuning and Performance Evaluation

ANDREA ANGEL ZEA

Department of Energy and Environment
Division of Electric Power Engineering
CHALMERS UNIVERSITY OF TECHNOLOGY
Göteborg, Sweden 2013

Power System Stabilizers for The Synchronous Generator
Tuning and Performance Evaluation
ANDREA ANGEL ZEA

Department of Energy and Environment
Division of Electric Power Engineering
Chalmers University of Technology
SE–412 96 Göteborg
Sweden
Telephone +46 (0)31–772 1000

Chalmers Bibliotek, Reproservice
Göteborg, Sweden 2013

Power System Stabilizers for The Synchronous Generator
Tuning and Performance Evaluation
ANDREA ANGEL ZEA
Department of Energy and Environment
Division of Electric Power Engineering
Chalmers University of Technology

Abstract

The electromechanical oscillations damping through the synchronous generator is analyzed in this work. Traditionally, this has been achieved using a conventional Power System Stabilizer PSS controller, which has the aim of enhancing the dynamic stability of the generator through the excitation control system, therefore a PSS tuning methodology is developed and tested. Moreover, other damping control alternative for the synchronous generator based on signal estimation theory is proposed in this thesis.
Initially, a detailed modelling of the Synchronous Machine Infinite Bus SM-IB system has been accomplished in order to study the electromechanical interaction between a single generator and the power system. The SM-IB system model is the base to analyze and to tune the PSS controller. It was concluded that it is not necessary to include the damper windings dynamics in the system phase lag analysis since, in the PSS frequency range of interest, the biggest phase lag difference including them was about 10°. This difference could be considered not sufficient to include the sub-transient model in the PSS tuning analysis. Therefore, the linearized transient model of the system is a suitable model for the tuning process.
Secondly, the main concepts for a PSS tuning methodology, which is based on linear control system theory, are established. Specifically, frequency response techniques are used to define the setting for the lead lag filters time constants and PSS gain. This is supported on the fact that the predominant trend in the industry is still to use frequency response based tuning methods [12], even more in the case of PSS providers who should tune the controller having detailed information about the generator but not exact details about the connecting grid. The methodology is implemented as a software tool in Matlab/Simulink R2011b using the mathematical model of the excitation system provided by the company VG Power AB and giving the option to chose between static and rotating type of exciters; it is also designed considering the rotor speed change as input signal to the PSS. The performance of the PSS with the achieved tuning is validated via simulations in the complete SM-IB system model. Furthermore, a sensitivity analysis of the local oscillation mode damping to changes in the system operating point is carried out verifying the robustness of the tuning process. In all analyzed cases, the minimum damping of the local mode was never less than 10%.
Finally, the application of a Phasor Power Oscillation Damping POD controller to the excitation control system in the synchronous generator is studied. Nowadays, POD for inter-area oscillation modes in power systems is also achieved through FACTS. Control structures using low-pass filter based and recursive least square based estimation methods to extract the oscillatory component of a signal has been successfully applied to control FACTS [3], [17] and [5] achieving damping. The same idea is used in this work to define an alternative controller for the generator which is based on a low-pass filter based signal estimation algorithm. The analysis is done again using the SM-IB system. The obtained results indicate that the alternative controller is able to damp successfully the local oscillation mode that appear after applying a disturbance to the system. However, deeper studies are needed in order to be able to compare fairly the performance of the PSS and the Phasor POD controller when they are applied to the synchronous generator. Additionally, the proposed control approach should be test in a power system model of higher order. These are recommended topics for future work.

Index Terms: Synchronous Generator, PSS Tuning, Signal Estimation, Phasor POD Controller.

Acknowledgements

I would like to express my gratitude to:

Massimo Bongiorno and **Stefan Lundberg**.
Thanks for your guidance and shared knowledge during this master thesis. Also for the interesting courses given during the master program!

Mats Wahlen and **VG Power AB**.
Thanks for offering a topic of my complete interest and for the opportunity to have a contact with the Swedish industry!

Mebtu Beza.
Many thanks for your support and help!

Hector Botero.
Thanks for your teachings and your example!

Colfuturo.
Thanks for the Scholarship!

Chalmers and **The Government of Sweden**.
Thanks for the IPOET Scholarship!

Diana and **Panos**.
Thanks for your company and friendship during this two years in Sweden!

Mamá.
Aquí se cumple no sólo mi sueño, sino el sueño que sembraste en mí! Gracias a tí por siempre y por todo!

Esperanza.
Tendrás un vuelo eterno en mi corazón!

Papá, **Olga**, **Sebas**, **Benja**, **Familia** y **Amigos**
Gracias por estar a mi lado!

Andrea Angel Zea
Göteborg, Sweden, 2013

Acronyms

AVR Automatic Voltage regulator

PSS Power System Stabilizer

SM-IB Synchronous Machine - Infinite Bus

POD Power Oscillation Damping

FACTS Flexible AC Transmission System

TCSC Thyristor Controlled Series Capacitor

AC Direct Current

DC Direct Current

PI Proportional and Integral

LMI Linear Matrix Inequality

LPF Low-Pass Filter

Contents

Chapter 1

Introduction

1.1 Problem Background

The increasing magnitude and complexity of interconnected power systems due to competitive energy markets, economy and population development have created the need to operate the power systems close to their capacity limits. This leads sometimes to stability problems or poor dynamic behaviours like power oscillations. These oscillations can cause a reduction of the system components lifetime, expensive operations of the electrical grids and in the worst case, risks of partial system collapses. On the other hand, in the synchronous generator, the damping that the field and damper windings provide to the rotor oscillations is weakened due to excitation control system action. The reason for this is that in the rotor circuits appear additional currents induced by the voltage regulation and those currents oppose to the currents induced by the rotor speed deviations [18]. Therefore, an additional stabilizing signal was needed and the Power System Stabilizer PSS was developed with this aim [14].

The PSS is a feedback controller, part of the control system for a synchronous generator, which provides an additional signal that is added to the input summing point at the Automatic Voltage Regulator AVR. The PSS main function is to damp generator rotor oscillations in the range from 0.1 to 2.5 Hz approximately, which according to [11], are oscillations due to electromechanical dynamics and are called electromechanical oscillations. By adding the stabilizing signal the PSS is expected to produce an electric torque component that counteracts the mechanical dynamics. The produced electric torque component should be in phase with the deviations of the generator rotor speed in order to be able to damp the oscillations.

Different input signals have been used to extract the rotor oscillations. The most common input signals are the active power, the terminal frequency and the shaft speed [1], [14], [18]. In the classical PSS, the input signal passes through a washout filter which is a high pass filter that prevents the PSS to act when slow changes (operating point changes) occur. This filter defines the frequency from which the PSS begins to operate. The PSS is also constituted by a phase compensation algorithm by using lead lag filters, which are introduced to supply the phase shift needed to compensate for the phase lag between the excitation system input and the resulting electric torque.

To provide effective damping and ensure the stability of the system, the PSS should be carefully tuned. The tuning process is a topic of big interest for excitation systems and PSS manufacturers, who should complete the commissioning of a controller with a suitable and robust tuning according to the specific generator where the PSS is added and to the different operating conditions of the system. Therefore, analytical methodologies to tune the PSS in order to achieve the mentioned conditions becomes of relevant importance. The task of controller tuning should be supported in formal methods and not only in the knowledge generated by the field experience. Several methods have been used and are available in the literature to tune the PSS. Those methods could be mainly classified in linear and non-linear approach, as described in [4]. Among the linear design methods are: Pole Placement, Pole-Shifting, Linear Quadratic Regulator Formulation, Linear Matrix Inequalities, Linear Optimal Control, Quantitative Feedback Theory, Eigenvalue Sensitivity Analysis, Sliding Mode Control and Conventional P-Vr Method. Among the

non-linear methods of design are: Adaptive Control, Genetic Algorithm, Tabu Search, Particle Swarm Optimization, Simulated Annealing, Neuronal Networks, Support Vector Machine, Fuzzy Logic, Rule-Based Method, Lyapunov Method, Frequency Response Methods, Dissipativity Methods, Agent Technology, Gain Scheduling Method, Phasor Measurement, Optimization Methods and H_∞ Based Optimization [4].

However, two important aspects should be considered at this point regarding the tuning and performance of the classical PSS for electromechanical oscillation damping:

- First, a difficulty of the PSS tuning appear when it is consider that the modes of oscillations that must be compensated by the controller vary with the operating point of the system and the network reactance seen at the generator terminals [21]. The lead lag filters are to be design to provide damping for a fixed oscillation frequency or a narrow range of frequencies close to it. However, the power system is a dynamic system and other poorly damped oscillations modes can appear. Therefore, the good performance of the PSS is limited to an operating point or a narrow frequency range for which it is tuned.

- Second, the PSS is defined to provide damping for local area oscillations. The traditional PSS tuning process is based on a Synchronous Machine Infinite Bus SM-IB model, which doesn't allow considering the entire dynamic interactions at which the generator will be exposed to. That may define the oscillations modes that the PSS should damp and therefore limiting its effectiveness in damping inter-area oscillations. Additionally, for damping both, local and inter-area modes, it is required a phase compensation over a wider frequency range, which may be difficult to achieve.

The classical PSS drawbacks makes it interesting to study other types of control structures. Power Oscillation Damping POD in the power system has been also achieved nowadays through FACTS controllers. The conventional control strategy for FACTS to provide POD is similar to the one used for the generator using the classical PSS (a cascade of washout and lead lag filters). However, the same limitations described before are valid in this case; adding the fact that the slow response of the washout filters causes a slow response for the FACTS control system. Consequently, other control structures are being investigated and implemented to control FACTS in order to provide a proper injection of active and reactive power to the grid that allows to obtain electromechanical oscillations damping, specifically for inter-area modes [3], [6]. Therefore, it is interesting to investigate if those other control structures, which differs mainly in the way how the oscillation angle is extracted, could be implemented in the generator control system to overcome the presented difficulties of the classical PSS based on lead lag filters. This analysis would be of interest for the academy and the industry.

Finally, this project will be developed in close collaboration with the company VG Power AB, manufacturer of synchronous generators and provider of excitation systems, which is interested in a software tool based on an analytical method to tune the classical PSS parameters. The advantage of the tool is that it will allow having an initial settings which could be slightly modified during the PSS commissioning process.

1.2 Purpose

The purpose of this master thesis project is to develop a methodology to tune the classical PSS applied to the synchronous generator with particular focus on the lead lag filters. Additionally, the aim of this work is extended to study the application of an alternative control structure to the generator for damping electromechanical oscillations, which is based on signal estimation theory.

1.3 Scope

The tuning algorithm to be developed is constrained to an analysis in a SM-IB model. Moreover, the analysis of the PSS performance and the application of the other control structure is conceived as a theoretical analysis with the results supported by simulations.

1.4 Method

The first step is to develop a SM-IB model in MATLAB. The AVR, exciter and PSS will be modelled in MATLAB/Simulink according to information provided by VG Power AB. The next step is to perform the PSS tuning analysis using the SM-IB model. For this task MATLAB Control System Toolbox will be used to build an automatic tool to tune the lead lag filters in the PSS compensation stage. A detailed study of Synchronous Machine Modelling, Control Theory, Frequency Domain Techniques and Modal Analysis needs to be done in order to define the final tuning methodology that will be programmed in MATLAB. Additionally, commissioning and field PSS tuning experience by VG Power AB will enrich the methodology.

After the MATLAB tool has been built and test, a theoretical analysis of the PSS performance to damp electromechanical oscillations will be carried out. Other control structure reported in the literature that is being used in the power system to damp oscillations will be analyzed considering aspect as principle of operation, advantages and drawbacks. A deep study of that control structure will open the possibility to evaluate if it can be implemented as a controller in the synchronous generator. Simulations will be performed.

Finally, all the studies and simulations will be presented in a final report of the thesis project including detailed description and instructions how to use the tuning software. It is also important to mention as part of the method of working in this project that periodical meetings will be held with VG Power AB engineers for technical discussions, transfer of information and required data and to evaluate the progress of the project. However, the thesis will be developed at Chalmers University of Technology.

Chapter 2

Synchronous Machine Infinite Bus Modelling

In this chapter the modelling stages of the SM-IB system necessary to study its dynamic behaviour are presented. A diagram of the SM-IB system is shown in Fig. 2.1. The synchronous machine is connected to the infinite bus through a transmission system represented by a transformer and a line with reactance and resistance X_t, X_L, R_t and R_L respectively.

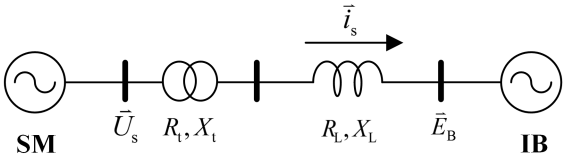

Fig. 2.1 Diagram of the SM-IB System

The SM-IB system can be considered as a theoretical simple system that allows to study the electromechanical interaction between a single generator and the power system. It is not useful for studies of large power systems but it helps to understand the effect of the field, damper circuits and the excitation system in the dynamic response of a single generator [11]. The SM-IB system model is also the base to analyze and to tune the PSS controller to enhance the dynamic stability of the generator through the excitation control system. Different degree of details are presented in the complete and linearized models of the SM-IB system described in this chapter. The linearized model will be a suitable model for PSS tuning while the complete one will allow to test the results reached from the PSS tuning process and from the application of other control structures to damp power oscillations in the power system. The parameters of the test generator and the models used for the excitation system are provided by VG Power AB and are presented in Appendix A.

2.1 SM-IB Complete Model

The model developed in this section includes a detailed mathematical model of the synchronous generator which consider stator and rotor windings flux dynamics and rotor mechanical dynamics. It also includes the mathematical model of the transmission system, current dynamics and the infinite bus, which is represented as a constant voltage. The modelled system is shown in Fig. 2.1.

It is assumed that the generator to be modelled has three stator windings and in the rotor, one field winding which is connected to a source of direct current, and three damper or amortisseur windings which is assumed to have a current flowing in closed circuits, as it is shown in the circuit of Fig. 2.2. From the figure it is also observed that the rotor circuit is in dq coordinates. In the model, the field flux is considered to be aligned to the d-axis, where there is also a damper winding 1d. The other two damper windings 1q and 2q are placed in the q-axis. The dq reference system is a rotating system and to express the stator circuit in

the same reference, the dq Transformation is used, specifically Power Invariant Transformation [11]. The transformations equations for three phase systems are presented in Appendix B. The angle θ in Fig. 2.2 is the transformation angle and it represents the angle by which the d-axis leads the magnetic axis of the a-phase winding [11].

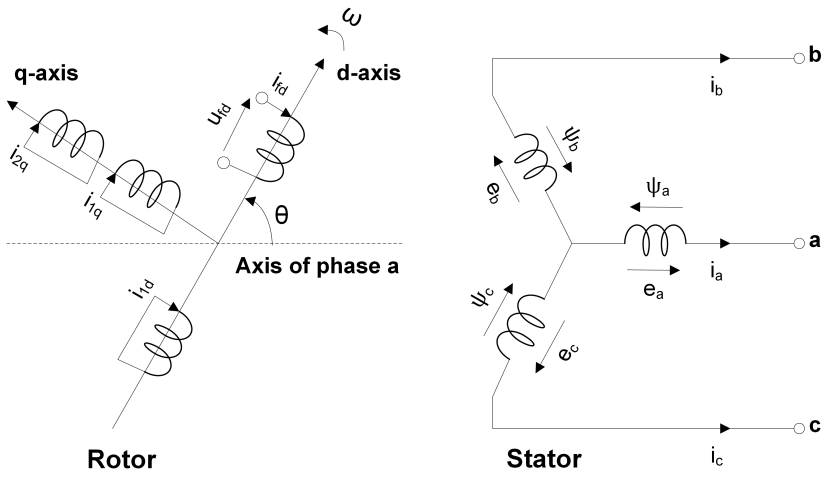

Fig. 2.2 Synchronous Machine Stator and Rotor Circuits

The equations of the synchronous machine that are presented as follows are stated under generator convention for polarities (positive direction of stator currents going out of the machine) and assuming positive direction of field and damper windings currents coming into the machine [11]. In the equations, including the ones of the external network, all quantities are presented in per unit except for the time which is presented in seconds, and balanced conditions are assumed which means that not zero sequence component is included.

Stator Voltage Equations

$$\begin{aligned} U_{sd} &= \tfrac{1}{\omega_0}\tfrac{d\psi_{sd}}{dt} - \omega_r\psi_{sq} - R_s i_{sd} \\ U_{sq} &= \tfrac{1}{\omega_0}\tfrac{d\psi_{sq}}{dt} + \omega_r\psi_{sd} - R_s i_{sq} \end{aligned} \tag{2.1}$$

Where U_{sd}, U_{sq}, i_{sd}, i_{sq}, ψ_{sd}, ψ_{sq} are the stator voltage, current and flux components in the dq reference system. ω_0 is the synchronous electrical angular speed, ω_r is the rotor speed and R_s is the stator resistance.

Rotor Voltage Equations

$$\begin{aligned} U_{fd} &= \tfrac{1}{\omega_0}\tfrac{d\psi_{fd}}{dt} + R_{fd} i_{fd} \\ 0 &= \tfrac{1}{\omega_0}\tfrac{d\psi_{1d}}{dt} + R_{1d} i_{1d} \\ 0 &= \tfrac{1}{\omega_0}\tfrac{d\psi_{1q}}{dt} + R_{1q} i_{1q} \\ 0 &= \tfrac{1}{\omega_0}\tfrac{d\psi_{2q}}{dt} + R_{2q} i_{2q} \end{aligned} \tag{2.2}$$

Where U_{fd}, i_{fd}, R_{fd} are the field voltage, current and resistance respectively. i_{1d}, i_{1q}, i_{2q}, ψ_{1d}, ψ_{1q}, ψ_{2q}, R_{1d}, R_{1q}, R_{2q} are the damper winding current, flux and resistance components in the dq reference system.

Stator Flux Linkage Equations

$$\begin{aligned}\psi_{sd} &= -L_{sd}i_{sd} + L_{md}i_{fd} + L_{md}i_{1d} \\ \psi_{sq} &= -L_{sq}i_{sq} + L_{mq}i_{1q} + L_{mq}i_{2q}\end{aligned} \tag{2.3}$$

Where L_{sd}, L_{sq}, L_{md} and L_{mq} are the stator and mutual inductance components in the dq reference system.

Rotor Flux Linkage Equations

$$\begin{aligned}\psi_{fd} &= -L_{md}i_{sd} + L_{fd}i_{fd} + L_{md}i_{1d} \\ \psi_{1d} &= -L_{md}i_{sq} + L_{md}i_{fd} + L_{1d}i_{1d} \\ \psi_{1q} &= -L_{mq}i_{sq} + L_{1q}i_{1q} + L_{mq}i_{2q} \\ \psi_{2q} &= -L_{mq}i_{sq} + L_{mq}i_{1q} + L_{2q}i_{2q}\end{aligned} \tag{2.4}$$

Where L_{fd} is the field inductance, L_{1d}, L_{1q} and L_{2q} are the damper windings inductance components in the dq reference system.

Inductances

The inductances introduced in the previous equations are defined as:

$$\begin{aligned}L_{sd} &= L_{md} + L_{s\lambda} \\ L_{sq} &= L_{mq} + L_{s\lambda} \\ L_{fd} &= L_{md} + L_{f\lambda} \\ L_{1d} &= L_{md} + L_{1d\lambda} \\ L_{1q} &= L_{mq} + L_{1q\lambda} \\ L_{2q} &= L_{mq} + L_{2q\lambda}\end{aligned} \tag{2.5}$$

Where the subscript λ means the leakage component of the inductance.

Electrical Airgap Torque

The electrical torque T_e produced by the generator is calculated as:

$$T_e = \psi_{sd}i_{sq} - \psi_{sq}i_{sd} \tag{2.6}$$

Equations of Motion

For power system analysis, it is used to consider the whole rotor of a generation unit (generator and turbine) as one rigid rotating mass [7]. The mechanical dynamics in the rotor are represented by the following equations considered as a single-mass model:

$$2H\frac{d\omega_r}{dt} = T_m - T_e - K_D\omega_r \tag{2.7}$$

$$\frac{1}{\omega_0}\frac{d\delta_r}{dt} = \omega_r - 1 \tag{2.8}$$

Where H is the inertia time constant of the entire rotor of the system expressed in seconds, T_m is the mechanical torque, T_e is the electrical torque, K_D is the damping torque coefficient given in p.u. torque/p.u. speed and δ_r is the angular position of the rotor with respect to a reference frame which is synchronously rotating. It is important to mention that the angular speed of a grid connected synchronous machine may be expressed as a deviation from the nominal speed [7] as can be seen from (2.8). Equation (2.7) is usually called *Swing Equation* and represents the acceleration of the rotor as a consequence of a torque unbalance on the shaft.

External Network Equations

Considering the system presented in Fig. 2.1, the following equations accomplishes the mathematical model of the SM-IB system:

$$\begin{aligned} U_{sd} &= E_{Bd} + R_E i_{sd} - \omega_r X_E i_{sq} + \tfrac{X_E}{\omega_0}\tfrac{di_{sd}}{dt} \\ U_{sq} &= E_{Bq} + R_E i_{sq} + \omega_r X_E i_{sd} + \tfrac{X_E}{\omega_0}\tfrac{di_{sq}}{dt} \end{aligned} \tag{2.9}$$

Where X_E is the total external reactance $X_t + X_L$, R_E is the total external resistance $R_t + R_L$, and E_{Bd} and E_{Bq} are the infinite bus voltage vector $\vec{E}_B$ components expressed in the dq reference system. Since the rotor position is taken as a reference, the infinite bus voltage vector $\vec{E}_B$ is defined referred to the rotor side as:

$$\vec{E}_B = E_{Bd} + jE_{Bq} = E_B \sin(\delta_r) + jE_B \cos(\delta_r) \tag{2.10}$$

The infinite bus is defined to have constant voltage, therefore E_B remains constant when a disturbance is applied to the system. If the system conditions change, E_B will change to represent a different operating condition of the external network [11].

Finally, the electrical equations of the SM-IB system can be drawn as a circuit. In Fig. 2.3 the equivalent circuit representation is shown.

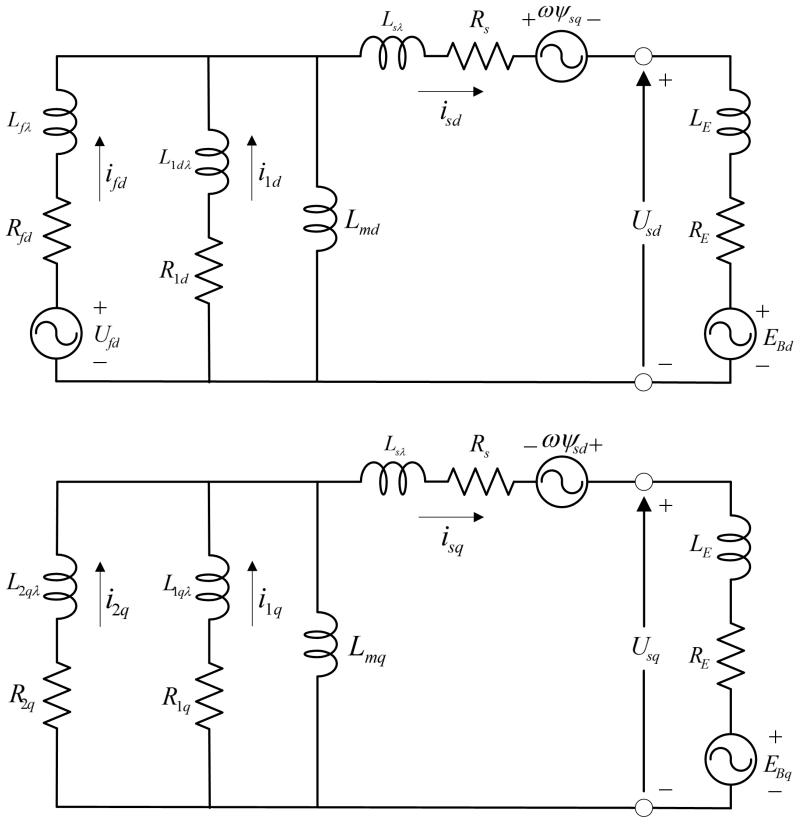

Fig. 2.3 SM-IB Equivalent Circuit - d and q Components

As a general observation, the purpose of the damper windings in the synchronous generator is to counteract changes of the magnetic airgap flux to obtain better dynamic performance of the system (damp out oscillations [11]) and to protect the field winding from high currents in the case of big disturbances on the stator side [7]. Additionally, according to the type of rotor construction and the frequency range in which the mathematical model should represent the machine characteristics, the number of rotor circuits (dampers or field) to be modelled is determined. If the model is used for system stability analysis, more than two or three rotor circuits in each axis are not necessary [11]. Therefore, the model presented in this section is a

complete model that consider all the dynamics in the generator and in the transmission network.

2.2 Excitation System Models

The excitation control system provides the direct current to the field winding. In addition to terminal voltage regulation, the control system performs other tasks as stabilizing and protecting functions. By controlling the current supplied to the field winding by the exciter, the AVR regulates the terminal voltage. A voltage error is obtained by comparing the measured terminal voltage with the reference voltage. This error is processed to calculate a voltage reference signal for the excitation. That reference alters the exciter output and thereby the generator field current, eliminating the terminal voltage error.

The exciter constitutes the power stage of the excitation system [11]. It supplies the DC power to the field winding in the synchronous generator. Generally, the exciters are classified as rotating or static. In rotating ones the excitation current is supplied either by an AC generator with rectifiers or by a DC generator. In static ones the excitation current is provided using static thyristor converters which are directly controlled by the AVR. In this case, an additional auxiliary service transformer or a generator output transformer are the used types of supply. The main disadvantage of the static exciters is that they need to use slip rings to feed current to the generator rotor [18].

Many models of excitations systems for power stability analysis can be found in the IEEE standard 421.5 2005 [1]. The excitation system models that will be considered in this work are the models provided by VG Power AB which have some similarities with the standard ones presented in [1]. Two types of exciter will be considered, static and rotating exciter as in shown in Fig. 2.4 and Fig. 2.5. The models represent the voltage transducer, the AVR and the exciter. V_{ref} and V_t are the reference and terminal voltage signals, K_p and K_i are the proportional and integral gain of the AVR, T_r is the time constant of the terminal voltage transducer, T_4 is the time constant of a low pass filter to represent a delay due to digital type of AVR, S_e is a function that represents the saturation of the exciter iron which wont be considered in this work so it is set to zero, K_E and T_E are the gain and time constant of the rotating exciter and K_d and T_d are the gain and time constant of a derivative filter that provides excitation system stabilization [1]. The AVR structure corresponds to a Proportional Integral PI controller which amplifies and integrates the voltage error. The control action is limited to the minimum and maximum ceiling voltage of the converter or power supply unit.

A signal coming from a PSS can be added to the voltage reference in the AVR input, this signal is used to modulate the excitation of the generator with the aim of achieving rotor oscillations damping as it will be explain as follows.

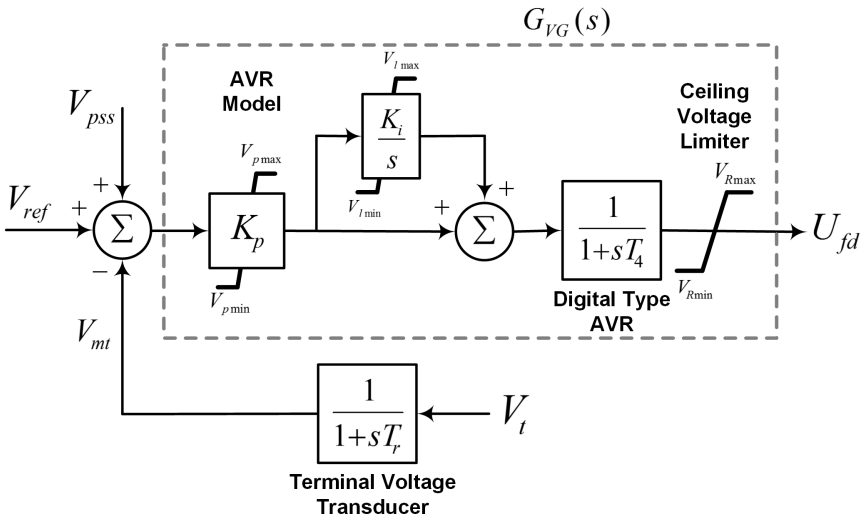

Fig. 2.4 VG Power AB Excitation System Model - Static Exciter

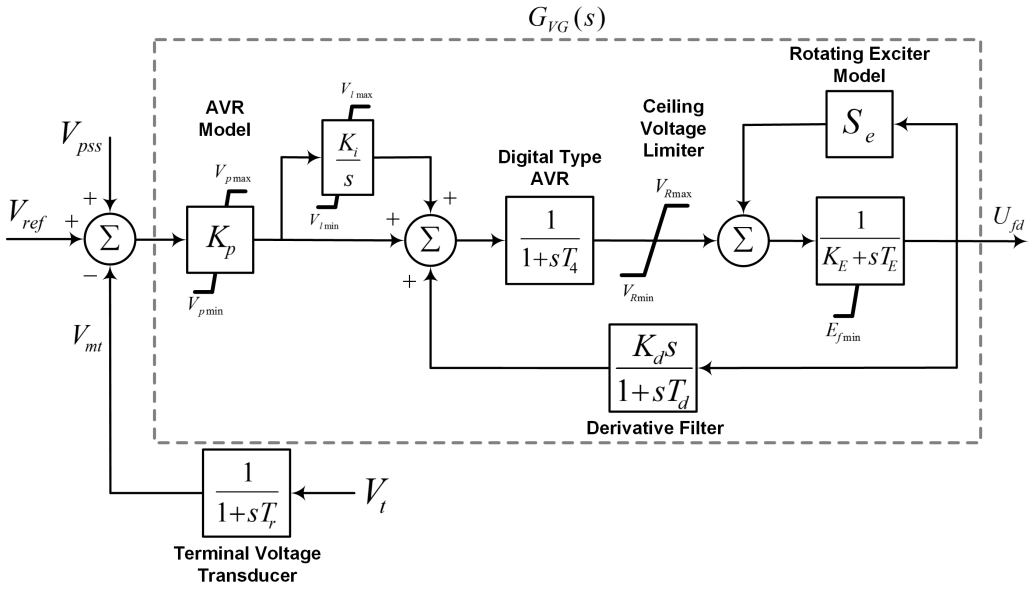

Fig. 2.5 VG Power AB Excitation System Model - Rotating Exciter

2.3 PSS Model

The PSS is a feedback controller, part of the control system for a synchronous generator, which acts through the excitation system, adding a signal to modulate the field voltage. The PSS main function is to damp generator rotor oscillations in the range from 0.1 to 2.5 Hz approximately, which according to [11], are oscillations due to electromechanical dynamics and are called electromechanical oscillations. To provide damping, the PSS should produce an electric torque component that counteracts the mechanical dynamics as is shown in (2.7). The created electric torque component should be in phase with the deviations of the generator rotor speed to constitute a damping torque component. To achieve this, the PSS must compensate the phase difference between the excitation system input and the electric torque.

The idea of power stabilization is that the voltage control system should take the control decision based on the voltage error only if there is no rotor speed deviations. But, if oscillations in the rotor speed appear, the voltage control system must produce a control signal based on the voltage error and on an additional signal from the PSS.

The input signals to the PSS are measured at the generator terminals and determine the type of specific structure of the controller. Among the most modern PSS are the ones with *Dual Input* which use the rotor speed deviation and the active power to calculate the stabilizing signal and are called Type PSS2B in IEEE standard 421.5 2005 [1]; and the *Multiband* which use the rotor speed deviation and particularly, have three working frequency bands dedicated to different frequency oscillation modes, they are also called Type PSS4B [1]. Figure 2.6 shows a block diagram of a generalized structure of the PSS with a single input that is commonly used [1]. Each block in the model corresponds to a main component which are described as follows:

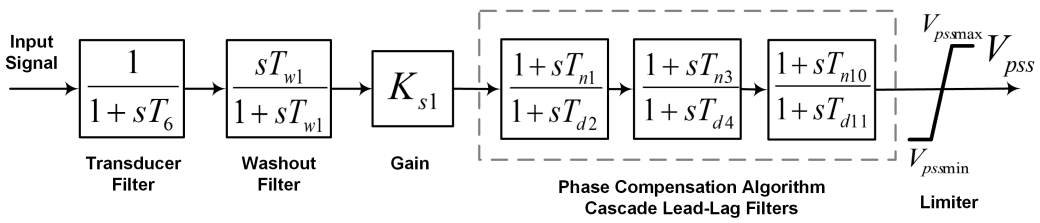

Fig. 2.6 General PSS Structure Model

Initially, a *Transducer Filter* represents the measurement transducer that gives a signal of the measured quantity. Then, a *Washout Filter* which is a high pass filter, is used to define the frequency from which the PSS begins to operate. The measured signal is passed through this filter to prevent the PSS to act when slow changes occur (operating point changes). The *Gain* determines the level of damping provided with the PSS. The PSS is also constituted by a *Phase Compensation* algorithm by using lead lag filters. The phase difference between the excitation system input and the resulting electrical torque is compensated using a cascade of lead lag filters. Finally, a *Limiter* is used to keep the PSS output voltage within a range of values that it can be added to the voltage error in the AVR.

The PSS model that will be used in this work for the theoretical PSS tuning analysis is the one represented in Fig. 2.6 using rotor speed deviations as input signal. If other input signal is used with this structure, additional phase shift could be required from the stabilizer. In the model T_6 is the transducer filter time constant, T_{w1} is the washout filter time constant, T_{n1}, T_{n3} and T_{n10} are the leading time constants, T_{d2}, T_{d4} and T_{d11} are the lag time constants and K_{s1} is the PSS gain.

2.4 SM-IB Linearized Reduced Order Model

Several simplifications can be applied to the complete model presented in Section 2.1 when the intention is to perform small signal analysis for PSS tuning. Small signal analysis in this work is referred to analysis in steady state or under small disturbances applied to the system. A disturbance is considered small if the effect that it has in the system can be analized with linearized equations without relevant lost of accuracy [11]. A linearized model is therefore only valid around a stationary operating point of the system.

Accordingly, the small signal stability is the ability of the system to remain in synchronism when small disturbances occur. As is stated in [11], the synchronous machine rotor oscillations due to lack of damping torque can be seen as a small signal stability problem. In that case, a linearized reduced order model of the SM-IB can provide good representation of the dynamic response of the system to analyze the damping effect that a PSS can introduce. Thus, in this section reduced order and linearized models of the SM-IB system shown in Fig. 2.1 are presented.

The main starting assumptions made to develop the reduced order models are discussed in [11] and listed as follows:

- The stator flux and transmission network current dynamics are neglected.
- The effect of changes in speed in the stator voltage equations is not considered.

The model is linearized around a operating point (x_0,u_0) and it is expressed in the form:

$$\Delta\dot{\mathbf{x}} = \mathbf{A}\Delta\mathbf{x} + \mathbf{B}\Delta\mathbf{u} \tag{2.11}$$

Where **A** is the *State Matrix* and **B** is the *Input Matrix*. $\Delta\mathbf{x}$ is the *States Vector* and $\Delta\mathbf{u}$ is the *Inputs Vector*. The notation with Δ represents a small signal variation around an equilibrium point [5].

2.4.1 Transient Model

The linearized *Transient Model* is a model developed adding the assumption that the damper windings effects are neglected. It includes the mechanical dynamics, the effect of the field flux variations and the effect of the excitation system. Equations (2.1) to (2.8) are linearized, reduced to an appropriate form and then combined with the external network equations in (2.9) to develop the linearized state-space model of the system that will be presented as follows. The complete mathematical derivation is in [11] where the reader is referred for more details.

Let's start considering the equations of motion and the field voltage equation of the synchronous machine combined with the external network equations to obtained the linearized state-space model of the

system [11]. For this model the state variables are the rotor angular speed, the rotor angular position and the field flux. The voltage of the infinite bus is defined to be constant therefore there is no input for it in the model. The inputs to the system are the mechanical torque and the field voltage, however the last one will be determined by the excitation system later in this subsection. With these states and inputs a linearized state-space model of the SM-IB system can be expressed as:

$$\begin{bmatrix} \Delta\dot{\omega}_r \\ \Delta\dot{\delta}_r \\ \Delta\dot{\psi}_{fd} \end{bmatrix} = \begin{bmatrix} A_{11} & A_{12} & A_{13} \\ A_{21} & 0 & 0 \\ 0 & A_{32} & A_{33} \end{bmatrix} \begin{bmatrix} \Delta\omega_r \\ \Delta\delta_r \\ \Delta\psi_{fd} \end{bmatrix} + \begin{bmatrix} B_{11} & 0 \\ 0 & 0 \\ 0 & B_{32} \end{bmatrix} \begin{bmatrix} \Delta T_m \\ \Delta U_{fd} \end{bmatrix} \tag{2.12}$$

Where,

$$A_{11} = -\frac{K_D}{2H} \qquad A_{12} = -\frac{K_1}{2H}$$

$$A_{13} = -\frac{K_2}{2H} \qquad A_{21} = \omega_0$$

$$A_{32} = -\frac{\omega_0 R_{fd}}{L_{f\lambda}} m_1 L'_{md} \quad A_{33} = -\frac{\omega_0 R_{fd}}{L_{f\lambda}}(1 - \frac{L'_{md}}{L_{f\lambda}} + m_2 L'_{md})$$

$$B_{11} = \frac{1}{2H} \qquad B_{32} = \frac{\omega_0 R_{fd}}{L_{md}}$$

and L'_{md} is the d-axis mutual transient inductance and it is defined using the d-axis stator transient inductance L'_{sd} as $L'_{md} = L'_{sd} - L_{s\lambda}$. Moreover, due to per unit values, $L'_{sd} = X'_{sd}$ where X'_{sd} is the d-axis stator transient reactance, a standard parameter of the synchronous machine commonly used. An aspect to mention at this point is that in this work it is not considered the representation of saturation in the inductances used in the model. The constants K_1 and K_2 are defined as:

$$K_1 = n_1(L_{md}(-i_{sd0} + i_{fd0}) + L_{mq} i_{sd0}) - m_1(-L_{mq} i_{sq0} + L'_{md} i_{sq0}) \tag{2.13}$$

$$K_2 = n_2(L_{md}(-i_{sd0} + i_{fd0}) + L_{mq} i_{sd0}) - m_2(-L_{mq} i_{sq0} + L'_{md} i_{sq0}) + \frac{L'_{md}}{L_{f\lambda}} i_{sq0} \tag{2.14}$$

Where the subscript 0 denotes the initial steady-state value of the variables and:

$$n_1 = \frac{E_B(R_{Tot}\sin\delta_{r0} + X_{Totd}\cos\delta_{r0})}{R^2_{Tot} + X_{Totq}X_{Totd}} \qquad n_2 = \frac{R_{Tot}}{R^2_{Tot} + X_{Totq}X_{Totd}}(\frac{L_{md}}{L_{md} + L_{f\lambda}})$$

$$m_1 = \frac{E_B(X_{Totq}\sin\delta_{r0} - R_{Tot}\cos\delta_{r0})}{R^2_{Tot} + X_{Totq}X_{Totd}} \qquad m_2 = \frac{X_{Totq}}{R^2_{Tot} + X_{Totq}X_{Totd}}(\frac{L_{md}}{L_{md} + L_{f\lambda}})$$

Defining $R_{Tot} = R_s + R_E$, $X_{Totd} = X_E + X'_{sd}$, $X_{Totq} = X_E + X_{sq}$. Additionally, the angle δ_{r0} represents the initial steady-state value of the angle by which the synchronous machine leads the infinite bus, taking as reference the infinite bus angle as is shown in Fig. 2.7 where δ_i is the internal rotor angle of the machine.

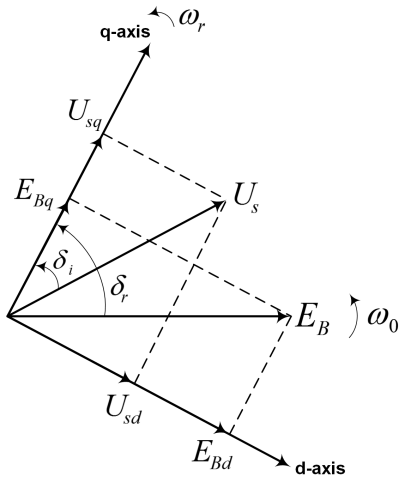

Fig. 2.7 SM-IB Voltage Phasor Diagram [11]

After substitutions and reorganization of the system equations (mathematical procedure that is clearly detailed in [11]), the linearized form of the electrical torque equation can be written as:

$$\Delta T_e = K_1 \Delta\delta_r + K_2 \Delta\psi_{fd} \tag{2.15}$$

The first term in (2.15) is in phase with $\Delta\delta_r$ and is a synchronizing torque component. The second term results from field flux variations which are determined by the third differential equation in (2.12). By rearranging and grouping terms in that equation it is obtained that:

$$\Delta\psi_{fd} = \frac{K_3}{1 + sT_3}(\Delta U_{fd} - K_4 \Delta\delta_r) \tag{2.16}$$

Observe that (2.16) is presented in Laplace domain. The constants of the equation are defined as follows, where T'_{d0} is the d-axis open circuit transient time constant of the machine:

$$K_3 = \frac{L_{f\lambda}}{L_{md}}\left(\frac{1}{1 - \frac{L'_{md}}{L_{f\lambda}} + m_2 L'_{md}}\right) \tag{2.17}$$

$$K_4 = \frac{L'_{md} L_{md}}{L_{f\lambda}} m_1 \tag{2.18}$$

$$T_3 = K_3 T'_{d0} \frac{L_{md}}{L_{fd}} \tag{2.19}$$

To add the effect of the excitation system in the linearized model, the change in the terminal voltage is expressed [11] as:

$$\Delta V_t = K_5 \Delta\delta_r + K_6 \Delta\psi_{fd} \tag{2.20}$$

Where,

$$K_5 = \frac{U_{sd0}}{V_{t0}}(-R_s m_1 + L_{s\lambda} n_1 + L_{mq} n_1) + \frac{U_{sq0}}{V_{t0}}(-R_s n_1 - L_{s\lambda} m_1 - L'_{md} m_1) \tag{2.21}$$

$$K_6 = \frac{U_{sd0}}{V_{t0}}(-R_s m_2 + L_{s\lambda} n_2 + L_{mq} n_2) + \frac{U_{sq0}}{V_{t0}}(-R_s n_2 - L_{s\lambda} m_2 + L'_{md}(\frac{1}{L_{f\lambda}} - m_2)) \tag{2.22}$$

Considering the block diagram of the excitation system with static exciter presented in Fig. 2.4, the next linear expression is derived:

$$s\Delta V_{mt} = \frac{1}{T_r}(\Delta V_t - \Delta V_{mt}) \tag{2.23}$$

Replacing (2.20) in (2.23) and changing from frequency to time domain, a new differential equation is obtained that will increase by one the order of the linearized model:

$$\Delta\dot{V_{mt}} = \frac{1}{T_r}(K_5 \Delta\delta_r + K_6 \Delta\psi_{fd} - \Delta V_{mt}) \tag{2.24}$$

The new state variable is the measured terminal voltage V_{mt}. On the other hand, again from the block diagram in Fig. 2.4 an expression for the field voltage is derived:

$$U_{fd} = (K_p + \frac{K_p K_i}{s})(\frac{1}{1+sT_4})(V_{ref} - V_{mt}) \tag{2.25}$$

Which in perturbed values and assuming constant voltage reference will be:

$$\Delta U_{fd} = (K_p + \frac{K_p K_i}{s})(\frac{1}{1+sT_4})(-\Delta V_{mt}) \tag{2.26}$$

Replacing (2.26) in the differential equation for the field flux changes in (2.12) and reorganizing, the complete steady-state model of the system is obtained:

$$\begin{bmatrix} \Delta\dot{\omega}_r \\ \Delta\dot{\delta}_r \\ \Delta\dot{\psi}_{fd} \\ \Delta\dot{V}_{mt} \end{bmatrix} = \begin{bmatrix} A_{11} & A_{12} & A_{13} & 0 \\ A_{21} & 0 & 0 & 0 \\ 0 & A_{32} & A_{33} & A_{34} \\ 0 & A_{42} & A_{43} & A_{44} \end{bmatrix} \begin{bmatrix} \Delta\omega_r \\ \Delta\delta_r \\ \Delta\psi_{fd} \\ \Delta V_{mt} \end{bmatrix} + \begin{bmatrix} B_{11} \\ 0 \\ 0 \\ 0 \end{bmatrix} \Delta T_m \tag{2.27}$$

Where,

$A_{34} = -B_{32}(K_p + \frac{K_p K_p}{p})(\frac{1}{1+pT_4})$, $A_{42} = \frac{K_5}{T_r}$, $A_{43} = \frac{K_6}{T_r}$, $A_{44} = -\frac{1}{T_r}$ and

p represents the time derivative of the signal. Finally, the equations that describe the linearized transient model can be represented in a block diagram as is shown in Fig. 2.8. More details regarding the process of building the linearized model and the block diagram of the SM-IB system for small signal stability analysis can be found in [9], [10] and [11]. With this modelling approach, the dynamic characteristics of the system are expressed through the *"K"* constants. Observe in the block diagram, that the terminal voltage transducer and the excitation system $G_{VG}(s)$ blocks are the same as in Fig. 2.4 and Fig. 2.5.

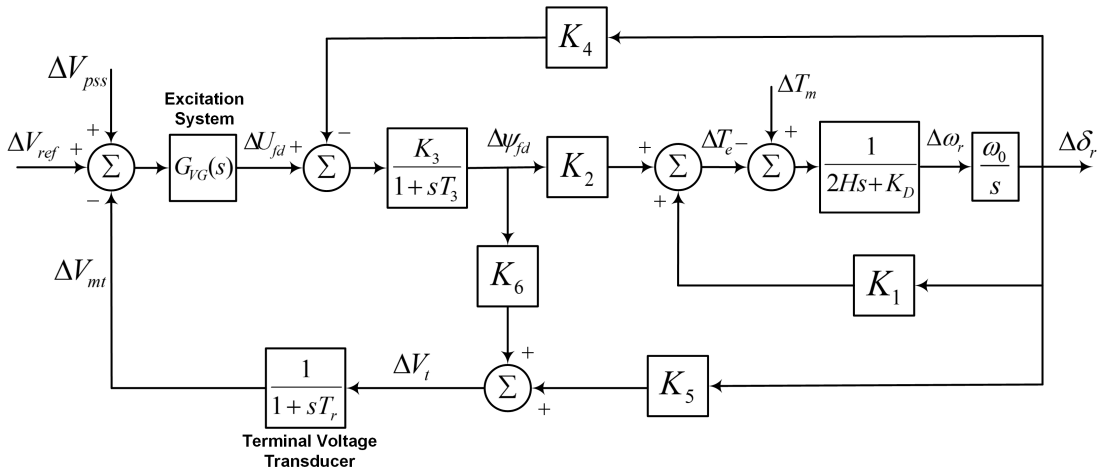

Fig. 2.8 Block Diagram SM-IB Linearized Transient Model [11]

2.4.2 Transient Model for System Phase Analysis

When the purpose of the modelling is the PSS tuning some modifications are made to the model of Fig. 2.8 in order to make it suitable to analize the phase compensation that the PSS should provide to the system. To add damping to the rotor oscillations, the PSS has to guarantee that the created torque component is in phase with the rotor speed deviations. To achieve this it has to compensate the phase lag that the excitation system and the field circuit of the generator introduce between the excitation system input and the electrical torque.

To determine the phase shift, the first step is to calculate the frequency response between the excitation system input and the electrical torque. To do that, the rotor speed and angle should remain constant due to when the excitation of the generator is modulated, the change that results in the electrical torque causes

variations in rotor speed and angle that will affect the electrical torque [11]. Therefore, the rotor angle variation effect is eliminated from the model and in that way the rotor speed is kept constant. The block diagram of the modified model, that will be called the *Transient Model* for system phase analysis and is used for investigating the phase lag in the system, is presented in Fig. 2.9.

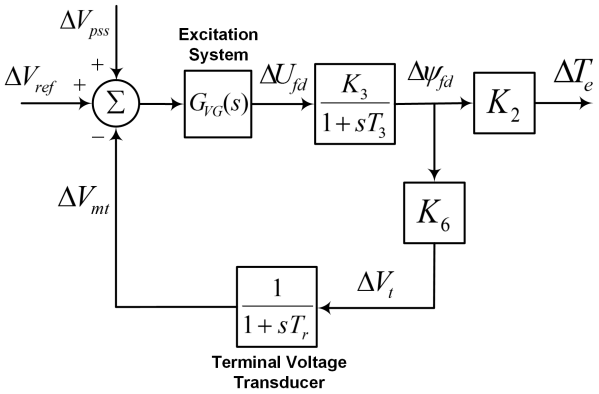

Fig. 2.9 Block Diagram SM-IB Transient Model for System Phase Analysis

2.4.3 Sub-Transient Model for System Phase Analysis

To evaluate the effect that damper windings could have in the phase characteristic of the generator within the PSS frequency range of interest or, what is the same, within the frequency range of electromechanical oscillations, the transient model of Fig. 2.9 is expanded to consider damper windings dynamics resulting in a model that is valid in the sub-transient time frame and that will be called the *Sub-Transient Model* for system phase analysis.

Taken into account the main starting assumptions and following the same procedure that was used in [11] to develop the transient model, the constants of this model are determined considering the four rotor circuit equations in (2.2) and (2.4). Analogue to the transient case, the linearized form of the electrical torque equation can be written as [11]:

$$\Delta T_e = K_1\Delta\delta_r + K_2\Delta\psi_{fd} + K_{21d}\Delta\psi_{1d} + K_{21q}\Delta\psi_{1q} + K_{22q}\Delta\psi_{2q} \tag{2.28}$$

Where,

$$K_1 = n_1(L_{md}(-i_{sd0} + i_{fd0}) + L''_{mq}i_{sd0}) - m_1(-L_{mq}i_{sq0} + L''_{md}i_{sq0}) \tag{2.29}$$

$$K_2 = n_2(L_{md}(-i_{sd0} + i_{fd0}) + L''_{mq}i_{sd0}) - m_2(-L_{mq}i_{sq0} + L''_{md}i_{sq0}) + \frac{L''_{md}}{L_{f\lambda}}i_{sq0} \tag{2.30}$$

$$K_{21d} = n_3(L_{md}(-i_{sd0} + i_{fd0}) + L''_{mq}i_{sd0}) - m_3(-L_{mq}i_{sq0} + L''_{md}i_{sq0}) + \frac{L''_{md}}{L_{1d\lambda}}i_{sq0} \tag{2.31}$$

$$K_{21q} = n_4(L_{md}(-i_{sd0} + i_{fd0}) + L''_{mq}i_{sd0}) - m_4(-L_{mq}i_{sq0} + L''_{md}i_{sq0}) - \frac{L''_{mq}}{L_{1q\lambda}}i_{sd0} \tag{2.32}$$

$$K_{22q} = n_5(L_{md}(-i_{sd0} + i_{fd0}) + L''_{mq}i_{sd0}) - m_5(-L_{mq}i_{sq0} + L''_{md}i_{sq0}) - \frac{L''_{mq}}{L_{2q\lambda}}i_{sd0} \tag{2.33}$$

and L''_{md} and L''_{mq} are the d-axis and q-axis mutual sub-transient inductances. They are defined using the d-axis and q-axis stator sub-transient inductances L''_{sd} and L''_{sq} as $L''_{md} = L''_{sd} - L_{s\lambda}$ and $L''_{mq} = L''_{sq} - L_{s\lambda}$. Moreover, due to per unit values, $L''_{sd} = X''_{sd}$ and $L''_{sq} = X''_{sq}$ where X''_{sd} and X''_{sq} are the d-axis and q-axis stator sub-transient reactances which are standard parameters of the synchronous machine commonly used.

In this case, n_1 and m_1 remain the same as in the transient case but changing the definition of X_{Totd} and X_{Totq} as $X_{Totd} = X_E + X''_{sd}$ and $X_{Totq} = X_E + X''_{sq}$. The other parameters are defined as:

$$n_2 = \frac{R_{Tot}L''_{md}}{(R^2_{Tot} + X_{Totq}X_{Totd})L_{f\lambda}} \qquad m_2 = \frac{X_{Totq}L''_{md}}{(R^2_{Tot} + X_{Totq}X_{Totd})L_{f\lambda}}$$

$$n_3 = \frac{R_{Tot}L''_{md}}{(R^2_{Tot} + X_{Totq}X_{Totd})L_{1d\lambda}} \qquad m_3 = \frac{X_{Totq}L''_{md}}{(R^2_{Tot} + X_{Totq}X_{Totd})L_{1d\lambda}}$$

$$n_4 = \frac{X_{Totd}L''_{mq}}{(R^2_{Tot} + X_{Totq}X_{Totd})L_{1q\lambda}} \qquad m_4 = -\frac{R_{Tot}L''_{mq}}{(R^2_{Tot} + X_{Totq}X_{Totd})L_{1q\lambda}}$$

$$n_5 = \frac{X_{Totq}L''_{mq}}{(R^2_{Tot} + X_{Totq}X_{Totd})L_{2q\lambda}} \qquad m_5 = -\frac{R_{Tot}L''_{mq}}{(R^2_{Tot} + X_{Totq}X_{Totd})L_{2q\lambda}}$$

After some mathematical manipulation of the rotor circuit equations, the flux variation in the rotor circuit windings can be expressed as:

$$\Delta\psi_{fd} = \frac{K_3}{1 + pT_3}(-K_4\Delta\delta + \Delta U_{fd} - K_{41d}\Delta\psi_{1d} - K_{41q}\Delta\psi_{1q} - K_{42q}\Delta\psi_{2q}) \tag{2.34}$$

$$\Delta\psi_{1d} = \frac{T_{1d}}{1 + pT_{1d}}(A_{42}\Delta\delta + A_{43}\Delta U_{fd} + A_{45}\Delta\psi_{1q} + A_{46}\Delta\psi_{2q}) \tag{2.35}$$

$$\Delta\psi_{1q} = \frac{T_{1q}}{1 + pT_{1q}}(A_{52}\Delta\delta + A_{53}\Delta U_{fd} + A_{54}\Delta\psi_{1d} + A_{56}\Delta\psi_{2q}) \tag{2.36}$$

$$\Delta\psi_{2q} = \frac{T_{2q}}{1 + pT_{2q}}(A_{62}\Delta\delta + A_{63}\Delta U_{fd} + A_{64}\Delta\psi_{1d} + A_{65}\Delta\psi_{1q}) \tag{2.37}$$

where,

$$A_{42} = -\frac{\omega_0 R_{1d}}{L_{1d\lambda}}m_1 L''_{md} \quad A_{43} = -\frac{\omega_0 R_{1d}}{L_{1d\lambda}}(m_2 L''_{md} - \frac{L''_{md}}{L_{f\lambda}})$$

$$A_{45} = -\frac{\omega_0 R_{1d}}{L_{1d\lambda}}m_4 L''_{md} \qquad A_{46} = -\frac{\omega_0 R_{1d}}{L_{1d\lambda}}m_5 L''_{md}$$

$$A_{52} = -\frac{\omega_0 R_{1q}}{L_{1q\lambda}}n_1 L''_{mq} \qquad A_{53} = -\frac{\omega_0 R_{1q}}{L_{1q\lambda}}n_2 L''_{mq}$$

$$A_{54} = -\frac{\omega_0 R_{1q}}{L_{1q\lambda}}n_3 L''_{mq} \quad A_{56} = -\frac{\omega_0 R_{1q}}{L_{1q\lambda}}(n_5 L''_{mq} - \frac{L''_{mq}}{L_{2q\lambda}})$$

$$A_{62} = -\frac{\omega_0 R_{2q}}{L_{2q\lambda}}n_1 L''_{mq} \qquad A_{63} = -\frac{\omega_0 R_{2q}}{L_{2q\lambda}}n_2 L''_{mq}$$

$$A_{64} = -\frac{\omega_0 R_{2q}}{L_{2q\lambda}}n_3 L''_{mq} \quad A_{65} = -\frac{\omega_0 R_{2q}}{L_{2q\lambda}}(n_4 L''_{mq} - \frac{L''_{mq}}{L_{1q\lambda}})$$

and,

$$K_3 = \frac{L_{f\lambda}}{L_{md}}\left(\frac{1}{1 - \frac{L''_{md}}{L_{f\lambda}} + m_2 L''_{md}}\right) \tag{2.38}$$

$$K_4 = \frac{L''_{md} L_{md}}{L_{f\lambda}} m_1 \tag{2.39}$$

$$K_{41d} = \frac{L_{md}}{L_{f\lambda}}\left(m_3 L''_{md} - \frac{L''_{md}}{L_{f\lambda}}\right) \tag{2.40}$$

$$K_{41q} = \frac{L''_{md} L_{md}}{L_{f\lambda}} m_4 \tag{2.41}$$

$$K_{42q} = \frac{L''_{md} L_{md}}{L_{f\lambda}} m_5 \tag{2.42}$$

$$T_3 = \frac{L_{f\lambda}}{\omega_0 R_{fd}\left(1 - \frac{L''_{md}}{L_{f\lambda}} + m_2 L''_{md}\right)} \tag{2.43}$$

$$T_{1d} = \frac{L_{1d\lambda}}{\omega_0 R_{1d}\left(1 - \frac{L''_{md}}{L_{f\lambda}} + m_3 L''_{md}\right)} \tag{2.44}$$

$$T_{1q} = \frac{L_{1q\lambda}}{\omega_0 R_{1q}\left(1 - \frac{L''_{mq}}{L_{1q\lambda}} + n_4 L''_{mq}\right)} \tag{2.45}$$

$$T_{2q} = \frac{L_{2q\lambda}}{\omega_0 R_{2q}\left(1 - \frac{L''_{mq}}{L_{2q\lambda}} + n_5 L''_{mq}\right)} \tag{2.46}$$

Adding the effect of the excitation system, the expression for the change in the terminal voltage will be:

$$\Delta V_t = K_5 \Delta\delta_r + K_6 \Delta\psi_{fd} + K_{61d} \Delta\psi_{1d} + K_{61q} \Delta\psi_{1q} + K_{62q} \Delta\psi_{2q} \tag{2.47}$$

Where,

$$K_5 = \frac{U_{sd0}}{V_{t0}}\left(-R_s m_1 + L_{s\lambda} n_1 + L''_{mq} n_1\right) + \frac{U_{sq0}}{V_{t0}}\left(-R_s n_1 - L_{s\lambda} m_1 - L''_{md} m_1\right) \tag{2.48}$$

$$K_6 = \frac{U_{sd0}}{V_{t0}}\left(-R_s m_2 + L_{s\lambda} n_2 + L''_{mq} n_2\right) + \frac{U_{sq0}}{V_{t0}}\left(-R_s n_2 - L_{s\lambda} m_2 + L''_{md}\left(\frac{1}{L_{f\lambda}} - m_2\right)\right) \tag{2.49}$$

$$K_{61d} = \frac{U_{sd0}}{V_{t0}}\left(-R_s m_3 + L_{s\lambda} n_3 + L''_{mq} n_3\right) + \frac{U_{sq0}}{V_{t0}}\left(-R_s n_3 - L_{s\lambda} m_3 + L''_{md}\left(\frac{1}{L_{1d\lambda}} - m_3\right)\right) \tag{2.50}$$

$$K_{61q} = \frac{U_{sd0}}{V_{t0}}\left(-R_s m_4 + L_{s\lambda} n_4 - L''_{mq}\left(\frac{1}{L_{1q\lambda}} - n_4\right)\right) + \frac{U_{sq0}}{V_{t0}}\left(-R_s n_4 - L_{s\lambda} m_4 - L''_{md} m_4\right) \tag{2.51}$$

$$K_{62q} = \frac{U_{sd0}}{V_{t0}}\left(-R_s m_5 + L_{s\lambda} n_5 - L''_{mq}\left(\frac{1}{L_{2q\lambda}} - n_5\right)\right) + \frac{U_{sq0}}{V_{t0}}\left(-R_s n_5 - L_{s\lambda} m_5 - L''_{md} m_5\right) \tag{2.52}$$

The mathematical derivation above allow redrawing the block diagram of the system as is presented in Fig. 2.10. This model is only suited for study the phase lag between the input to the excitation system and the resulting electric torque in the synchronous machine, under the assumption that the rotor speed is constant.

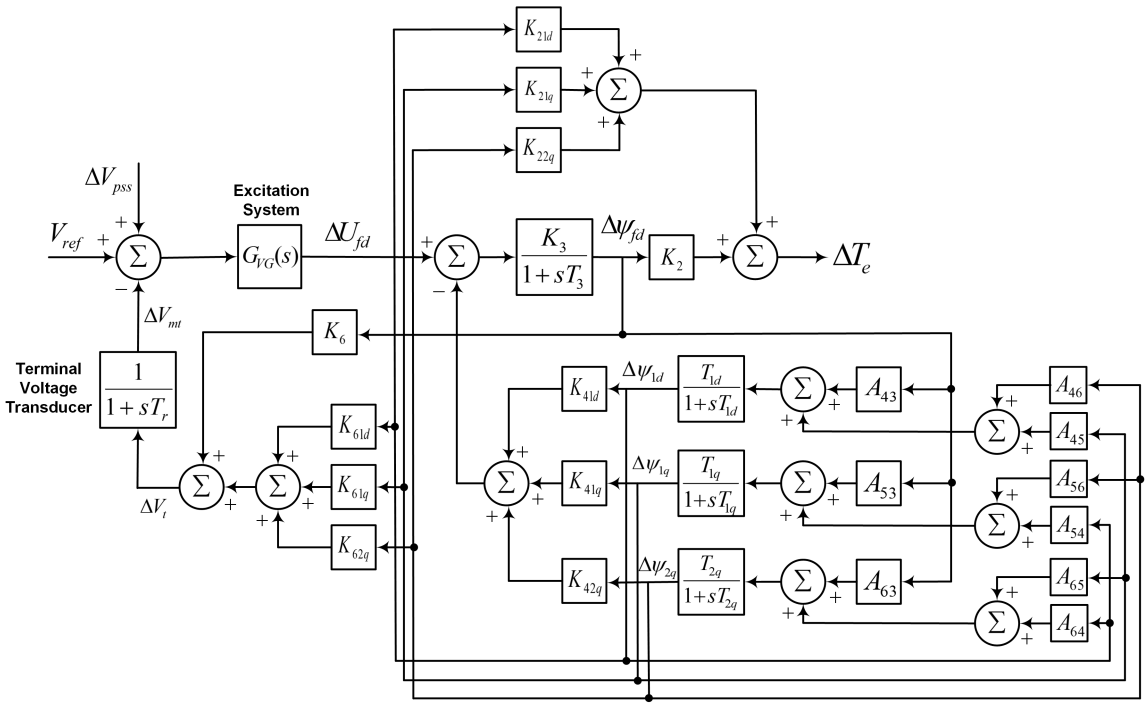

Fig. 2.10 Block Diagram SM-IB Sub-Transient Model for System Phase Analysis

2.5 System Phase Analysis

In this section the phase lag of the synchronous generator from the excitation system input to the electrical torque is analyzed. The parameters of the machine are given in Appendix A. The system phase lag is calculated using the linearized transient and sub-transient models presented in Subsections 2.4.2 and 2.4.3 which assume constant generator rotor speed and angle. Static and rotating exciter models provided by VG Power AB are used in the phase calculation, which is also performed in two different operation points described as follows:

- **OP1**: $X_E = 0.2$ p.u, $P = 0.9$ p.u and $Q = 0.1$ p.u.
- **OP2**: $X_E = 0.6$ p.u, $P = 0.4$ p.u and $Q = 0.1$ p.u.

The results are shown in the Bode diagrams of Fig. 2.11 and Fig. 2.12.

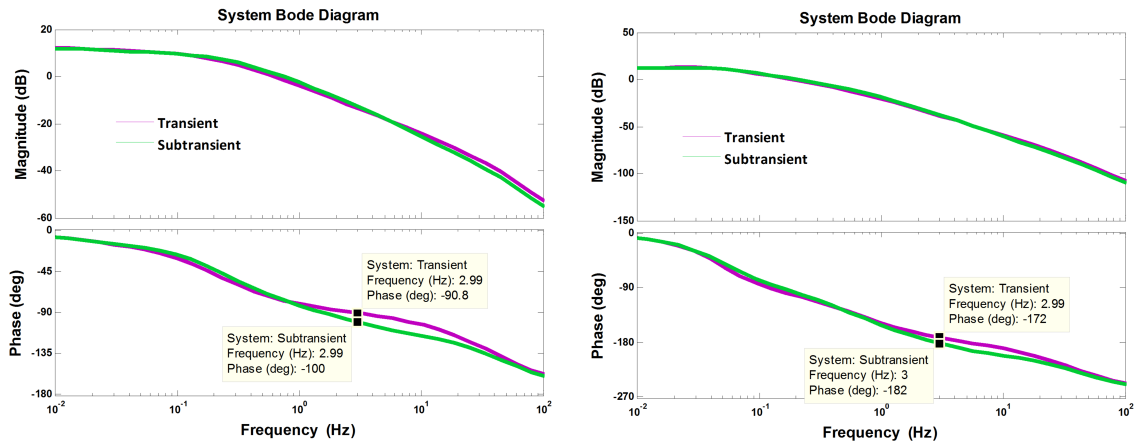

Fig. 2.11 System Bode Diagram - OP1. *Left*: Static Exciter. *Right*: Rotating Exciter

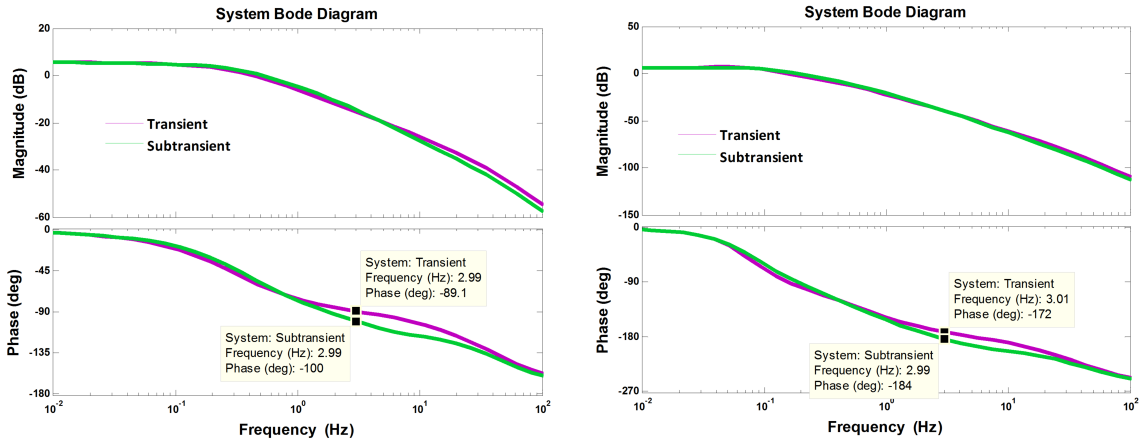

Fig. 2.12 System Bode Diagram - OP2. *Left*: Static Exciter. *Right*: Rotating Exciter

From the phase plots the following conclusions are reached, which are important for the phase characterization of generators using VG Power AB excitation system models:

- There is a larger phase lag for excitation systems with the rotating exciter than with the static exciter.
- At low frequencies, up to 1 Hz there is not representative phase difference between the transient and sub-transient models. At 3 Hz, which is the maximum upper limit of PSS frequency range of interest, the biggest phase difference between the two models is presented, however in the four cases shown in Fig. 2.11 and Fig. 2.12 that difference is about 10° which could be considered not sufficient to include the sub-transient model in the system phase analysis during the PSS tuning process.
- For both kind of exciters, from low frequencies up to 1.5 Hz approximately, the phase lag is larger in the first operation point OP1 which represents a strong external power system and a high loaded synchronous generator. In Chapter 3 will be showed that it is exactly the operating conditions where the PSS should be tuned.
- Finally, it can be concluded that it is not necessary to include the damper windings dynamics in the PSS tuning. Moreover, if the small phase lag introduced by the sub-transient characteristic wants to be taken into account, it is possible to treat it as a PSS design criteria which makes to increase the compensation angle some few degrees.

2.6 Synchronizing and Damping Torque Coefficients Calculation

The variation in the electrical torque ΔT_e due to small disturbances consists of one part which is proportional to the rotor angle variation and is called *Synchronizing Torque* component and one part which is proportional to the rotor speed variation and is called *Damping Torque* component [7] as:

$$\Delta T_e = K_S \Delta\delta_r + K_D \Delta\omega_r \tag{2.53}$$

Where K_S and K_D are the synchronizing and damping torque coefficients respectively. The value of these coefficients depends on the parameters and the operation point of the generator, the parameters of the connecting grid and the parameters of the excitation control system. K_S and K_D must be positive to guarantee the stability of the system [7].

Using the model shown in Fig. 2.8, the effect of the excitation system and the PSS on the synchronizing and damping torque components can be evaluated through the changes in field flux caused by them, considering the electrical torque equation presented in (2.15) as:

$$\begin{aligned} \Delta T_e &= K_1 \Delta\delta_r + K_2 \Delta\psi_{fd} = K_1 \Delta\delta_r + K_2 \Delta\psi_{fd}|_{exar} + K_2 \Delta\psi_{fd}|_{pss} \\ \Delta T_e &= K_1 \Delta\delta_r + \Delta T_e|_{exar} + \Delta T_e|_{pss} \end{aligned} \tag{2.54}$$

From (2.16) and Fig. 2.8, the variation in the field flux due to the excitation system and the armature reaction [11] can be rewritten as:

$$\Delta\psi_{fd}|_{exar} = \frac{K_3}{1+sT_3}(-K_4\Delta\delta_r - \frac{G_{VG}(s)}{1+sT_r}(K_5\Delta\delta_r + K_6\Delta\psi_{fd})) \tag{2.55}$$

In the same way, the variation in the field flux due to the PSS can be written as:

$$\Delta\psi_{fd}|_{pss} = \frac{K_3}{1+sT_3}G_{VG}(s)(-\frac{\Delta V_t}{1+sT_r} + \Delta V_{pss}) \tag{2.56}$$

Where $G_{VG}(s)$ represents the transfer function of the excitation system. In the next two subsections, the calculations of the torque components will be developed replacing $G_{VG}(s)$ with the transfer function of the static and rotating exciter respectively.

2.6.1 Using Excitation System with Static Exciter

Considering the model presented in Fig. 2.4, $G_{VG}(s)$ for the static exciter is given by:

$$G_{VG}(s) = (K_p + \frac{K_pK_i}{s})(\frac{1}{1+sT_4}) \tag{2.57}$$

After replacing (2.57) in (2.55), grouping terms and reorganizing, and inserting $\Delta\psi_{fd}|_{exar}$ in (2.54), the change in the torque component can be expressed as:

$$\Delta T_e|_{exar} = \frac{-K_2K_3[sK_4(1+sT_r)(1+sT_4) + sK_pK_5 + K_pK_iK_5]\Delta\delta_r}{s^4T_3T_4T_r + s^3(T_4T_r + T_3(T_4+T_r)) + s^2(T_3+T_4+T_r) + s(1+K_pK_3K_6) + K_pK_iK_3K_6} \tag{2.58}$$

The interest here is to get the torque coefficients at a certain rotor oscillation frequency, thus the Laplace operator in (2.58) will be replaced by $s = \alpha + j\omega$. Observe that in this case s is defined as a complex number instead of $j\omega$. The concept of *Complex Frequency*, is used in [11], which considers that the properties of sinusoids functions, when $s = j\omega$, are shared by *damped* sinusoids functions, when $s = \alpha + j\omega$. Consequently, it is possible to have also a phasor representation of a *damped* sinusoid function in the form [11]:

$$v = V_m e^{\alpha t}\cos(\omega t + \theta) = Re(\underline{v}e^{st}) \tag{2.59}$$

Where $\underline{v} = V_m\angle\theta$ is the phasor for both sinusoid and *damped* sinusoid functions.

Therefore, the expression obtained for the electrical torque component has the following general form:

$$\Delta T_e|_{exar} = R\Delta\delta_r + jI\Delta\delta_r \tag{2.60}$$

Where R and I represent the real and imaginary components of the torque $\Delta T_e|_{exar}$. Now, from Fig. 2.8 it can be noticed that:

$$\Delta\omega_r = \frac{s\Delta\delta_r}{\omega_0} = \frac{(\alpha+j\omega)\Delta\delta_r}{\omega_0} \tag{2.61}$$

After solving for $j\Delta\delta_r$, it is obtained that:

$$j\Delta\delta_r = \frac{\omega_0}{\omega}\Delta\omega_r - \frac{\alpha}{\omega}\Delta\delta_r \tag{2.62}$$

Inserting (2.62) in (2.60) and reorganizing:

$$\Delta T_e|_{exar} = (R - I\frac{\alpha}{\omega})\Delta\delta_r + (\frac{\omega_0}{\omega})I\Delta\omega_r = K_S|_{exar}\Delta\delta_r + K_D|_{exar}\Delta\omega_r \tag{2.63}$$

Where, $K_S|_{exar}$ and $K_D|_{exar}$ are the synchronizing and damping torque coefficients due to the change in field flux caused by the excitation system action and the armature reaction.

Let's now consider the effect of the PSS in the torque coefficients. Inserting (2.57) in (2.56) and defining ΔV_t and ΔV_{pss} from Fig. 2.8 and Fig. 2.6 respectively as:

$$\Delta V_t = K_6 \Delta \psi_{fd} \tag{2.64}$$

$$\Delta V_{pss} = K_{s1}(\frac{1+sT_{n1}}{1+sT_{d2}})(\frac{1+sT_{n3}}{1+sT_{d4}})(\frac{sT_{\omega 1}}{1+sT_{\omega 1}})(\frac{1}{1+sT_6})\Delta\omega_r = G_{pss}(s)\Delta\omega_r \tag{2.65}$$

It is obtained an expression for $\Delta\psi_{fd}|_{pss}$ which is inserted in (2.54) to have the change in the torque component:

$$\Delta T_e|_{pss} = \frac{K_2K_3(sK_p + K_pK_i)(1+sT_r)G_{pss}(s)\Delta\omega_r}{s(1+sT_3)(1+sT_4)(1+sT_r) + K_3K_6(sK_p + K_pK_i)} \tag{2.66}$$

Again, replacing s with $\alpha + j\omega$, the expression obtained in this case has the following general form:

$$\Delta T_e|_{pss} = R\Delta\omega_r + jI\Delta\omega_r \tag{2.67}$$

From (2.61), $j\Delta\omega_r$ can be expressed as:

$$j\Delta\omega_r = \frac{j(\alpha + j\omega)\Delta\delta_r}{\omega_0} = \frac{\alpha}{\omega_0}(j\Delta\delta_r) - \frac{\omega}{\omega_0}\Delta\delta_r \tag{2.68}$$

Inserting (2.62) in (2.68), then in (2.67) and reorganizing:

$$\Delta T_e|_{pss} = -I(\frac{\alpha^2}{\omega\omega_0} + \frac{\omega}{\omega_0})\Delta\delta_r + (R + I\frac{\alpha}{\omega})\Delta\omega_r = K_S|_{pss}\Delta\delta_r + K_D|_{pss}\Delta\omega_r \tag{2.69}$$

Finally, the total synchronizing and damping torque coefficients are given by:

$$K_S = K_1 + K_S|_{exar} + K_S|_{pss} \tag{2.70}$$

$$K_D = K_D|_{exar} + K_D|_{pss} \tag{2.71}$$

2.6.2 Using Excitation System with Rotating Exciter

The same procedure is followed using the model presented in Fig. 2.5. In this case, $G_{VG}(s)$ for rotating exciter is given by:

$$G_{VG}(s) = (K_p + \frac{K_pK_i}{s})(\frac{1+sT_d}{(1+sT_4)(1+sT_d)(sT_E + K_E + S_e) + sK_d}) = (K_p + \frac{K_pK_i}{s})G_{rot}(s) \tag{2.72}$$

The torque components in this case are:

$$\Delta T_e|_{exar} = \frac{-K_2K_3[sK_4(1+sT_r) + sK_pK_5G_{rot}(s) + K_pK_iK_5G_{rot}(s)]\Delta\delta_r}{s^3T_3T_r + s^2(T_r+T_3) + s(1+K_pK_3K_6G_{rot}(s)) + K_pK_iK_3K_6G_{rot}(s)} \tag{2.73}$$

$$\Delta T_e|_{pss} = \frac{K_2K_3(sK_p + K_pK_i)(1+sT_r)G_{rot}(s)G_{pss}(s)\Delta\omega_r}{s(1+sT_3)(1+sT_r) + K_3K_6(sK_p + K_pK_i)G_{rot}(s)} \tag{2.74}$$

In the calculations for rotating exciter case, the third lead lag filter is added to the PSS transfer function $G_{pss}(s)$ presented in (2.65). Finally, K_S and K_D are computed in the same way than in static case.

2.6.3 Sensitivity Analysis

A sensitivity analysis is presented in Fig. 2.13 and Fig. 2.14 to evaluate the impact of excitation system in the damping and synchronizing torque coefficients with both kind of exciters and under different system operating conditions. The value of reactive power is fixed to $Q = 0.1$ p.u. The parameters used for the calculations are given in Appendix A.

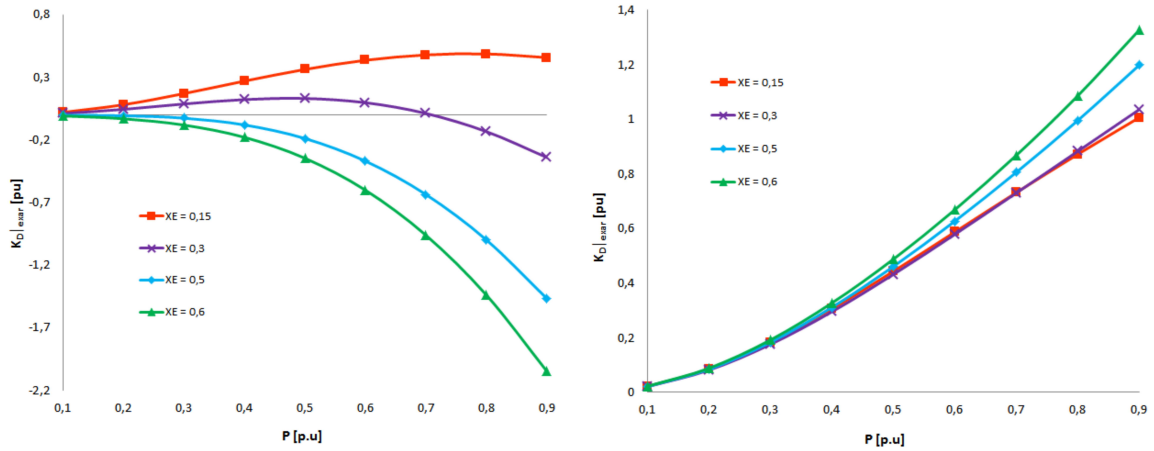

Fig. 2.13 Damping $K_D|_{exar}$ Torque Coefficients as Function of P. *Left*: Static Exciter. *Right*: Rotating Exciter.

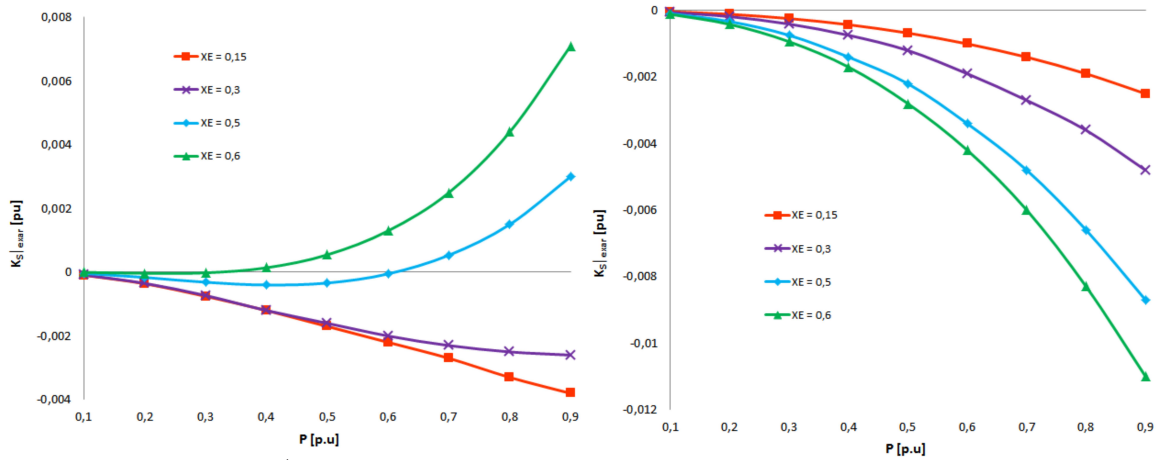

Fig. 2.14 Synchronizing $K_S|_{exar}$ Torque Coefficients as Function of P. *Left*: Static Exciter. *Right*: Rotating Exciter.

From Fig. 2.13 it is observed that with static exciter, the damping coefficient becomes negative as the external reactance increases and it gets worse as the machine is more loaded. For a value of reactance around 0.3 p.u, the coefficient becomes negative for high active power and for very low values of X_E, it is always positive. The damping coefficient with rotating exciter is always positive independent of the external reactance value, and it gets better as the generator active power increases; the reason could be the stabilizing loop in that control structure which add damping ability to the system. In general, it was also observed that the reactive power has a negative impact in the damping toque coefficients decreasing its values.

On the other hand, from Fig. 2.14 it is observed an opposite behaviour of the synchronizing torque coefficient. With rotating exciter it is always negative and decreases as the active power increases. With static exciter the coefficient is always negative for low values of X_E and always positive for high values of X_E while for values of the external reactance around 0.5 p.u the coefficient becomes positive for high active power values.

The points in Fig. 2.13 and Fig. 2.14 are calculated for different complex frequencies as it was explained in Section 2.6.1. Each complex frequency corresponds to the real and imaginary part of the eigenvalue associated to the local oscillation mode in each operating point; those local modes appear in a range from 0.9 Hz to 1.4 Hz approximately. To evaluate the coefficients as function of the local mode oscillation frequency, Fig. 2.15 is built for fixed values: $X_E = 0.5$ p.u, $P = 0.9$ p.u, $Q = 0.1$ p.u. It is observed that again the damping coefficient with rotating exciter is always positive in the whole frequency range although it becomes very close to zero after 1 Hz. The opposite case happens for the damping coefficient with static exciter which is always negative and worse at low frequencies. The synchronizing coefficient with static exciter is positive until around 1 Hz and with rotating exciter is negative from about 0.3 Hz.

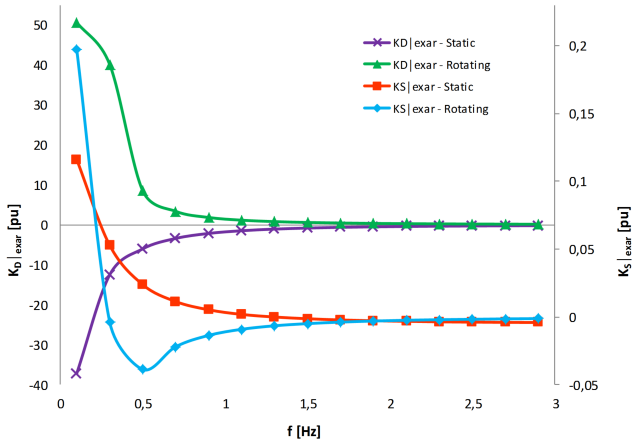

Fig. 2.15 Synchronizing $K_S|_{exar}$ and Damping $K_D|_{exar}$ Torque Coefficients as Function of f [Hz]

It should be taken into account that, from (2.70) and without considering the PSS component, the net synchronizing torque coefficient K_S in the presented cases is not negative since K_1, which is always positive and with higher magnitude than $K_S|_{exar}$, makes it positive. An example of this is illustrated in Fig. 2.16 for static and rotating exciter and as a function of the local mode oscillation frequency.

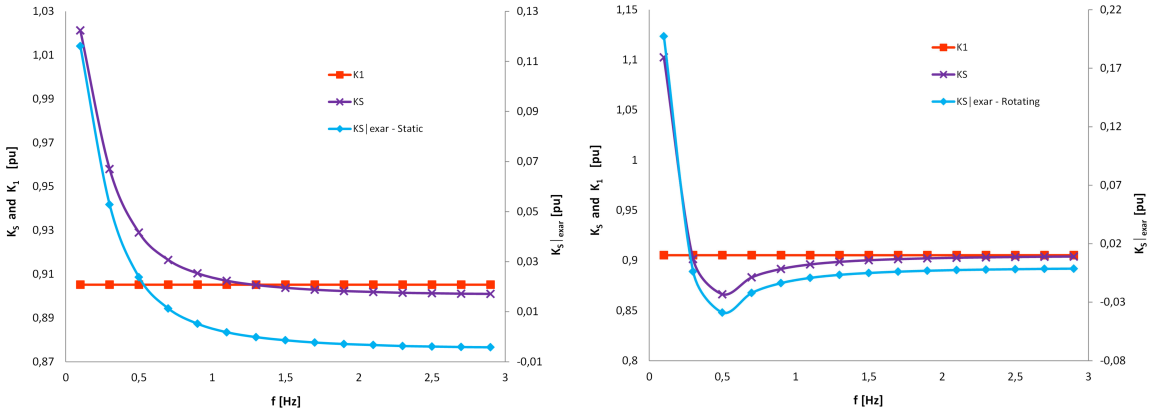

Fig. 2.16 Synchronizing K_S Torque Coefficient as Function of f. *Left*: Static Exciter. *Right*: Rotating Exciter.

Finally, the results show how the excitation system may negatively impacts the synchronizing and damping torque components. Also, it was mathematically demonstrated the need of a PSS to increase the damping torque component specially in the case of excitation systems with static exciters and at low frequencies. In the next chapter a PSS tuning methodology based on frequency response techniques is presented. A proper tuning of this controller will allow reaching better damping conditions for the system.

Chapter 3

PSS Tuning

In the academic and industry community of power systems, the PSS tuning is a topic that has been widely researched for many years. Several methods have been proposed and tested based on linear and non-linear control system theories. Among the classical linear methods are the pole placement and frequency response methods, and more complex ones as LMI, Multivariable Control and Linear Optimal Control [4]. Techniques based on state space feedback, H_∞ robust controller design and intelligent methods have been also applied. Classical linear methods offer good results but might suffer from lack of robustness. On the other hand, advanced linear and non-linear methods are useful specially in the case of coordinated tuning of hundreds of PSS but might result either in oversimplification of the power system model used or in too complex tuning algorithms [22]. In addition they may be difficult to implement in some practical situations, and some of those methods are still in research stages and are not developed enough for general applications. Consequently, the predominant trend in the industry is still to use the frequency response based tuning method [12] even more in the case of a PSS provider company as VG Power AB, who should tune the controller having detailed information about the generator but not exact details about the connecting grid. Therefore, in this chapter the main concepts of a PSS tuning methodology based on frequency response techniques are summarized. The models presented in the previous chapter will be used here to tune the PSS and to test the obtained results. The parameters of the SM-IB system are given in Appendix A.

3.1 Eigenvalues Calculation

The first step in the PSS tuning methodology is to perform an eigenvalues calculation of the SM-IB linearized transient model whose state-space equation was presented in (2.27) and block diagram in Fig. 2.8. The linearized model, which includes the field and excitation system dynamics, can be expressed in the general form:

$$\Delta\dot{\mathbf{x}} = \mathbf{A}\Delta\mathbf{x} + \mathbf{B}\Delta\mathbf{u} \tag{3.1}$$

$$\Delta\mathbf{y} = \mathbf{C}\Delta\mathbf{x} + \mathbf{D}\Delta\mathbf{u} \tag{3.2}$$

Where, $\mathbf{A}$ is the *State Matrix*, $\mathbf{B}$ is the *Input Matrix*, $\mathbf{C}$ is the *Output Matrix* and $\mathbf{D}$ is the *Feedforward Matrix*. $\Delta\mathbf{x}$ is the *States Vector*, $\Delta\mathbf{u}$ is the *Inputs Vector* and $\Delta\mathbf{y}$ is the *Outputs Vector*. The calculation is based on the information contained in matrix $\mathbf{A}$ which is the Jacobian matrix of the system whose elements are evaluated at the equilibrium point where the system is being analyzed. The modes of the system dynamic response are related to the *Eigenvalues* λ_i of matrix $\mathbf{A}$, the ones that determine the stability of the linearized system [11].

The definition of eigenvalues is that λ is an eigenvalue of $\mathbf{A}$ if there exists a nonzero column vector $\mathbf{w}$ that satisfies:

$$\mathbf{A}\mathbf{w} = \mathbf{w}\lambda \tag{3.3}$$

w is called the *Right Eigenvector* associated with the eigenvalue λ. To find λ, (3.3) can be rewritten as:

$$(\mathbf{A} - \lambda\mathbf{I})\mathbf{w} = \mathbf{0} \tag{3.4}$$

Where **I** is a diagonal identity matrix and **0** a column vector of zeros. Equation 3.4 has a non-trivial solution $\mathbf{w} \neq 0$ if and only if [18]:

$$\det(\mathbf{A} - \lambda\mathbf{I}) = \mathbf{0} \tag{3.5}$$

Equation 3.5 is called the *Characteristic Equation* of the system. The *n* solutions of $\lambda = \lambda_1, \lambda_2, ..., \lambda_n$ are the eigenvalues of **A** which may be real or complex values and *n* is the order of **A**.

If the system is excited, its free motion time response is determined in terms of the eigenvalues λ_i by a linear combination of terms with the form $e^{\lambda_i t}$ [11]. Each term $e^{\lambda_i t}$ corresponds to the $i-th$ mode of the system. If λ_i is a real value, the $i-th$ mode is a non-oscillatory mode which should be negative to be a decaying mode. On the other hand, complex eigenvalues appear in conjugate pairs, each pair corresponds to an oscillatory mode. In this case, λ is defined as $\lambda = \alpha \pm j\omega_{osc}$ where the real component determines the damping and the imaginary component determines the frequency of oscillation. Then, the frequency of oscillation in Hz and damping ratio ζ in $\%$ are given by [11]:

$$f_{osc} = \frac{\omega_{osc}}{2\pi} \tag{3.6}$$

$$\zeta = 100\frac{-\alpha}{\sqrt{\alpha^2 + \omega_{osc}^2}} \tag{3.7}$$

The system will be stable if all the eigenvalues have a negative real part in the complex plane. A more accurate measure of the stability is reached using the damping ratio which consider both the real and the imaginary part of the eigenvalues. The larger the imaginary part, the more negative the real part must be in order to provide the same damping in an oscillation mode [22].

3.2 Lead Lag Filters Tuning

Through the eigenvalues analysis of the system without PSS the less damped mode is identified for an operation point, this mode could have negative or critical damping. Negative damping is presented when $\zeta < 0\%$ and critical damping when $0\% < \zeta < 5\%$. In those cases, if a disturbance occurs in the system, it is considered that poorly damped dynamic responses are created. To overcome that situation and provide damping torque with the PSS, the next step in the tuning process is to compute the phase lag of the system at the frequency of the identified mode. The last is done with the model described in Subsection 2.4.2 and *Bode Diagram* frequency response technique. Once the phase shift that the PSS should provide to the system is known, the parameters of the cascade lead lag filters stage in the PSS structure shown in Fig. 2.6 can be tuned.

Two ways of tuning the filters are presented here: *Method 1* [20], [22], [15] and *Method 2*. Both give the wanted phase compensation at the selected frequency, ω_{osc}.

Method 1

In this case the parameters are calculated as follows:

$$
\begin{aligned}
N = \frac{\theta_{pss}}{55^\circ} &= \left\{ \begin{array}{ll} 1 & \theta_{pss} \leqslant 55^\circ \\ 2 & \theta_{pss} \leqslant 110^\circ \\ 3 & 110^\circ < \theta_{pss} \leqslant 180^\circ \end{array} \right\} \\
\sigma &= \frac{1 - \sin\frac{\theta_{pss}}{N}}{1 + \sin\frac{\theta_{pss}}{N}} \\
T_{n_l} &= \frac{1}{\omega_{osc}\sqrt{\sigma}} \\
T_{d_p} &= \sigma T_{n_l}
\end{aligned}
\tag{3.8}
$$

Where θ_{pss}, given in degrees, is the angle that the PSS should compensate at the oscillation frequency ω_{osc}. N is the number of filters in cascade which are defined according to θ_{pss}. The restriction of 55° compensation per filter is to ensure acceptable phase margin and noise sensitivity at high frequencies [22]. T_{n_l} are the lead time constants with $l = 1, 3, 10$ and T_{d_p} are the lag time constants with $p = 2, 4, 11$. This way of calculation can be applied for lead and for lag compensation effect, that depends on the sign of θ_{pss}.

Method 2

In this case the parameters are calculated considering that a lead lag filter can be defined as:

$$
\frac{1 + sT_{n_l}}{1 + sT_{d_p}} = K_f e^{j\frac{\theta_{pss}}{N}} = K_f(\cos\frac{\theta_{pss}}{N} + j\sin\frac{\theta_{pss}}{N}) \tag{3.9}
$$

Where K_f is the filter gain and N follows the same definition than in 3.8. Taking into account that $s = \lambda = \alpha + j\omega_{osc}$ and neglecting the real part α of the frequency component, then $s = j\omega_{osc}$ is inserted in 3.9 to group real and imaginary parts and to solve for the time constants:

$$
\begin{aligned}
T_{n_l} &= \frac{K_f}{\omega_{osc}}\left(\frac{\cos\frac{\theta_{pss}}{N}}{\tan\frac{\theta_{pss}}{N}} + \sin\frac{\theta_{pss}}{N} - \frac{1}{K_f\tan\frac{\theta_{pss}}{N}}\right) \\
T_{d_p} &= \frac{1}{\omega_{osc}\sin\frac{\theta_{pss}}{N}}\left(\cos\frac{\theta_{pss}}{N} - \frac{1}{K_f}\right)
\end{aligned}
\tag{3.10}
$$

The gain K_f must not be less than about 2 to avoid T_{d_p} taking negative values. It was also observed that K_f should have a maximum value due to filter stability reasons. According to the cases analyzed in this work, a maximum value for K_f could be about 10. The effect of varying K_f is to move the compensation central frequency of the filter which will have an impact in the compensated system phase characteristic. Also, the higher K_f the smaller the PSS gain K_{s1} should be to guarantee the system stability.

Some important aspects related to the lead lag filters tuning process must be considered and they are listed as follows:

- **Objective System Phase at ω_{osc}:**
  In the SM-IB modelling task presented in Chapter 2, the dynamics of other machines in the power system were neglected therefore their effect on the phase characteristic of the SM-IB system is eliminated. In addition, the phase lag of the system varies according to the operation point of the generator and the external reactance. Considering this, an acceptable phase compensation for different system conditions should be selected. According to [11], undercompensation by about 10° over the complete

frequency range of interest can provide enough tolerance to support the assumptions made in the modelling process of the SM-IB. Even more, in [16] is said that undercompensation between $20°$ and $40°$ at ω_{osc} is desirable. This is to avoid the PSS to contribute negatively to the synchronizing torque as can be seen in Fig. 3.1 which is built extending the example case presented in Subsection 2.6.3 but now presenting the torque coefficients due to the PSS effect.

In this case, the calculation is done for a system with fixed external reactance $X_E = 0.1$ p.u, fixed reactive power $Q = 0.1$ p.u and fixed active power $P = 0.9$ p.u. What is changing now is the objective system phase at the analyzed oscillation frequency, which implicitly change the angle θ_{pss} that the PSS should compensate. A fixed PSS gain $K_{s1} = 10$ pu is also assumed. Observe that as the angle that the lead lag filters have to compensate for increases, the synchronizing torque coefficient for static exciter decreases. At exact compensation the PSS effect with static exciter would be to decrease the synchronizing torque component of the system but with rotating exciter it seems to be the best condition. In contrast, the bigger the angle to be compensated by the PSS the more damping torque component will be achieved with both exciters, result that is predictable considering the theory discuss until now.

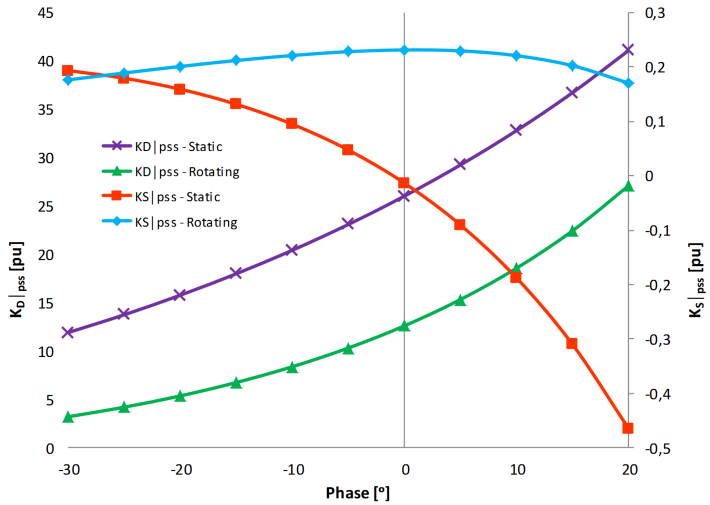

Fig. 3.1 Synchronizing $K_S|_{pss}$ and Damping $K_D|_{pss}$ Torque Coefficients as Function of the Objective System Phase at Analyzed Frequency [deg]

- **System Operation Point for Tuning:**
  According to [14], [15], [16] when the PSS is a rotor speed input PSS as the one analyzed in this work, the filters should be tuned for a system condition that represents the highest gain and the greatest phase lag. Those conditions are reached under generator full load and strongest external transmission system.

Finally, a comment about the washout filter is that its time constant T_{w1} depends on the oscillatory frequency. The lower the oscillatory frequency, the higher T_{w1} must be. In other words, it should be big enough to pass the stabilizing signals at the frequencies of interest but not so big that causes terminal voltage changes as a result of PSS action when the operation point change [13]. T_{w1} can be set in the range from 1 s to 20 s. In this work a value of 7 s will be assumed as it is reported by VG Power AB as a common value to be used with this parameter. In Fig. 3.2 is presented the Bode diagram of the washout filter in the PSS frequency range of interest. Observe that with $T_{w1} = 7$ s the phase contribution by the filter is about $1°$ in almost all the range. For this reason, the washout filter effect wont be considered in the phase analysis of the system.

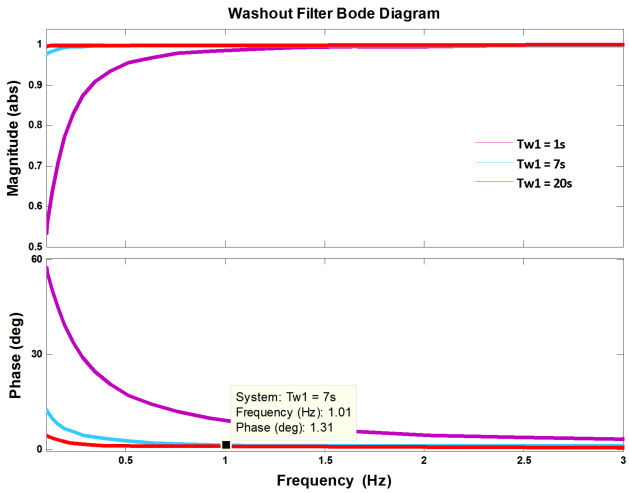

Fig. 3.2 Washout Filter Bode Diagram

3.3 Gain Tuning

When the phase compensation stage has been defined, the next step is to set the PSS gain K_{s1}. Commonly, the chosen gain is related to the instability gain as is described in the following comments about two ways of getting the instability gain of the system:

- One way is using the *Root Locus Plot* of the system, which is a frequency response technique that indicates how the poles and zeros of the open loop system are modified when the controller gain K_{s1} takes different values. Theory about root locus technique can be found in [20]. The block diagram including the PSS used to compute the plot is shown in Fig. 3.3. As the open loop gain takes different values, the roots or eigenvalues of the transfer function from ΔV_{ref} to ΔV_{pss} change. For a certain value of gain, the closed loop system, with positive feedback in the case of the PSS, will be critically or marginally stable, which means that the real part of a pair of eigenvalues is zero. It is a common practice to set the PSS gain to one third of the gain where instability starts [15], [16]. The instability gain must be determined at the same system operating condition mentioned in the previous section for lead lag filters tuning.

- If the root locus plot can not be built, the other way to obtain the instability gain is by a field test usually called the *Gain Margin Test*. It consists of slowly increase the gain from zero until the value that cause the instability. Details about the test can be found in [16]. Again, the recommendation is to set the gain to one third of the obtain gain value.

It is important to mention that setting the gain in one third of the instability gain value is a guide based on field experiences of many years, but it is not an exact method. In order to tune the gain more accurately it is recommended to analyze the root locus of the system in detail and evaluate the paths of critical modes. The closed loop system including the PSS has several eigenvalues and consequently several modes, but only the local mode of the generator oscillating against the infinite bus and the ones associated with the PSS transfer function become critical or relevant to analize [15], [19].

In conclusion, the PSS gain should be set to the minimum value that satisfies a damping requirement for the mode to be damped, in order to avoid compromising the stability of the system. The maximum value allowed would be one third of the value at which the damping of any critical mode becomes zero [12]. Nevertheless, it is common in the industry a conservative design of the gain in a value less than the optimum that limits the performance of the controller but assures the stability of the system. In this work the gain will be chosen through the root locus analysis and according to the performance requirements that will be presented in the next section.

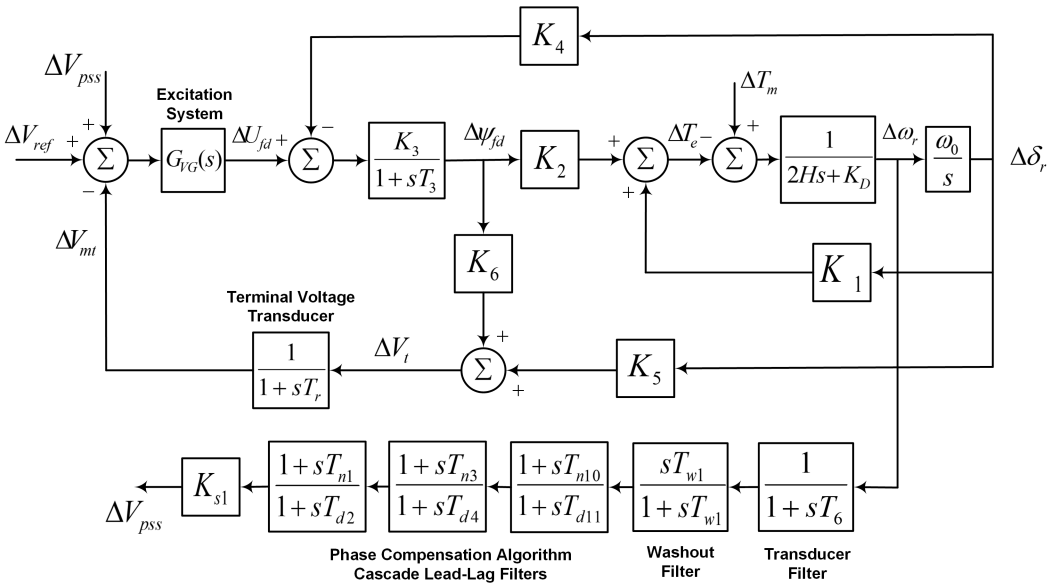

Fig. 3.3 Block Diagram SM-IB with PSS for Root Locus Analysis

3.4 Tuning Performance Requirements

As it has been discussed until now, the nature of the generator and the assumed infinite bus where it is connected provide the local oscillation mode where the PSS tuning task is focussed. The tuning objective then is to provide the best damping for that mode, and an acceptable phase compensation in the whole frequency range of interest. Certain tuning conditions and performance requirements for that case have been established in the literature [15], [16], [19] as:

- To get the maximum damping in the range from 0.2 Hz to 3 Hz, the compensated system should have a phase lag less than $90°$ in the whole range. This is more important than perfect phase compensation results at specific frequencies.
- The phase lag of the compensated system at the local mode frequency should be less than $45°$.
- Some phase lag at lowest frequencies, from 0.2 HZ to 0.5 Hz, is needed since phase lead specially at those frequencies will cause the PSS to deteriorate the synchronizing torque component.
- The change in local mode frequency with and without PSS in operation should be less than 10% to limit the effect of the PSS on the synchronizing torque coefficient.
- Not exact damping percentage is recommended to satisfy a damping requirement, it is more a user decision, despite that is said that excess of local mode damping is unnecessary and it is obtained at the expense of transient stability.

However, specific requirements associated to the external power system dynamics may change the tuning objective, this refers to obtain the PSS parameters so as to contribute as much as possible with the damping of a specific mode, usually an inter-area mode, in the wide area of the system [12].

3.5 Sensitivity Analysis

To examine the sensitivity of the local mode damping to changes in the system operation point, the parameters of the PSS are tuned for the synchronous machine presented in Appendix A using the static exciter. Two cases are reviewed: one where the tuning objective is the local oscillation mode and one where the tuning objective is a specific mode with different oscillation frequency. In both cases, the tuning is made considering a strong external power system $X_E = 0.2$ p.u and high load for the synchronous generator where $P = 0.9$ p.u and $Q = 0.1$ p.u.

3.5.1 Tuning for Local Oscillation Mode

In the mentioned operation point for tuning, the local oscillation mode appears at a frequency of 1.348 Hz with a damping of 0.1942%. The system phase lag at the oscillation frequency is $-84.05°$, the objective system phase at that frequency is set to $-15°$ and as a result, $\theta_{pss} = 69.05°$. In Table 3.1 the obtained parameters using both ways of lead lag filters tuning presented in section 3.2 are summarized. In Fig. 3.4 the root locus plots used to tune the gain K_{s1} are shown and a value of 25 p.u is chosen for both cases in order to be able to compare the results.

Table 3.1: PSS Parameters - Tuning for Local Oscillation Mode

	Parameter								
	$\mathbf{T_{n1}}$	$\mathbf{T_{d2}}$	$\mathbf{T_{n3}}$	$\mathbf{T_{d4}}$	$\mathbf{T_{n10}}$	$\mathbf{T_{d11}}$	$\mathbf{K_{s1}}$	$\mathbf{T_{w1}}$	$\mathbf{T_6}$
Method 1	0.2245	0.0621	0.2245	0.0621	1	1	25	7	0
Method 2	0.2450	0.0675	0.2450	0.0675	1	1	25	7	0

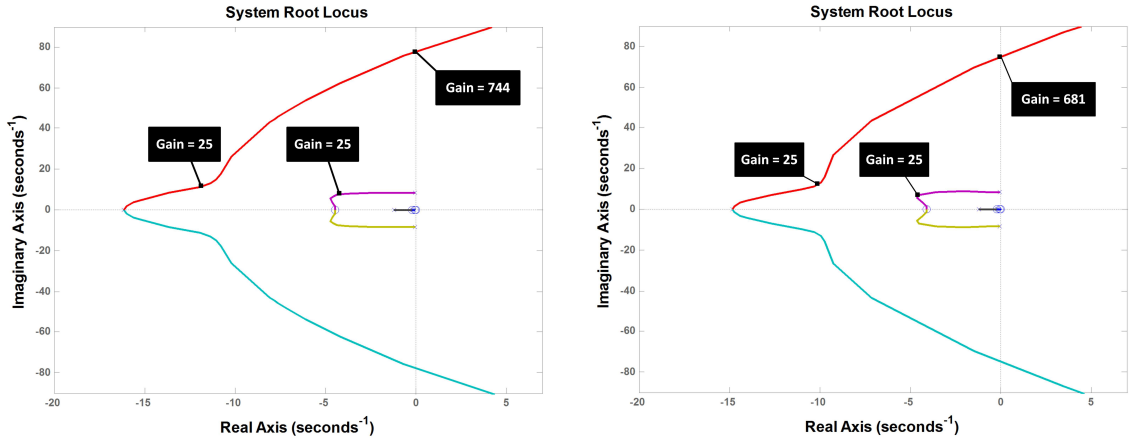

Fig. 3.4 System Root Locus Plots. *Left*: Method 1. *Right*: Method 2

The phase compensation provided by the PSS with both tuning methods is presented in Fig. 3.5 through the Bode diagram of the lead lag filters. Observe that there is not representative difference between the two methods and that at the local mode frequency the compensation provided is $69°$.

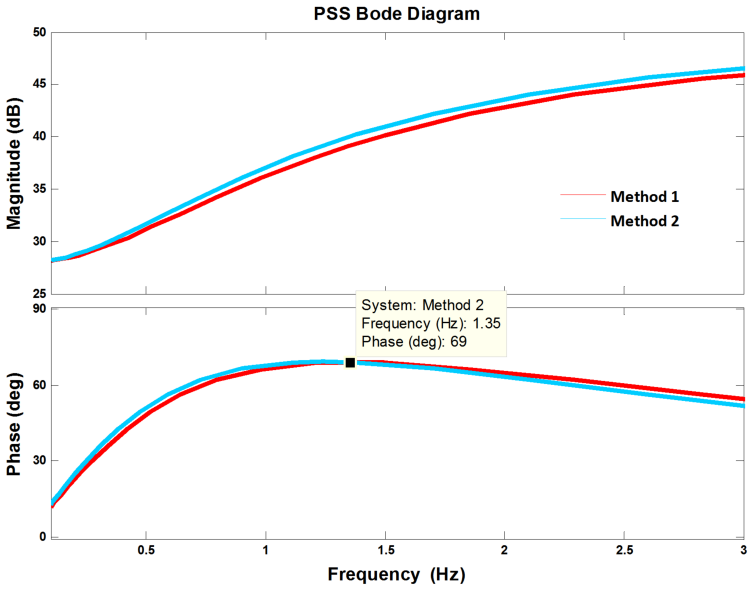

Fig. 3.5 PSS Bode Diagram - Tuning for Local Oscillation Mode

The sensitivity of local mode damping to changes in the system operating point is shown in Fig. 3.6

where a constant value of reactive power was assumed $Q = 0.1$ p.u. The main observations after the analysis are:

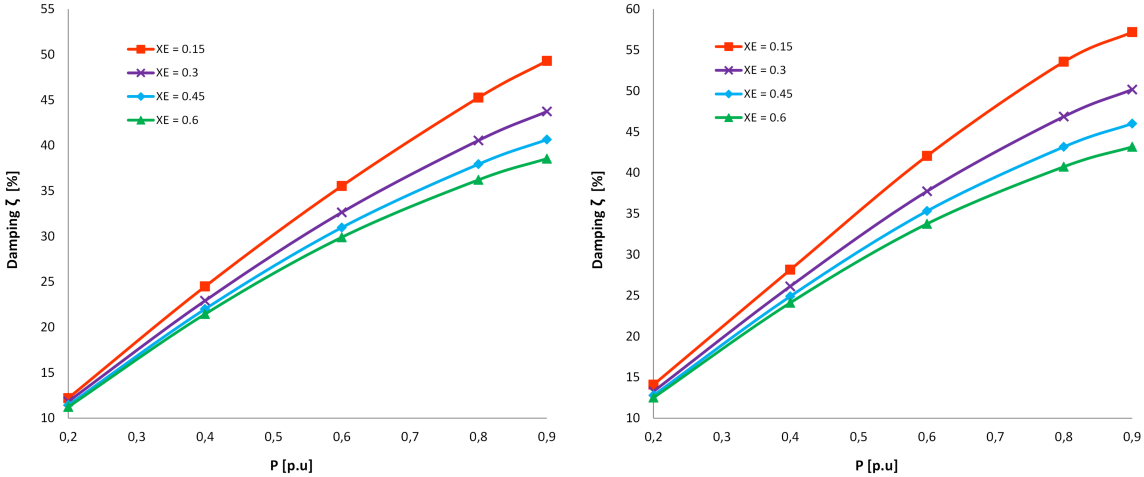

Fig. 3.6 Sensitivity of Local Mode Damping. *Left*: Method 1. *Right*: Method 2

- As the external reactance increases (the external system becomes weaker) the damping of the local mode of oscillation decreases, also the frequency of it as is shown in Fig. 3.7.
- As the active power increases the damping of the local mode of oscillation increases, however the opposite occurs when the magnitude of the reactive power increases.
- For the analyzed case with $Q = 0.1$ p.u, the minimum damping of the local mode is never less than 10% which can be considered a sufficient level of damping to do not put on risk the stability of the system in all operating conditions. As the reactive power increases, the minimum damping slightly decreases.
- For an undercompensation of $-15°$, it is observed that the *Method 1* gives smaller damping, however as the undercompensation decreases or θ_{pss} increases, the *Method 2* becomes the method giving smaller damping.
- It can be seen from Fig. 3.7 that if the reactive power increases the local mode has higher frequencies for strong power systems, X_E up to 0.4 p.u approximately and smaller frequencies for weak power systems, X_E higher than 0.4 p.u.
- As a general comment, it was observed during the simulations that, the average delta damping gain when adding the PSS is higher with the static exciter than with the rotating exciter.

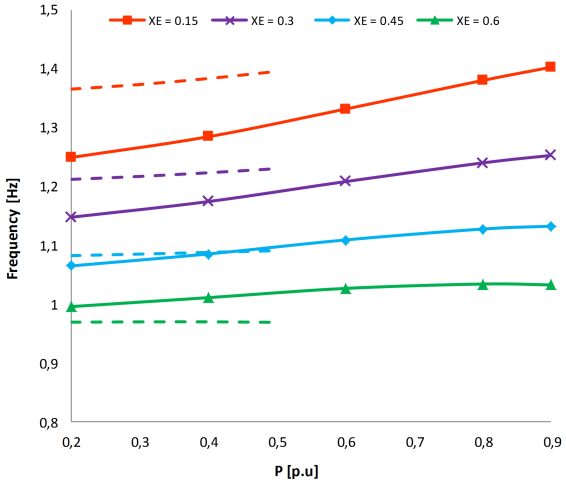

Fig. 3.7 Local Oscillation Mode. *Solid*: $Q = 0.1$. *Dashed*: $Q = 0.5$

3.5.2 Tuning for a Different Oscillation Frequency

Now, to examine the case when the PSS is tuned for a frequency different than the natural local mode of oscillation, a frequency of 0.5 Hz is chosen. The system phase lag at that frequency is $-70.15°$, the objective system phase at that frequency is set to $-15°$ and as a result, $\theta_{pss} = 55.15°$. In Table 3.2 the obtained parameters using both ways of lead lag filters tuning presented in section 3.2 are summarized. Similarly to the previous case, the gain K_{s1} is tuned using the root locus plot and a value of 25 p.u is chosen for both cases in order to be able to compare the results.

Table 3.2: PSS Parameters - Tuning for Different Oscillation Frequency

	Parameter								
	$\mathbf{T_{n1}}$	$\mathbf{T_{d2}}$	$\mathbf{T_{n3}}$	$\mathbf{T_{d4}}$	$\mathbf{T_{n10}}$	$\mathbf{T_{d11}}$	$\mathbf{K_{s1}}$	$\mathbf{T_{w1}}$	$\mathbf{T_6}$
Method 1	0.5254	0.1929	0.5254	0.1929	1	1	25	7	0
Method 2	0.7657	0.2657	0.7657	0.2657	1	1	25	7	0

The phase compensation provided by the PSS with both tuning methods is presented in Fig. 3.8 through the Bode diagram of the lead lag filters. Observe that at 0.5 Hz in both cases the phase provided is $55°$ as expected. However, the phase compensation at the local mode frequency differs about $7°$.

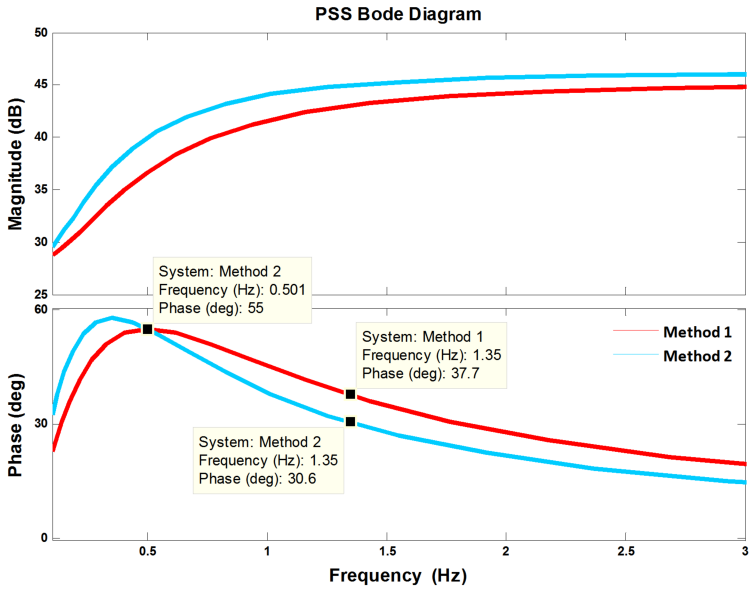

Fig. 3.8 PSS Bode Diagram - Tuning for Different Oscillation Frequency

The sensitivity of local mode damping to changes in the system operating point is shown in Fig. 3.9 where a constant value of reactive power was assumed $Q = 0.1$ p.u. What is observed in this case is:

- As the external reactance increases (the external system becomes weaker) the damping of the local mode of oscillation also increases. This result is expected since weak external power systems have natural local oscillation modes of lower frequencies and the PSS was tuned for lower frequency therefore it provides better compensation in lower frequency range and consequently better damping.

- Comparing with the first tuning case, the reached level of damping for low active power values is higher in this tuning case, but for medium and high generator load better damping results are obtained when the tuning is performed for the local oscillation mode.

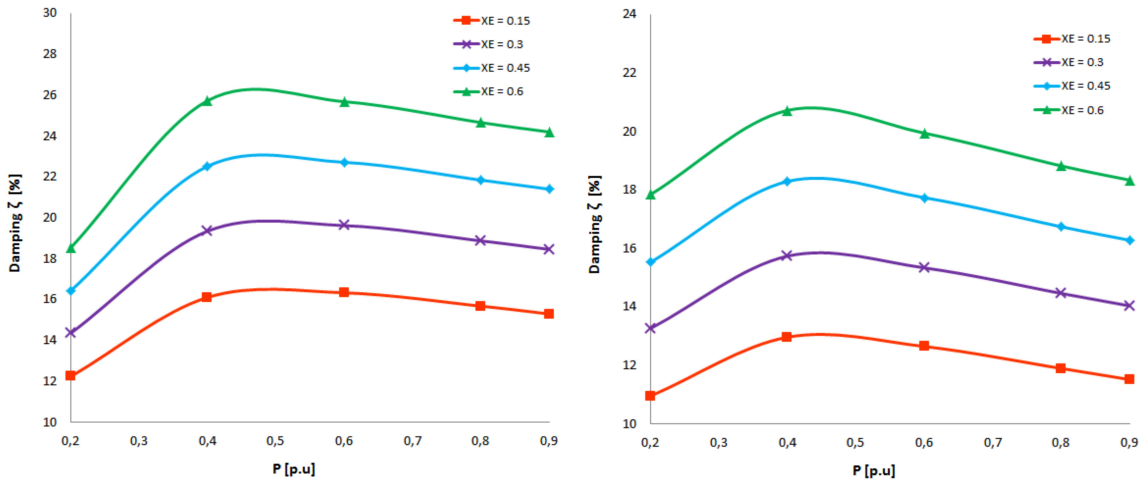

Fig. 3.9 Sensitivity of Local Mode Damping. *Left*: Method 1. *Right*: Method 2

Through the Bode diagram of the system, from the excitation system input to the electrical torque, that is presented in Fig. 3.10, without and with compensation, it is possible to observe the difference in the phase compensation provided by the PSS in the analyzed tuning cases. It is noticed that when the tuning is done for the specific frequency of 0.5 Hz, phase lead can occur at low frequencies causing deterioration of the synchronizing torque. Therefore, the tuning algorithm would have to be improved in order to handle this situation. In addition, it is seen that the phase compensation after 0.5 Hz is obviously reduced affecting the damping of the natural local modes. Particularly, at 1.34 Hz the reached phase values are about $-46°$ with the Method 1 and about $-53°$ with the Method 2.

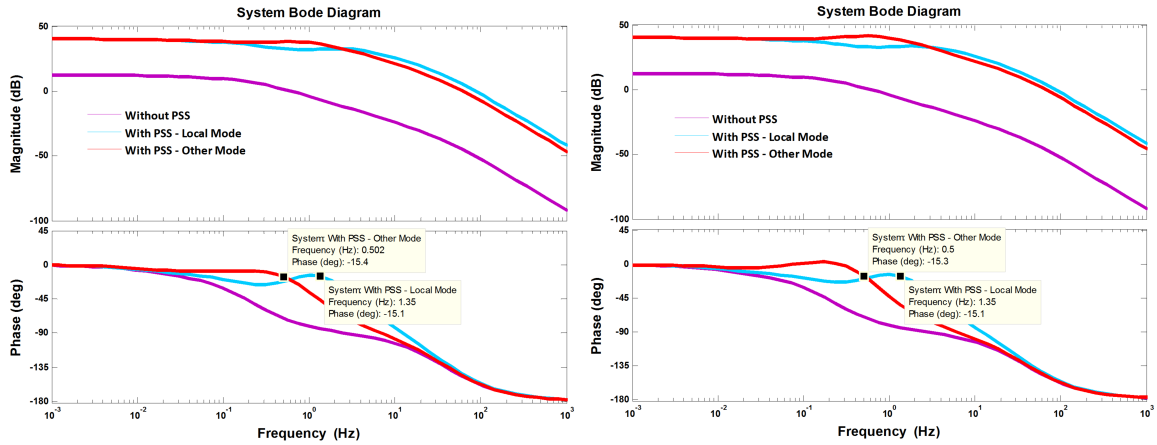

Fig. 3.10 System Bode Diagram. *Left*: Method 1. *Right*: Method 2

3.6 PSS Tuning Performance Evaluation

In this final section the results of time domain simulations of the SM-IB system when disturbances are applied are presented. Different cases are analyzed using the models presented in Chapter 2. Again the analysis is done for static exciter.

3.6.1 PSS Gain Sensitivity

The PSS performance with Method 1 tuning for local oscillation mode presented in Subsection 3.5.1 is evaluated using the complete model of the system which is not linearized. In this case, the order of the model described in Section 2.1 is reduced neglecting the stator flux and transmission network current dynamics, and also the effect of changes in speed in the stator voltage equations. The assumptions are made to facilitate the understanding of the electromechanical dynamics in the system [5].

According to the sensitivity analysis, an interesting operation point to perform the simulations is: weak external power system $X_E = 0.6$ p.u, generator active power $P = 0.4$ p.u and reactive power $Q = 0.4$ p.u since at these conditions low level of damping may be presented. The disturbances are steps of 15% in the voltage reference and in the mechanical torque, which are applied at 2 s of the simulation. Different values of the PSS gain are tested. The results are presented as follows.

Voltage Reference Step

The rotor angle speed and terminal voltage response are shown in Fig. 3.11. In Fig. 3.12 is presented the control action which is the output signal of the PSS.

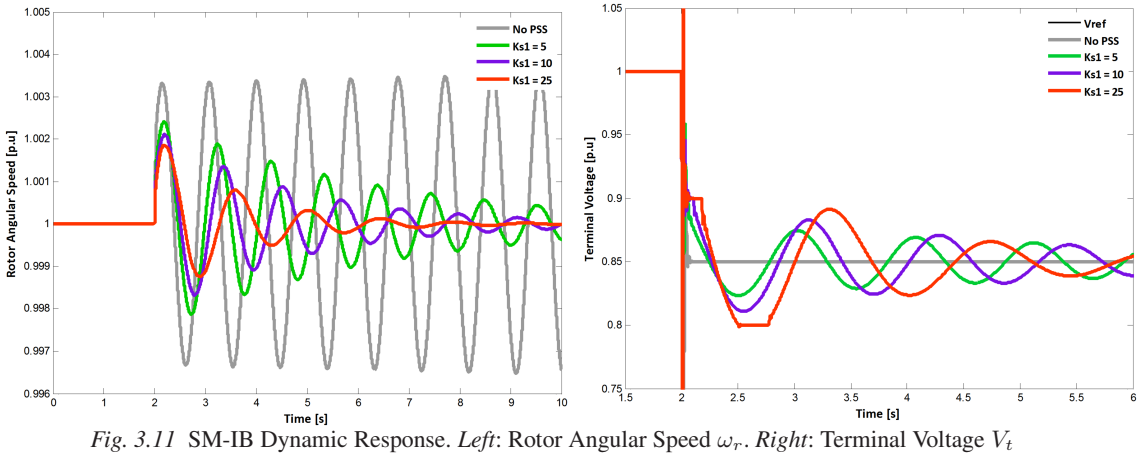

Fig. 3.11 SM-IB Dynamic Response. *Left*: Rotor Angular Speed ω_r. *Right*: Terminal Voltage V_t

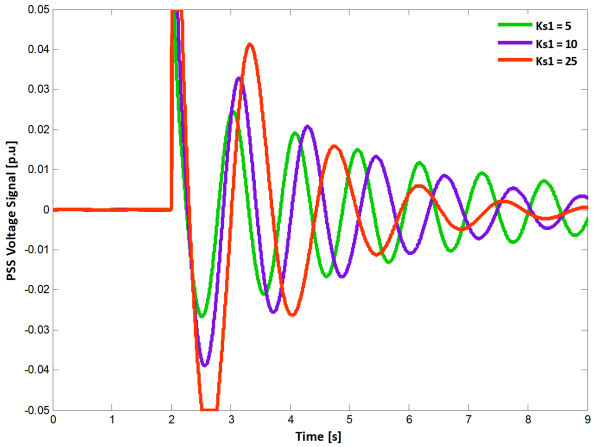

Fig. 3.12 Control Action - PSS Output Signal V_{pss}

Mechanical Torque Step

The rotor angle speed and electrical torque response are shown in Fig. 3.13. In Fig. 3.14 is presented the control action which is the output signal of the PSS.

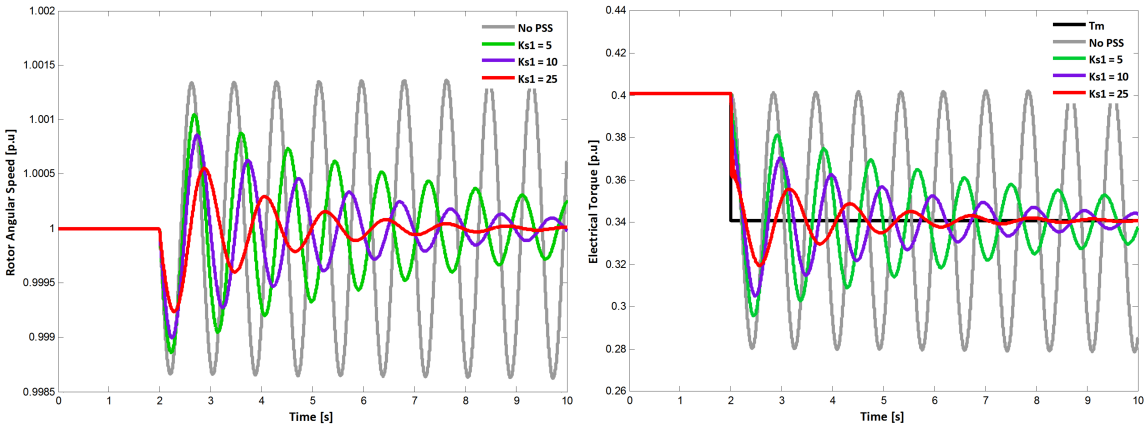

Fig. 3.13 SM-IB Dynamic Response. *Left*: Rotor Angular Speed ω_r. *Right*: Electrical Torque T_e

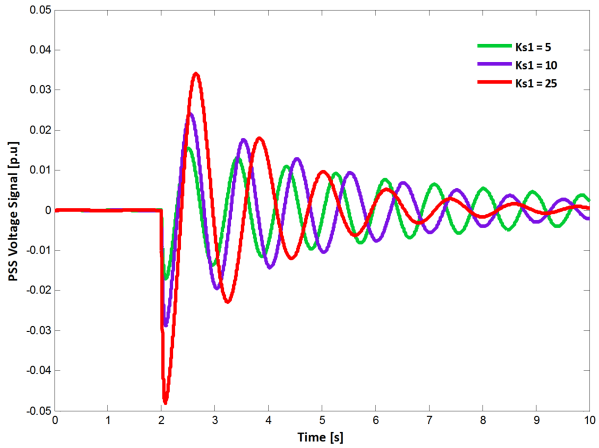

Fig. 3.14 Control Action - PSS Output Signal V_{pss}

The main conclusions from the simulations results are:

- The PSS tuning obtained using the transient linearized model of the system works adequately to damp out the oscillation created by the disturbance in the system model that is not linearized.
- The industry practice of a conservative design of the PSS gain is validated since reducing drastically the gain affects the performance of the controller but not in a critical way. The oscillation takes few seconds more to disappear but they are acceptable if the objective is to protect the system from a instability produced by high gains. Also reducing the gain, the PSS control action does not have to be limited.
- It is observed that without PSS, the disturbance applied drives the system to the be almost critically stable since the magnitude of the created oscillation remains constant with time, therefore the PSS is definitely needed.
- In the case of the step in the voltage reference, the terminal voltage response is influenced by the fact that the output signal of the PSS is limited in the first swing for the three test gain values. In the highest gain case, the AVR also reaches its limits.
- The control action when the step is applied to the mechanical torque is less severe than in the case of step in the voltage reference, however the damping results are good.

3.6.2 Impact of Tuning Operation Point

In this case, the impact of tuning operation point is evaluated in the linearized transient model. The linearized model is chosen to observe also the impact of the linearization in time domain simulations. The Method 1 tunings from Subsections 3.5.1 and 3.5.2 are used but changing the PSS gain to $K_{s1} = 10$ in both

cases. The simulation is performed in the same operation point ($X_E = 0.6$ p.u, $P = 0.4$ p.u, $Q = 0.4$ p.u) and a mechanical torque step of 15% is applied. The rotor angle speed and electrical torque response are shown in Fig. 3.15. In Fig. 3.16 are presented the terminal voltage and the PSS control action.

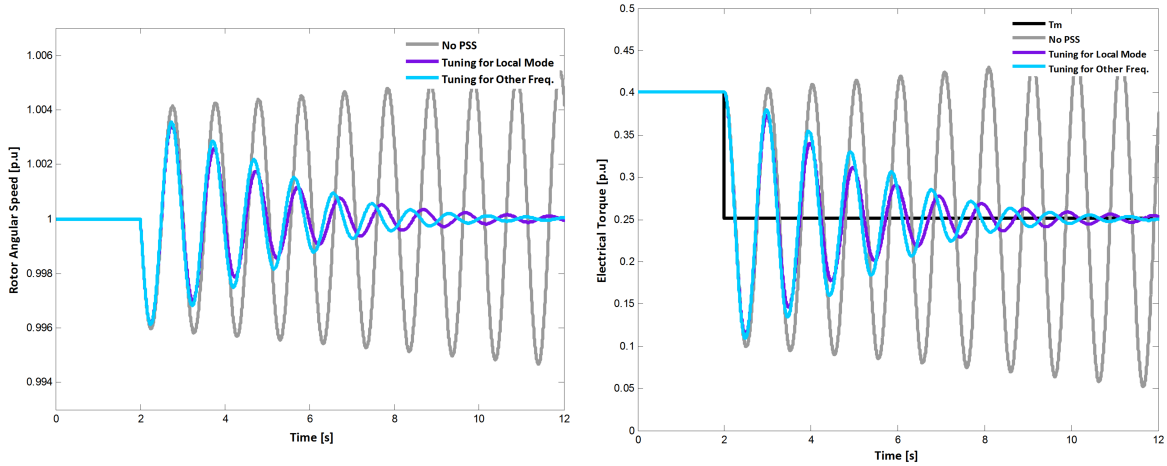

Fig. 3.15 SM-IB Dynamic Response. *Left*: Rotor Angular Speed ω_r. *Right*: Electrical Torque T_e

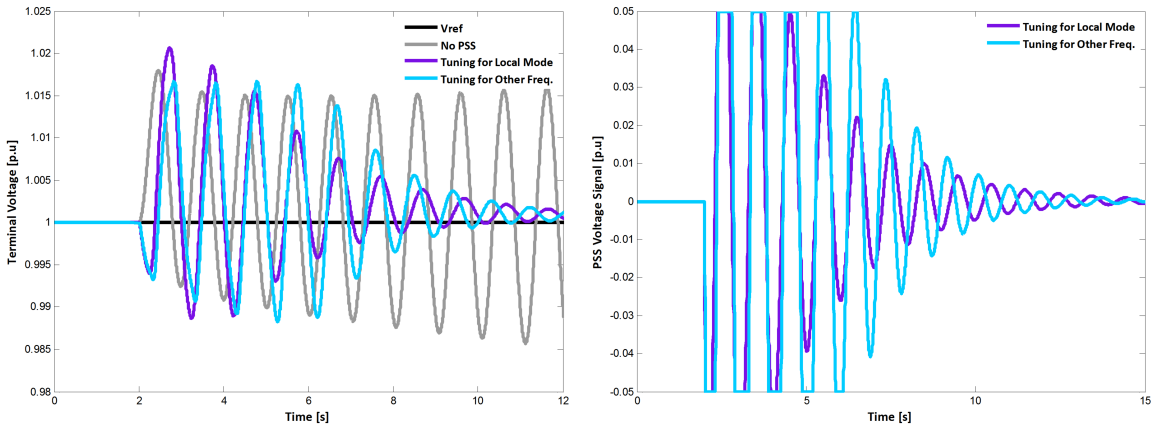

Fig. 3.16 SM-IB Dynamic Response. *Left*: Terminal Voltage V_t. *Right*:PSS Output Signal V_{pss}

It is important to have in mind that an step of 15% is a big disturbance for the linearized model, however it was applied to it with the aim to compare the models results. The main conclusions from the simulations results are:

- Both PSS tunings work adequately to damp out the oscillation. At the tested operation point, the oscillation that is triggered with the disturbance has a frequency about 1.01 Hz. At that frequency, it is observed from the Bode diagram presented in Fig. 3.17 that the compensated system has an under-compensation of $6.87°$ and of $28.2°$ with the two analized tuning cases. Slightly better performance is observed with the tuning made for local oscillation mode, also in that case the control action is less severe. According to the sensitivity analysis, at the test operation point, both tunings should provide similar level of damping, however the better performance of the tuning for the local mode could be explained due to the $20°$ compensation difference. Finally, it is important to remember that both tunings were performed for frequencies different than 1.01 Hz.

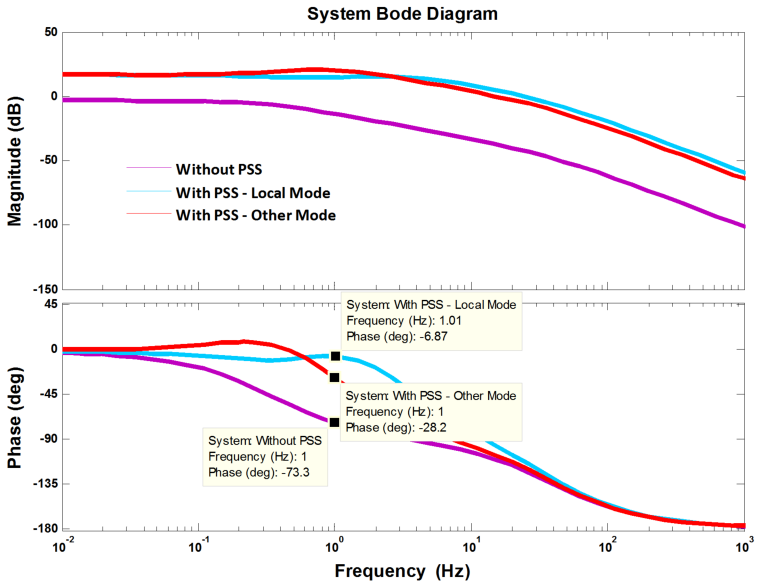

Fig. 3.17 System Bode Diagram

- Comparing Fig. 3.15 with Fig. 3.13, it is noticed that the linearization has an impact in the gain of the system, this can be seen from the magnitude difference in the variables dynamic response. In addition, from the rotor speed simulations with *No PSS* in both cases, it can be observed that the linearization also decreases the oscillation frequency of the response. Despite of this fact, the PSS shows to be robust enough to handle with the simplification of being tuned using a linearized model.
- In the linearized model simulation also appears that without PSS the system is inherently unstable under the level of disturbance applied.

Chapter 4

Control Structure Based on Signal Estimation

Nowadays, POD for inter-area oscillation modes in power systems is also achieved through FACTS controllers. The conventional control strategy for FACTS to provide POD is similar to the one used for the generator, using a cascade of washout and lead lag filters [3]. However, the PSS limitations, like the fact that its good performance is limited to an operating point and that it is conceptually built to provide local stabilization, are also valid in this case. In addition, the slow response of the washout filters causes a slow response for the FACTS control system. Consequently, other control structures are being investigated and implemented to control FACTS in order to provide a proper injection of active and reactive power to the grid, that allows to obtain electromechanical oscillations damping [3], [6], [17]. Those other control structures are based on signal estimation theory. Low-pass filter based and recursive least square based estimation methods to extract the oscillatory component of a signal were used and reported in [3], [17] and [5] to control FACTS achieving POD successfully.

Despite the fact that PSS has shown good performance to damp out local oscillation modes through the excitation system of a synchronous generator which is connected to an infinite bus, the same idea that has been used to damp oscillations with FACTS will be used in this work to define an alternative controller for the generator. In this chapter the controller, which is based on a low-pass filter based signal estimation algorithm and it is also applied to the excitation system, will be tested again using a SM-IB system. No reference has been found in the literature of such a kind of controller used in the synchronous generator to replace the PSS action.

4.1 LPF Based Estimation Algorithm

A signal estimation method based on low-pass filters is described in this section. The method was proposed in [3] to separate the average and oscillatory component of a power signal; the extracted power oscillation component was used to define the reactance reference for a TCSC in order to damp low frequency oscillations in the power system. In [2] is presented the single-phase implementation of the estimation algorithm which consider a single-phase signal as input signal. In this work, the single phase implementation considering as input signal the generator rotor angular speed change $\Delta\omega_r$ will be used.

According to [3], [2] and [5], where the algorithm is clearly explained, the input signal can be defined as to have an average and an oscillatory component as:

$$\Delta\omega_r(t) = \Delta\omega_{r0}(t) + \Delta\omega_{rosc}(t) \tag{4.1}$$

The oscillatory component is defined as:

$$\Delta\omega_{rosc}(t) = Re[\Delta\underline{\omega}_{rph}(t)e^{j\theta_{osc}(t)}] = \Delta\omega_{rph}(t)\cos(\omega_{osc}t + \varphi(t)) \tag{4.2}$$

And it can be rewritten as:

$$\Delta\omega_{rosc}(t) = \frac{1}{2}\Delta\underline{\omega}_{rph}(t)e^{j\theta_{osc}(t)} + \frac{1}{2}\Delta\underline{\omega}^*_{rph}(t)e^{-j\theta_{osc}(t)} \tag{4.3}$$

Where, $\Delta\omega_{rph}, \omega_{osc}$ and φ are the amplitude, angular frequency and phase of the oscillatory component respectively. $\Delta\underline{\omega}_{rph} = \Delta\omega_{rph}e^{j\varphi}$ is the complex phasor of the oscillatory component and $\theta_{osc}(t) = \omega_{osc}t$ is the oscillation angle.

Inserting (4.3) in (4.1) and solving for the complex phasor:

$$\Delta\underline{\omega}_{rph}(t) = [2(\Delta\omega_{rosc}(t) - \Delta\omega_{r0}(t)) - \Delta\underline{\omega}^*_{rph}(t)e^{-j\theta_{osc}}(t)]e^{-j\theta_{osc}(t)} \tag{4.4}$$

Therefore, the estimation algorithm is defined applying low-pass filtering to (4.1) and (4.4) to obtain the estimate for the average and the complex phasor of the input signal as is showed in the following equations, where H_0 and H_{ph} are the low-pass filter functions [3], [2], [5]:

$$\Delta\hat{\omega}_{r0}(t) = H_0\{\Delta\omega_r(t) - \Delta\hat{\omega}_{rosc}(t)\} \tag{4.5}$$

$$\Delta\underline{\hat{\omega}}_{rph}(t) = H_{ph}\{[2(\Delta\omega_r(t) - \Delta\hat{\omega}_{r0}(t)) - \Delta\underline{\hat{\omega}}^*_{rph}(t)e^{-j\theta_{osc}}(t)]e^{-j\theta_{osc}(t)}\} \tag{4.6}$$

Using the estimate for the phasor in (4.6) and the definition of the oscillatory component in (4.3), the estimate of the last one will be:

$$\Delta\hat{\omega}_{rosc}(t) = \frac{1}{2}\Delta\underline{\hat{\omega}}_{rph}(t)e^{j\theta_{osc}(t)} + \frac{1}{2}\Delta\underline{\hat{\omega}}^*_{rph}(t)e^{-j\theta_{osc}(t)} \tag{4.7}$$

The block diagram of the single-phase estimation algorithm is showed in Fig. 4.1. It is important to mention that even though the algorithm is presented here for generator rotor speed as input signal, any other oscillatory input signal could be applied.

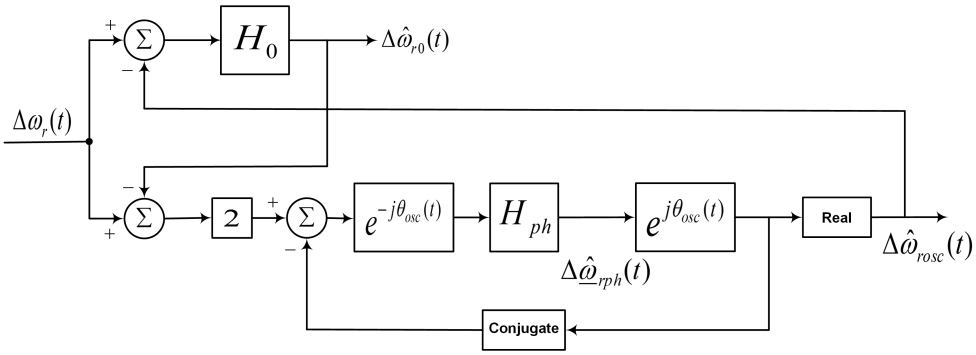

Fig. 4.1 Block Diagram of LPF Based Estimation Algorithm using Generator Rotor Speed Input

The low-pass filter functions H_0 and H_{ph} are defined in Laplace domain as follows. Observe that the same cut-off frequency value is used for both filters, however not necessarily it has to be like that. The important point is the adequate selection of the parameter to be able to separate the average and the oscillatory components. The parameter selection depends on the oscillatory frequency and will be described later in this chapter.

$$H_0(s) = H_{ph}(s) = \frac{\alpha_{LPF}}{s + \alpha_{LPF}} \tag{4.8}$$

Therefore, (4.5) can be rewritten in Laplace domain as:

$$\frac{\Delta\hat{\omega}_{r0}(s)}{\Delta\omega_r(s) - \Delta\hat{\omega}_{rosc}(s)} = \frac{\alpha_{LPF}}{s + \alpha_{LPF}} = H_0(s) \tag{4.9}$$

$$s\Delta\hat{\omega}_{r0} = -\alpha_{LPF}\Delta\hat{\omega}_{r0}(s) - \alpha_{LPF}\Delta\hat{\omega}_{rosc}(s) + \alpha_{LPF}\Delta\omega_r(s) \tag{4.10}$$

And, taken inverse Laplace transform to (4.10), the state space equation of the estimate for the average component is obtained:

$$\frac{d\Delta\hat{\omega}_{r0}(t)}{dt} = -\alpha_{LPF}\Delta\hat{\omega}_{r0}(t) - \alpha_{LPF}\Delta\hat{\omega}_{rosc}(t) + \alpha_{LPF}\Delta\omega_r(t) \tag{4.11}$$

Considering that the estimate oscillating phasor has a real and an imaginary part as:

$$\Delta\underline{\hat{\omega}}_{rph}(t)e^{j\theta_{osc}(t)} = \Delta\hat{\omega}_{rosc}(t) + j\Delta\hat{\omega}_{r\beta}(t) \tag{4.12}$$

Equation 4.6 can also be expressed in Laplace domain as:

$$\Delta\hat{\omega}_{rosc}(s) + j\Delta\hat{\omega}_{r\beta}(s) = \frac{\alpha_{LPF}}{s - j\omega_{osc} + \alpha_{LPF}}[2(\Delta\omega_r(s) - \Delta\hat{\omega}_{r0}(s)) - (\Delta\hat{\omega}_{rosc}(s) - j\Delta\hat{\omega}_{r\beta}(s))] \tag{4.13}$$

Separating the real and imaginary part, the following equations are obtained:

$$s\Delta\hat{\omega}_{rosc}(s) = -2\alpha_{LPF}\Delta\hat{\omega}_{r0}(s) - 2\alpha_{LPF}\Delta\hat{\omega}_{rosc}(s) - \omega_{osc}\Delta\hat{\omega}_{r\beta}(s) + 2\alpha_{LPF}\Delta\omega_r(s) \tag{4.14}$$

$$s\Delta\hat{\omega}_{r\beta}(s) = \omega_{osc}\Delta\hat{\omega}_{rosc}(s) \tag{4.15}$$

Again, taken inverse Laplace transform to (4.14) and (4.15), the state space equations of the estimate for the oscillatory (real) and imaginary components of the complex phasor are obtained:

$$\frac{d\Delta\hat{\omega}_{rosc}(t)}{dt} = -2\alpha_{LPF}\Delta\hat{\omega}_{r0}(t) - 2\alpha_{LPF}\Delta\hat{\omega}_{rosc}(t) - \omega_{osc}\Delta\hat{\omega}_{r\beta}(t) + 2\alpha_{LPF}\Delta\omega_r(t) \tag{4.16}$$

$$\frac{\Delta\hat{\omega}_{r\beta}(t)}{dt} = \omega_{osc}\Delta\hat{\omega}_{rosc}(t) \tag{4.17}$$

Finally, the state space model of the LPF based estimation algorithm is defined by (4.11), (4.16) and (4.17) which in a matrix way is:

$$\frac{d}{dt}\begin{bmatrix} \Delta\hat{\omega}_{r0}(t) \\ \Delta\hat{\omega}_{rosc}(t) \\ \Delta\hat{\omega}_{r\beta}(t) \end{bmatrix} = \begin{bmatrix} -\alpha_{LPF} & -\alpha_{LPF} & 0 \\ -2\alpha_{LPF} & -2\alpha_{LPF} & -\omega_{osc} \\ 0 & \omega_{osc} & 0 \end{bmatrix}\begin{bmatrix} \Delta\hat{\omega}_{r0}(t) \\ \Delta\hat{\omega}_{rosc}(t) \\ \Delta\hat{\omega}_{r\beta}(t) \end{bmatrix} + \begin{bmatrix} \alpha_{LPF} \\ 2\alpha_{LPF} \\ 0 \end{bmatrix}\Delta\omega_r(t) \tag{4.18}$$

The characteristic frequency response of the algorithm from the input signal to the estimated oscillatory component is presented in the Bode diagram of Fig. 4.2. The response also depends on the parameters α_{LPF} and ω_{osc} whose selection will be explained in the next section.

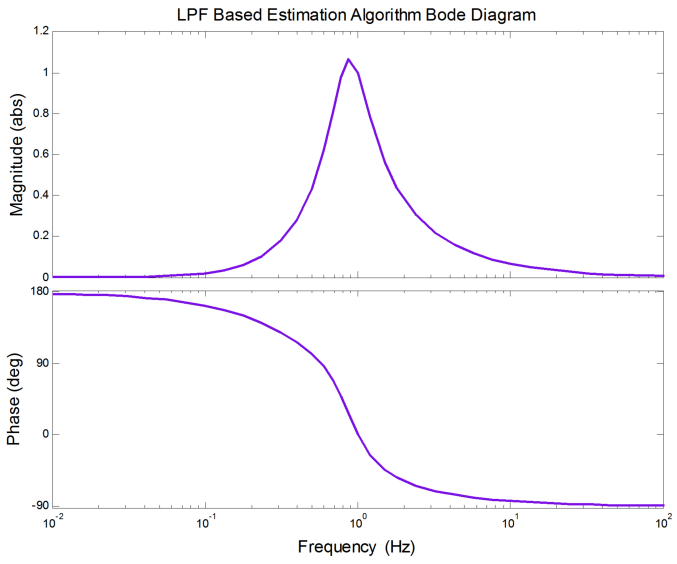

Fig. 4.2 Bode Diagram from $\Delta\omega_r(t)$ to $\Delta\hat{\omega}_{rosc}(t)$

4.2 Controller Applied to the Synchronous Generator

Basically, using a LPF based estimation algorithm, the oscillatory component of the generator rotor speed deviation when an oscillation mode appears is extracted and, adding a phase shift (as with the lead lag filters in the PSS) that oscillatory component can be applied to the summing input point of the AVR (as with the PSS) to produce an electrical torque component in phase with the rotor speed deviation.

The phase compensation is done separating the magnitude and angle of the complex phasor $\Delta\underline{\hat{\omega}}_{rph}(t)$ and adding a phase shift θ_{est} as is shown in Fig. 4.3. The magnitude remains unchanged while the phase is shifted to compensate the phase lag in the generator. Then, the real part of the estimate oscillating compensated phasor $\Delta\underline{\hat{\omega}}_{rph,com}(t)e^{j\theta_{osc}(t)}$ is the compensated oscillatory component $\Delta\underline{\hat{\omega}}_{rosc,com}(t)$ of the input signal.

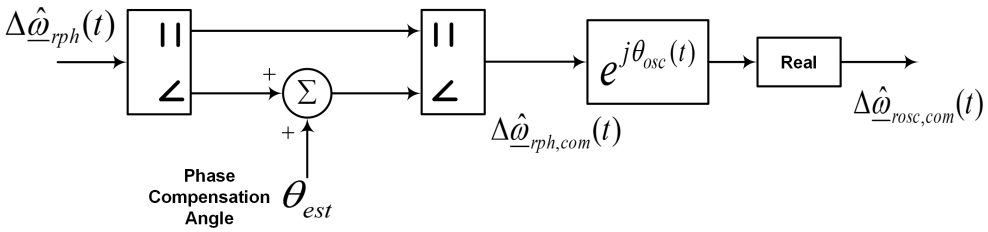

Fig. 4.3 Block Diagram of Phase Compensation of the Complex Phasor

Consequently, the complete structure of the controller based on signal estimation, which will be called from now on as *Phasor POD Controller*, is shown in the block diagram of Fig. 4.4. As in the PSS, the gain K_{est} allows to determine the level of damping provided by the controller and the limiter allows to keep the controller output voltage V_{est} within an appropriate range of values to be added to the voltage error in the AVR. A general block diagram of the controlled system is presented in Fig. 4.5 where the feedback damping controller is applied to the synchronous generator. And the effect of the phase shift and gain can be seen through the Bode diagram of the algorithm in Fig. 4.6.

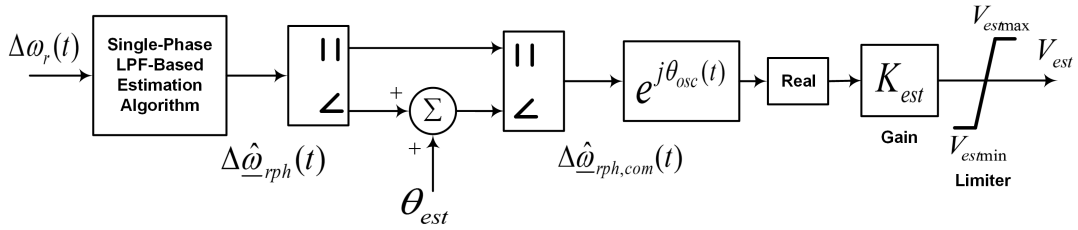

Fig. 4.4 Block Diagram of Damping Controller Based on Signal Estimation

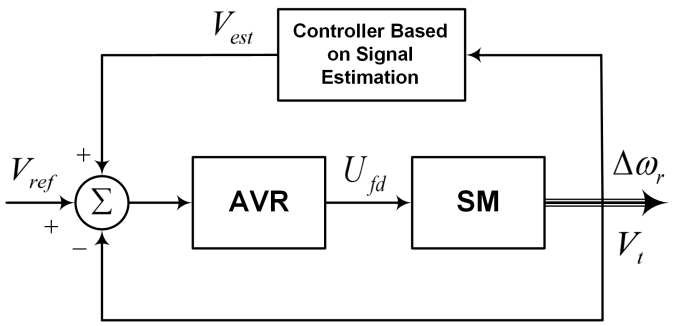

Fig. 4.5 General Block Diagram of Damping Controller Closed Loop with the Synchronous Machine

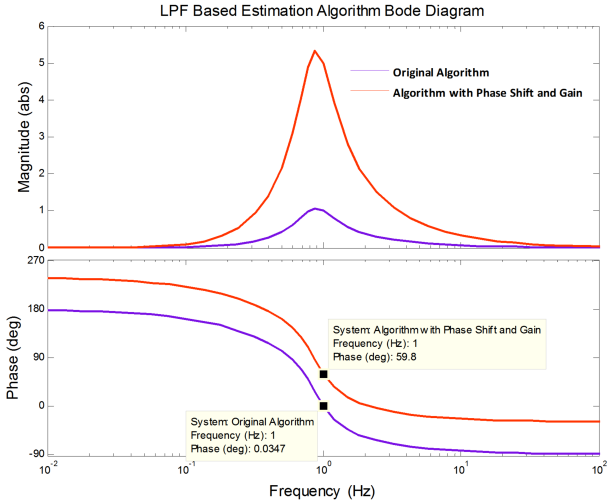

Fig. 4.6 Bode Diagram from $\Delta\omega_r(t)$ to $\Delta\hat{\omega}_{rosc}(t)$ with Phase Shift and Gain

From Fig. 4.6 it can be seen that for an oscillation frequency of 1 Hz ($\omega_{osc} = 2\pi$), the phase of the oscillatory component in the original algorithm is approximately $0°$ and the gain is 1 p.u. For the same oscillation frequency, setting $K_{est} = 5$ p.u and $\theta_{est} = 60°$, it is observed how the gain and phase characteristic are modified. The performance of the controller when it is applied to the generator to damp local oscillation modes is influenced by the parameters tuning that will be presented as follows.

4.2.1 Parameters Selection

Oscillation Frequency $\omega_{\mathbf{osc}}$

The frequency of the oscillation presented in the SM-IB system when a disturbance is applied needs to be well known in order to tune the controller. From the eigenvalue analysis of the linearized system this frequency can be obtained and represents the local oscillation mode.

LPF Cut-off Frequency $\alpha_{\mathbf{LPF}}$

The cut-off frequency α_{LPF} of the low-pass filters H_0 and H_{ph} must be smaller than the oscillation frequency ω_{osc} in order to be able to separate the average and oscillatory components of the input signal [5]. In [3] is recommended that α_{LPF} should be about 0.2-0.5 times ω_{osc}. In [5] is proved that for α_{LPF} larger than 0.4 times ω_{osc}, the dynamic performance of the estimator starts to decrease; it is also mentioned that typically α_{LPF} is selected to be 0.1 times ω_{osc}. The effect of different values of α_{LPF} in the frequency response of the estimator is presented in Fig. 4.7 which is calculated using an oscillation frequency of 1 Hz.

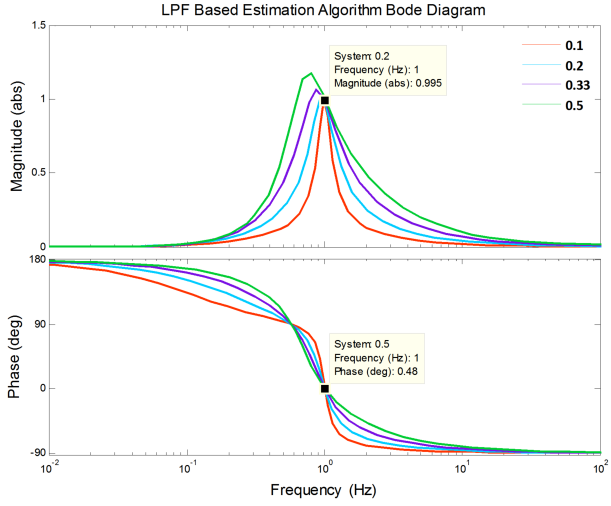

Fig. 4.7 Bode Diagram from $\Delta\omega_r(t)$ to $\Delta\hat{\omega}_{rosc}(t)$. Sensitivity to α_{LPF}

Setting α_{LPF} to 0.1 times ω_{osc} the algorithm gives the best frequency selectivity but the estimation can be slow, on the contrary, when it is 0.5 times ω_{osc} the possibility of not extracting the right frequency is increased (the selectivity is deteriorated) even a faster estimation can be achieved. In this case, it is also observed from the magnitude diagram that if another oscillation frequency different than the frequency of interest appears, it could be amplified. Therefore, the selection of the cut-off frequency should be done considering an acceptable compromise among the mentioned factors.

Compensation Angle $\theta_{\mathbf{est}}$

θ_{est}, given in degrees, is the angle that the controller should compensate at the oscillation frequency ω_{osc}. This angle depends on the selected objective system phase at ω_{osc} as was discussed in Section 3.2.

Controller Gain $\mathbf{K_{est}}$

The gain will be set in such a way that a fair comparison can be made between the Phasor POD controller and the PSS. Through the Bode diagram, it will be confirmed that at the analyzed oscillation frequency, both controllers have the same gain. An example for an oscillation frequency of 1 Hz is shown in Fig. 4.8 where the gain of the controller should be tuned about 11 p.u in order to be able to compare the level of damping that both controllers can provide for the oscillation mode.

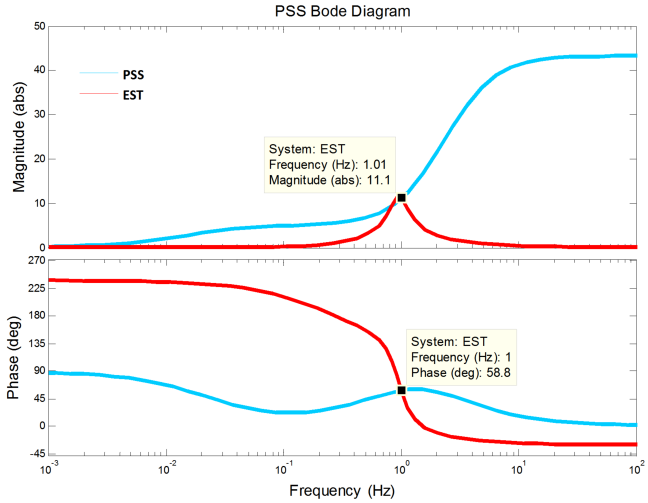

Fig. 4.8 PSS and Phasor POD Controller Bode Diagrams

4.3 Simulations Results

In this section the results of time domain simulations of the SM-IB system when a disturbance is applied are presented. Different cases are analyzed using the presented models. As in the PSS performance evaluation, the analysis is carried out for static exciter.

4.3.1 With Complete Model

The Phasor POD controller performance is verified using the complete model of the system. In this case, the order of the model described in Section 2.1 is reduced neglecting the stator flux and transmission network current dynamics, and also the effect of changes in speed in the stator voltage equations. The assumptions are made to facilitate the understanding of the electromechanical dynamics in the system [5].

The Phasor POD controller is tuned for the same operation point used to tune the PSS, which consider a strong external power system $X_E = 0.2$ p.u and high load for the synchronous generator where $P = 0.9$ p.u and $Q = 0.1$ p.u. In that point, the local oscillation mode appears at a frequency of 1.348 Hz and the system phase lag at the oscillation frequency is $-84.05°$. The objective system phase at that frequency is set to $-15°$. The parameter selection is summarized in Table 4.1.

Table 4.1: Phasor POD Controller Parameters

Parameter	Value	Unit
$\mathbf{f_{osc}}$	1.348	Hz
$\alpha_{\mathbf{LPF}}$	$0.2(2\pi f_{osc})$	rad/s
$\theta_{\mathbf{est}}$	69.05	deg
$\mathbf{K_{est}}$	5	p.u

The value of the controller gain K_{est} being tuned as was explained in Subsection 4.2.1 should be set to 18 p.u, however the best results are obtained when the gain take a reduced value of 5 p.u. On the other hand, the simulations are performed in the same tuning operation point. The applied disturbance is a step of 15% in the voltage reference of the AVR at 2 s of the simulation. The results are presented in Fig. 4.9 and Fig. 4.10 and include a simulation using the PSS for comparison. The PSS is tuned as it was presented in Subsection 3.5.1 with a gain $K_{pss} = 5$ p.u.

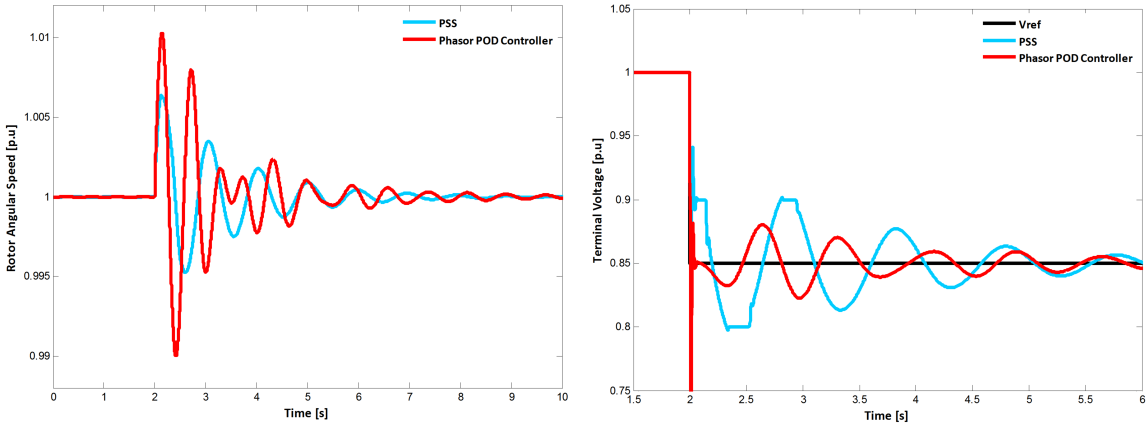

Fig. 4.9 SM-IB Dynamic Response. *Left*: Rotor Angular Speed ω_r. *Right*: Terminal Voltage V_t

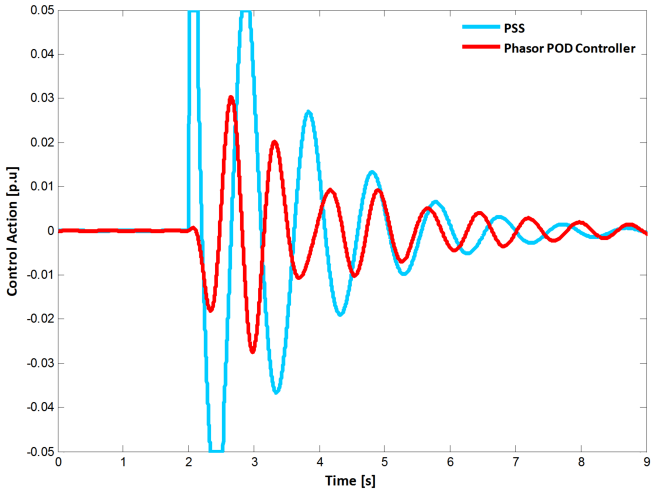

Fig. 4.10 Control Action - PSS V_{pss} and Phasor POD Controller V_{est} Output Signals

The time needed to damp the oscillation created by the disturbance is approximately the same with both controllers, however the control action is significantly lower with the Phasor POD controller than with the PSS. The effect of the control action magnitude can be also observed in the terminal voltage response. Due to the aggressive action of the PSS, the AVR hits its lower and upper limits in the first swings, while with the Phasor POD controller the terminal voltage is less modulated.

4.3.2 With Linear Transient Model

The simulation presented here using the linearized transient model consider the Phasor POD controller tuned to compensate all the phase lag in the synchronous generator, therefore $\theta_{est} = 84.05°$ and a value of $K_{est} = 18$ p.u. The simulation is carried out for the same operation point, with the same PSS tuning and under the same disturbance than in the previous case with the complete model. The results are presented in Fig. 4.11 and Fig. 4.12.

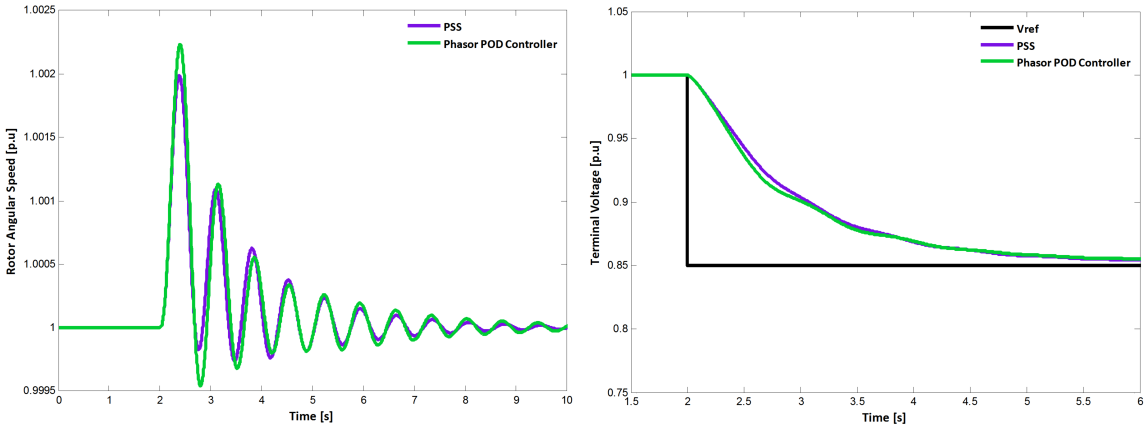

Fig. 4.11 SM-IB Dynamic Response. *Left*: Rotor Angular Speed ω_r. *Right*: Terminal Voltage V_t

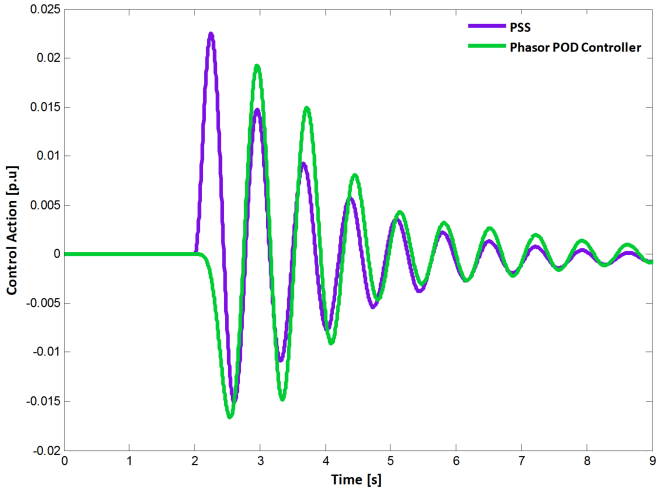

Fig. 4.12 Control Action - PSS V_{pss} and Phasor POD Controller V_{est} Output Signals

The effects of the system linearization were discussed in Subsection 3.6.2, and even this test with linearized model is less realistic, it helps to illustrate the similarities in the system response when using both controllers.

4.4 Critical Comparison - PSS vs. Phasor POD Controller

Finally, the control approach evaluated in this chapter to damp electromechanical oscillations has been widely researched and its advantages demonstrated when it is applied to FACTS. Still more studies are needed in order to be able to compare fairly the performance of the PSS and the Phasor POD controller when it is applied to the synchronous generator. Furthermore, this control approach should be test in a power system model different than the SM-IB model, where it can be possible to reproduce inter-area oscillations modes for which it is well recognized that the PSS effectiveness is not that good as for local oscillations modes. In that case, the benefits of the proposed damping control design could be highlighted.

In Table 4.2 is presented a critical comparison between the PSS and the Phasor POD controller regarding important aspects that determine the performance of a controller.

Table 4.2: Controller Analytical Comparison

	Controller	
	PSS	**Phasor POD**
Response Speed	Generally a *slow speed of action* is presented [18].	The estimation algorithm separates the average and oscillatory component of the input signal with a small time constant, therefore a *fast response* can be achieved.
Phase Compensation	The lead lag filters have a limit in the phase compensation that can be provided per filter due to stability reasons.	No restriction in the phase compensation.
System Order	*Higher order* introduced by the lead lag, washout and low-pass filters, therefore the controller has more poles and zeros. See Fig. 2.6.	*Lower order* since the control structure only needs two low-pass filters. See Fig. 4.4
Tuning	*More parameters* to tune. Require knowledge of the connecting grid. Tuning usually performed for a fixed local oscillation mode achieving good damping performance on it but limiting the performance on different operating points or for different mode frequencies. Classical and advanced methods have been applied.	*Less parameters* to tune also higher robustness due to less parameters. Good performance can be achieved independent of the oscillation frequency value if the oscillation mode is well known and the phase angle to compensate is chosen correctly.
Parameters Adaptation	Usually, the PSS technology nowadays is develop to set a fixed tuning of the parameters.	There are more advanced algorithms with the same principle that make possible to adapt the oscillation frequency and the phase shift in real time. An adaptive version of the controller would lead in a satisfactory action of it in a wider range of operating points.

Chapter 5

PSSVG 1.0 Software Tool

This chapter aims to be a user manual for the PSS tuning software tool PSSVG 1.0 built in Matlab R2011b. The concepts and theoretical background for PSS tuning were presented in Chapters 2 and 3 and should be taken into account in the final decision for the parameters values. The tuning methodology is based on linear control system theory, specifically frequency response techniques are used to define the setting for the lead lag filters time constants and controller gain when the PSS is analyzed on a SM-IB system. The software will be for the use of VG Power AB company, to have an initial tuning during commissioning of the controller in generation power plants. The calculated tuning might be adjusted with field test and the company PSS tuning experience. The tool has implemented the mathematical model of the excitation system provided by VG Power AB giving the option to chose between static and rotating exciters, it is also designed considering the rotor speed change as input signal to the PSS. Finally, detailed explanation is given for the main algorithm which uses the local oscillation mode as oscillation frequency to tune the lead lag filters, additionally the program for tuning the filters at a different oscillation frequency will be briefly described.

5.1 Algorithm Flow Chart

The general algorithm under PSSVG 1.0 is built is presented in Fig. 5.1. The steps are described as follows:

- First, The parameters of the SM-IB, AVR, exciter, and tuning operation point should be input in order to calculate the linear transient model constants of the SM-IB system (see Subsection 2.4.1).
- Second, an eigenvalue analysis of the system without PSS is computed (see Section 3.1) to identify the local oscillation mode of the system at the tuning operation point. In the main algorithm, the tuning is carried out for that oscillation frequency, however there is an alternative algorithm to perform the tuning for a manually input oscillation frequency.
- In the next step, the software computes the phase lag of the system at the specific oscillation frequency. The user should input the objective system phase at the analyzed frequency taking into account the previously calculated phase lag and the discussion presented in Section 3.2.
- According to the phase shift to compensate, the software calculates the lead lag filters time constants and the number of filter required using the two methods of tuning presented in Section 3.2.
- Then, from the root locus plot and considering the recommendations presented in Section 3.3 a gain should be selected by the user.
- The gain and phase margin are calculated by the software to have an idea of the relative stability of the system with the actual tuning.
- Later, the software computes again the phase of the system but now with compensation through the PSS. At the oscillation frequency, the system phase should be the selected one. However depending on the phase characteristic of the system it is important to analyze the phase of the compensated system at different frequencies into the PSS frequency range of interest.

- Finally, an eigenvalue analysis of the system with PSS is computed now to evaluate the level of damping reached with the actual tuning.

- If the obtained results are accepted, the tuning would be the final tuning, if not, the process and analysis should be done again changing the objective system phase at the analyzed frequency and the selected gain. This will be repeated until an acceptable tuning is reached.

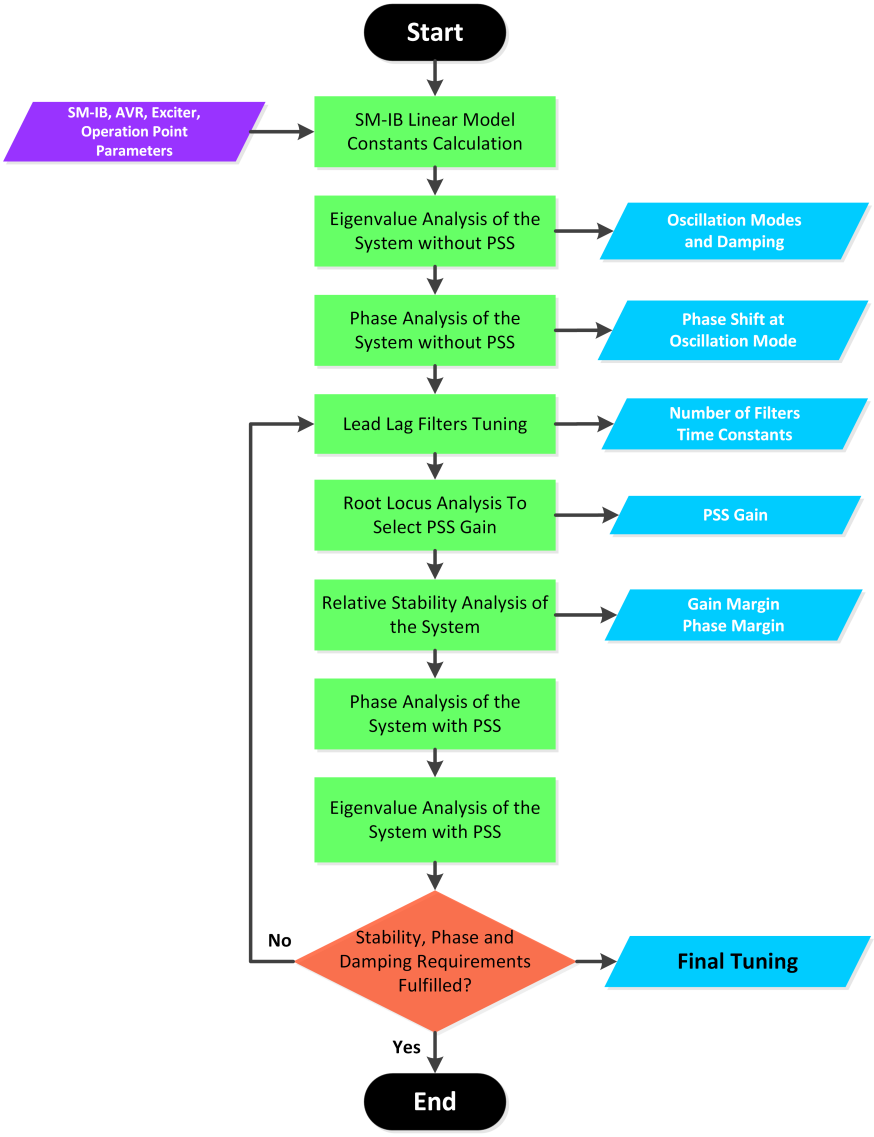

Fig. 5.1 PSS Tuning Algorithm

5.2 Matlab and Simulink Files

A file structure for the main algorithm is presented in Fig. 5.2. A file called **MainProgram** executes three scripts: *SMIBPar*, *SMIBNoPSS* and *SMIBPSS*. **SMIBPar** load the parameters previously input by the user. **SMIBNoPSS** computes the three first algorithm steps by calling the functions: *Ks_VG*, *ModalNoPSS_VG* and *PhaseNoPSS_VG*. ModalNoPSS_VG calls the Simulink model *SM_ExcSys_VG* (see Subsection 2.4.1) and PhaseNoPSS_VG calls the Simulink model *SM_IB_Trans* (see Subsection 2.4.2). The results of SMIBNoPSS are inputs to **SMIBPSS** which executes the rest of the algorithm steps calling the following functions and Simulink models: *FilterTuning_O*, *FilterTuning_M*, *SM_ExcSys_VG_RL* (see Section 3.3), *GPhMargin* (wich calls *SM_ExcSys_VG_M*), *PhasePSS_VG* (which calls *PSS*), *ModalPSS_VG* (which calls *SM_PSS_VG*), *TeCoeff_VG* and *ResFig*.

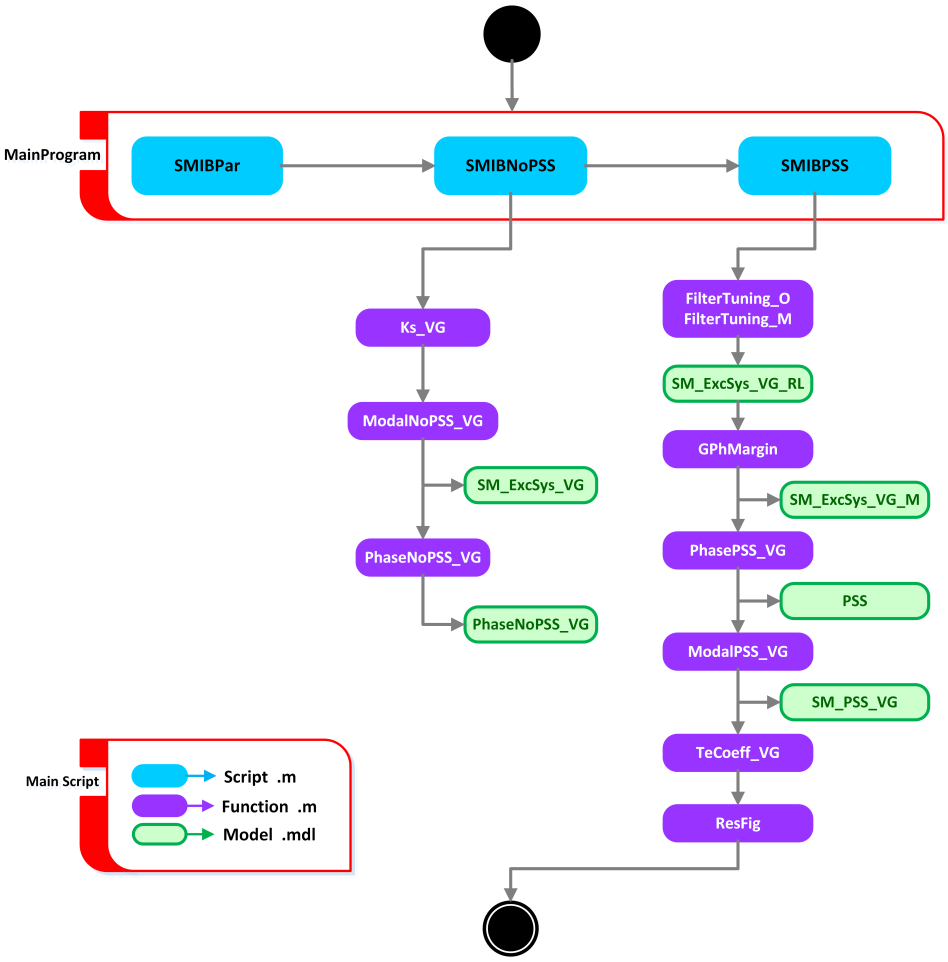

Fig. 5.2 PSSVG 1.0 Files Structure

Simulink block diagram models are masked under a function block as in the example shown in Fig. 5.3 for *SM_ExcSys_VG* model. Giving double click to the block it will display a window with the system parameters. To find the block diagram it is needed to right click the block and select ***"Look Under Mask"*** option. The model will appear in a new window as is presented in Fig. 5.4. In this case, the block *AVR-Exciter* is also masked, the same procedure described before should be done to reach the block diagram of the AVR and exciter model. In general, all Simulink models (.mdl extension) follow the same masked design.

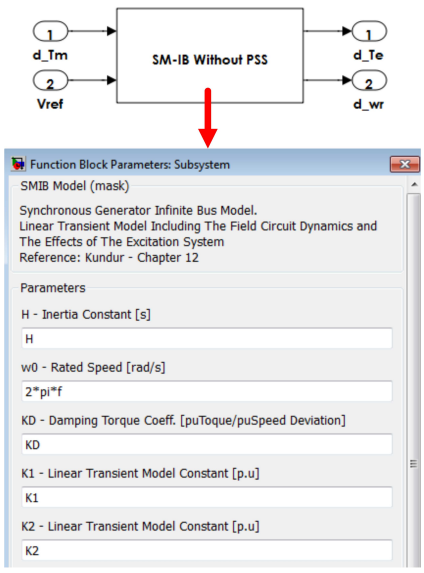

Fig. 5.3 Simulink Models Masked as a Subsystem Function Block

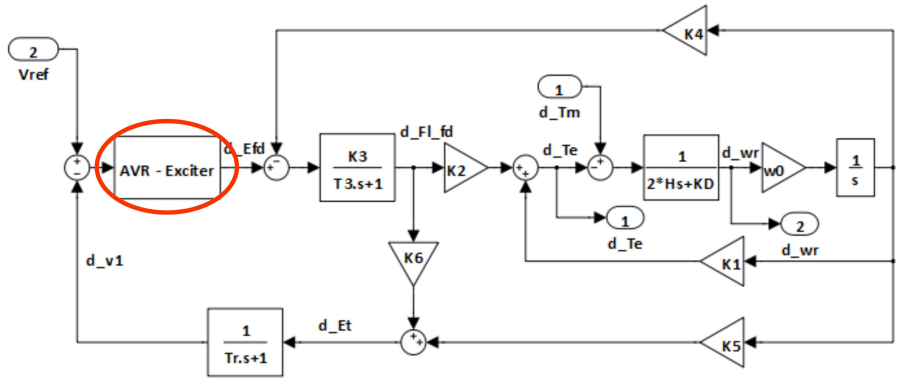

Fig. 5.4 Block Diagram Model Under the Mask

5.3 How to Run a Case

An example step by step about how to run a case for PSS tuning is presented as follows:

1. Open the folder *ModalFrequencyTuning*, where the user can find the main algorithm files.

2. Open the file *SMIBPar* and fill on it the required system parameters. Observe that X_T, X_L, P, Q and the type of exciter are parameters that do not need to be input in the file since they will be asked when the program is running.

3. As is presented in Fig. 5.5, right click to the file *MainProgram* and select the option ***"run"***.

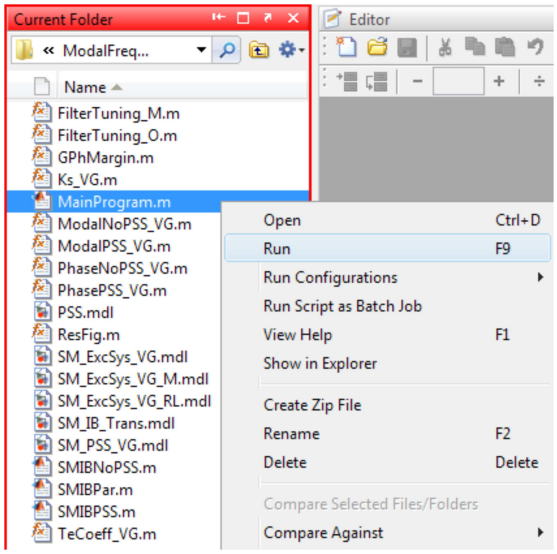

Fig. 5.5 Run the Main Algorithm

4. In the command window, the user is asked to define the tuning operation point and the type of exciter as can be seen in Fig. 5.6.

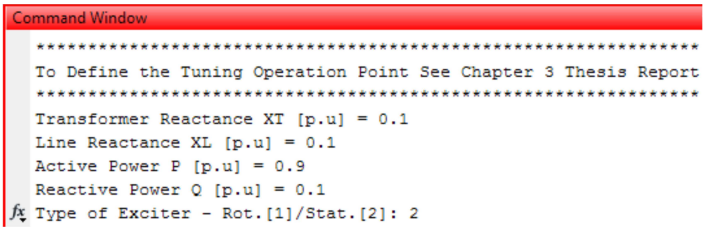

Fig. 5.6 Defining Tuning Operation Point

5. Once the user has input the data, the program display the eigenvalue and phase analysis of the system without PSS and asks the user to input the objective system phase at the analyzed frequency and the lead lag filters tuning type. Then the filters time constants are displayed in the command window.

6. A root locus plot of the system will pop up in a new window as it is shown in Fig. 5.7. The user should analyze the plot and input the selected gain for the PSS in the command window.

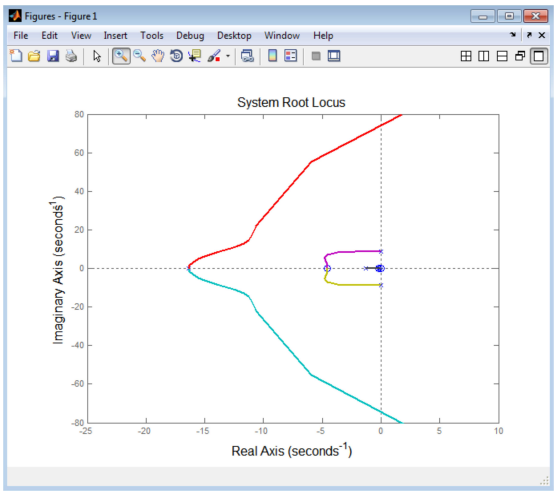

Fig. 5.7 Root Locus Plot Window

7. After the gain has been input, the following results are displayed in the command window:

   - Gain and Phase Margins.
   - System phase limits at the PSS frequency range 0.1 Hz - 3 Hz.
   - Eigenvalue analysis of the system with PSS.
   - Synchronizing and damping torque coefficients at analized oscillation frequency.

8. A group of plots as the PSS Bode diagram, the Bode diagram of the system without PSS and with PSS, the system phase in the frequency range of interest and the system zero-pole map will pop up in several windows as is shown in Fig. 5.8 and Fig. 5.9. These plots help the user to analyze the particular case together with the numerical results.

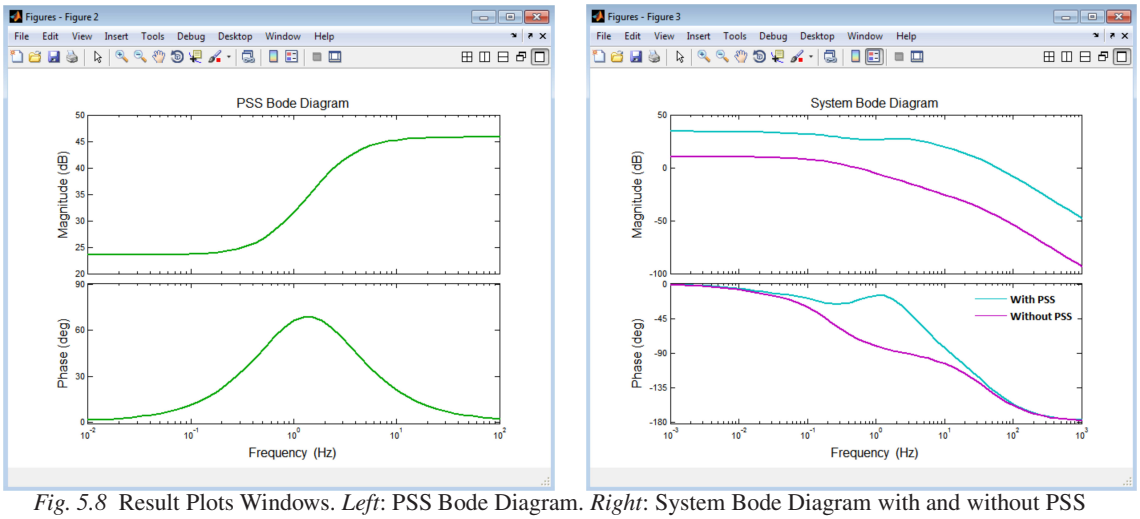

Fig. 5.8 Result Plots Windows. *Left*: PSS Bode Diagram. *Right*: System Bode Diagram with and without PSS

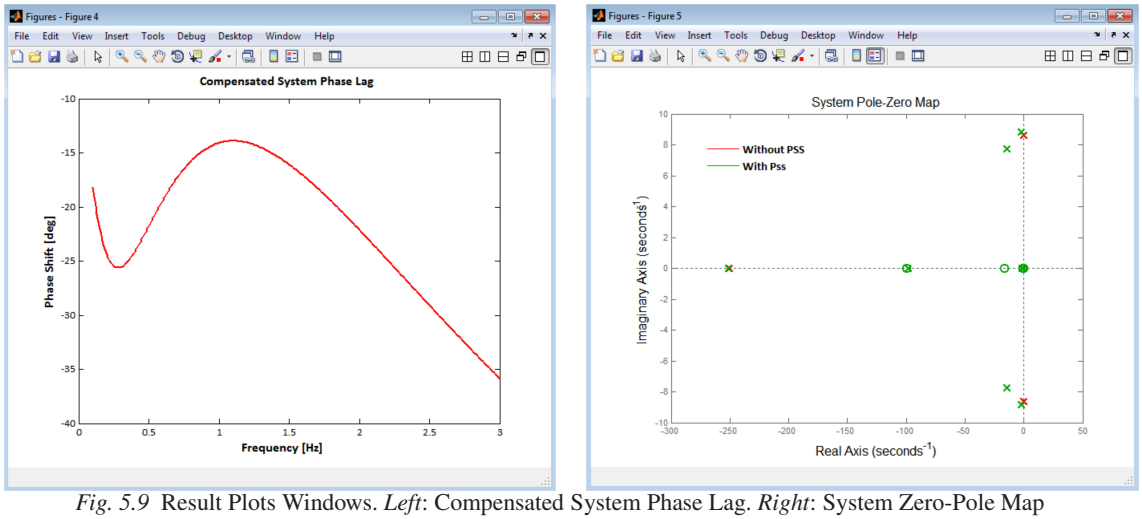

Fig. 5.9 Result Plots Windows. *Left*: Compensated System Phase Lag. *Right*: System Zero-Pole Map

9. At the end, the program asks if the user wants to save the final tuning in a **.mat** file.

10. Finally, after analyzing the results about damping, torque coefficients, phase and gain margins and compensated system phase lag, the user should decide if keep the tuning or change any of the input data to run the process again for a new case.

5.4 Numerical Results in The Command Window

The complete numerical results are display in the command window as is presented in Fig. 5.10. The command window can be printed as a **.pdf** file to generate a separate file with the results.

```
*************************************************************
To Define the Tuning Operation Point See Chapter 3 Thesis Report
*************************************************************
Transformer Reactance XT [p.u] = 0.1
Line Reactance XL [p.u] = 0.1
Active Power P [p.u] = 0.9
Reactive Power Q [p.u] = 0.1
Type of Exciter - Rot.[1]/Stat.[2]: 2
-------------------------------------------------------------
         System Eigenvalues with Damping > 0% & < 5%
-------------------------------------------------------------
 Eigenvalue  Damp.[%]  Freq.[Hz]
    3.0000    0.1942    1.3482
    4.0000    0.1942    1.3482

-------------------------------------------------------------
             System Eigenvalues with Damping > 5%
-------------------------------------------------------------
 Eigenvalue  Damp.[%]  Freq.[Hz]
     1   100      0
     2   100      0
     5   100      0
     6   100      0

-------------------------------------------------------------
    System Phase Lag at Frequency of Critically Damped Mode
-------------------------------------------------------------
 Freq.[Hz] Ph.Shift[deg]
    1.3482  -84.0503

*************************************************************
To Define the Objective System Phase See Chapter 3 Thesis Report
*************************************************************
Objective System Phase at Analyzed Frequency [deg] = -15
Filter Tuning Type - Method 1[O]/Method 2[M]: O
-------------------------------------------------------------
             Phase Shift to Compensate with the PSS
-------------------------------------------------------------
 Ph.Shift[deg]
   69.0503

-------------------------------------------------------------
           PSS Lead Lag Filters Time Constants
-------------------------------------------------------------
    Tn1[s]    Td2[s]    Tn3[s]    Td4[s]    Tn10[s]   Td11[s]
    0.2245    0.0621    0.2245    0.0621    1.0000    1.0000

*************************************************************
To Define the PSS Gain See Chapter 3 Thesis Report
*************************************************************
Input Gain Value Ks1 [p.u] = 10
-------------------------------------------------------------
                      Selected PSS Gain
-------------------------------------------------------------
   Ks1[pu]
    10

-------------------------------------------------------------
             Relative Stability of the System with PSS
-------------------------------------------------------------
  G.Marg[dB] f_G[Hz] Ph.Marg[deg] f_Ph[Hz]
   37.5070   12.4281   73.8975    1.5996

-------------------------------------------------------------
     System Phase Limits at PSS Frequency Range 0.1-3 [Hz]
-------------------------------------------------------------
       Without PSS          With PSS
-------------------------------------------------------------
     Freq   Ph.Shift     Freq    Ph.Shift
     [Hz]    [deg]       [Hz]     [deg]
    3.0000  -90.8737    3.0000  -36.4297
    0.1000  -30.6032    1.0900  -13.9595

-------------------------------------------------------------
             System Eigenvalues with Damping > 5%
-------------------------------------------------------------
 Eigenvalue  Damp.[%]  Freq.[Hz]
    1.0000  100.0000         0
    2.0000  100.0000         0
    3.0000  100.0000         0
    4.0000  100.0000         0
    5.0000   17.3197    1.3796
    6.0000   17.3197    1.3796
    7.0000   90.6450    1.0703
    8.0000   90.6450    1.0703
    9.0000  100.0000         0
   10.0000  100.0000         0

-------------------------------------------------------------------
             Synchronizing and Damping Torque Coefficients
                  at Analized Oscillation Frequency
-------------------------------------------------------------------
         Total             due to AVR         Net         due to PSS
-------------------------------------------------------------------
     Sync.     Damp.      Sync.     Damp.     Sync.     Sync.     Damp.
    1.4818   16.7408   -0.0038    0.1974    1.3705    0.1113   16.5434

Save Final Tuning? Y/N : N
```

Fig. 5.10 Command Window Displayed Numerical Results

5.5 Program for Tuning at a Different Oscillation Frequency

An additional folder called *SpecificFrequencyTuning* can be found in the main folder of the software tool. In this folder are the files of the algorithm to tune the lead lag filters for a different oscillation frequency. This algorithm follows the same logic and steps as the main algorithm. Also, the same Simulink models are used. In this case, the main file that should be run is called **OtherFrequencyTuning** as is presented in Fig. 5.11.

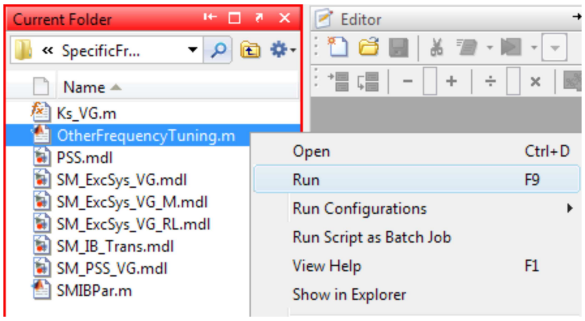

Fig. 5.11 Run the Alternative Algorithm

During the execution process, the program ask the user to input the frequency for analysis as is presented in the example of the Fig. 5.12. The system phase lag at that frequency is displayed in the command window and should be consider to define the objective system phase at the analyzed oscillation frequency.

```
*****************************************************************
Tuning the Lead-Lag Filters for a Frequency Different Than
The One Obtained From The Eigenvalue Analysis
*****************************************************************
Input Frequency for Analysis (0.1-2) [Hz] = 0.4
-----------------------------------------------------------------
             System Phase Lag at Input Frequency
-----------------------------------------------------------------
 Freq.[Hz] Ph.Shift[deg]
    0.4000 -120.3827

*****************************************************************
To Define the Objective System Phase See Chapter 3 Thesis Report
*****************************************************************
Objective System Phase at Analyzed Frequency [deg] = -15
-----------------------------------------------------------------
           Phase Shift to Compensate with the PSS
-----------------------------------------------------------------
 Ph.Shift[deg]
  105.3827
```

Fig. 5.12 Asking to Input Frequency for Anlaysis

Finally, with the previous information the program asks the user to chose the lead lag filters tuning type and follows the same steps as in Section 5.3 for the rest of the tuning process and results.

5.6 Comments and Tuning Tips

Some aspects to be taken into account about the software tool and the tuning task are listed below:

- The objective system phase at analyzed frequency is programmed as to be always negative, this means to obtain undercompensation. When the value is asked during the tuning process, it can be input positive or negative but the program will always assume that the objective system phase is a negative value. Therefore, it is not possible to tune the lead lag filters overcompensating the system phase for the analyzed frequency.
- The lead lag filter time constants are tuned to be equal for all filters, more advanced tuning algorithms would be needed to tune each filter in the cascade link with a different purpose. In that case, it would be possible to get a desired compensation not only for an specific frequency but for a range of frequencies.

- There is not representative difference in the results obtain between the two lead lag filters tuning methods presented in Chapter 3. For Method 2, the program has an internal value for K_f equal to 2. This filter gain should not be modified, furthermore it must not be less than 2 or more than 10. The effect of varying it is to move the compensation central frequency of the filter. The higher K_f the more phase lead the compensated system will have at low frequencies badly influencing the synchronizing torque at those frequencies. Also the higher K_f the smaller the PSS gain K_{s1} should be to guarantee the system stability.

- Generally, it was observed that the system phase lag is higher when the excitation system use a rotating exciter, this means that the PSS should compensate a higher angle. However, as was discussed in Chapter 2 in the synchronizing and damping torque coefficient analysis for this type of exciter, the damping coefficient due to the excitation system is always possitive, this condition support choosing more undercompensation in cases with this kind of exciters.

- According to many system root locus plot analysis for different levels of phase compensation, it was observed that the less the PSS compensation angle θ_{pss} the higher the optimal PSS gain K_{s1} can be, introducing higher level of damping.

- It is consider that a damping of 5% for an oscillation mode is acceptable to do not risk the system stability, however there is not an standardised criteria presented in the literature for the required damping in a power system. Additionally, it should be taken into account that the gain and phase margins should be positive at the frequency range of interest. Also, the obtained PSS tuning should produce positive synchronizing and damping torque coefficients to the system due to the PSS.

- Finally, the tool needs to be tested for different systems considering several kind of synchronous generator design connected to different external grids, in order to be able to evaluate and validate the results.

Chapter 6

Conclusions and Future Work

6.1 Conclusions

Based on the literature review, the performed analysis, and the simulations results it is possible to conclude that:

- The synchronous machine rotor oscillations due to lack of damping torque can be seen as a small signal stability problem [11]. In that case, a linearized model of the SM-IB can provide good representation of the dynamic response of the system to analyze the damping effect that a PSS can introduce.

- It is not necessary to include the damper windings dynamics in the PSS tuning analysis because the additional phase lag introduced by the sub-transient characteristic is not relevant compared with the increase in mathematical dimension of the system. If the small phase lag difference wants to be taken into account, it is possible to treat it as a PSS design criteria which makes to increase the compensation angle some few degrees. For the analyzed machine, in the PSS frequency range of interest, the biggest phase lag difference including the damper windings dynamics was about $10°$. This difference could be considered not sufficient to include the sub-transient model in the PSS tuning analysis.

- The results show how the excitation system may negatively impacts the synchronizing and damping torque components. Specifically, for the analized machine, the damping torque coefficient using static exciter with high active power and weak external connecting grid reaches values about -2 p.u. Therefore, it is mathematically demonstrated also the need of a PSS to increase the damping torque component specially in the case of excitation systems with static exciters and at low frequencies.

- A PSS tuning methodology, which is based on linear control system theory, is established in this work. Specifically, frequency response techniques are used to define the setting for the lead lag filters time constants and PSS gain. This is supported on the fact that the predominant trend in the industry is still to use frequency response based tuning methods [12].

- The performance of the PSS with the achieved tuning is validated via simulations in the complete SM-IB system model. Furthermore, a sensitivity analysis of the local oscillation mode damping to changes in the system operating point is carried out verifying the robustness of the tuning process. The sensitivity analysis is also extended to a PSS tuning performed for an oscillation frequency different than the natural local oscillation mode and once again good damping levels of the local mode are achieved, fact that confirms the reliable tuning. In all analyzed cases, the minimum damping of the local mode was never less than 10%.

- The idea of applying control structures based on signal estimation theory to FACTS to damp oscillations in the power system has been used in this work to define an alternative controller for the generator. This controller is based on a low-pass filter based signal estimation algorithm. The obtained results indicate that the alternative controller is able to damp successfully the local oscillation mode that appear after applying a disturbance to the SM-IB system.

- A critical comparison between the PSS and the Phasor POD controller reveals several advantages of the Phasor POD controller in aspects as speed of action, robustness, tuning requirements and possibility of parameters adaptation. However, the industry still prefer the conventional stabilization based on lead lag filters and the reason could be that acceptable results are obtained with a relative easy way on tuning. Also, because more research is needed to guarantee the stability of the system when another control structure or technique is applied with the same aim [4].

6.2 Future Work

Based on the obtained results, it is recommended to continue in the following working lines:

- PSS tuning algorithm improvement including optimization to expand the performance requirement to a frequency range, which should be the PSS frequency range of interest. Some proposed objective functions are the square error between the objective system phase and the real phase of the compensated system, or the square error between a objective oscillation mode damping and the real achieved damping.
- Deeper analysis of the Phasor POD controller applied to synchronous generator in aspects as its impact on the system stability and on the synchronizing torque component of the machine. Additionally, to study the controller in a higher order power system model where inter-area oscillations can be reproduced and more complex dynamic interactions appear allowing to test the controller limits of performance. This will also lead to the possibility of a stronger comparison between the PSS and the Phasor POD controller.

References

[1] *IEEE Recommended Practice for Excitation System Models for Power System Stability Studies*, Std 421.5 2005 ed., IEEE Power Engineering Society 2005.

[2] L. Ängquist and M. Bongiorno, "Auto-normalizing phase-locked loop for grid-connected converters," *IEEE Energy Conversion Congress and Exposition ECCE*, pp. 2957–2964, September 2009.

[3] L. Ängquist and C. Gama, "Damping algorithm based on phasor estimation," *Power Engineering Society Winter Meeting. IEEE*, vol. 3, pp. 1160–1165, 2001.

[4] A. Ba-muqabel and M. Abido, "Review of conventional power system stabilizer design methods," *GCC Conference. IEEE*, March 2006.

[5] M. Beza, "Control of energy storage equipped shunt-connected converter for electric power system stability enhancement," Licentiate of Engineering Thesis, Chalmers University of Technology, Department of Energy and Enviroment, Gothenburg, Sweden, May 2012.

[6] M. Beza and M. Bongiorno, "Power oscillation damping controller by static synchronous compensator with energy storage," *Energy Conversion Congress. IEEE*, pp. 2977–2984, September 2011.

[7] J. Bladh, "Hydropower generator and power system interaction," Ph.D Thesis, Uppsala University, Department of Engineering Sciences, Electricity, Uppsala, Sweden, November 2012.

[8] M. Bongiorno, "Power electronic solutions for power systems. lecture 3: Tools for analysis and control of power converters," Department of Energy and Enviroment, Chalmers University of Technology, Department of Energy and Enviroment, Göteborg, Sweden, Tech. Rep., 2012.

[9] F. Demello and C. Concordia, "Concepts of synchronous machine stability as affected by excitation control," *Power Apparatus and Systems, IEEE Transactions on PAS88*, no. 4, p. 316 to 329, April 1969.

[10] W. Heffron and R. Phillips, "Effects of modern amplidyne voltage regulator in underexcited operation of large turbine generators," *AIEE Transactions*, vol. PAS-71, pp. 692–697, August 1952.

[11] P. Kundur, *Power System Stability and Control*. Palo Alto,California: Electric Power Research Institute, 1994.

[12] P. Kundur and Others, "A pss tuning toolbox and its applications," *Power Engineering Society, General Meeting*, vol. 4, pp. 2090–2094, July 2003.

[13] ——, "Application of power systems stabilizers for enhancement of overall system stability," *IEEE Transactions on Power Systems*, vol. 4, no. 2, pp. 614–626, May 1989.

[14] E. Larsen and D. Swann, "Applying power system stabilizers. part i: General concepts," *IEEE Transactions on Power Apparatus and Systems*, vol. PAS-100, no. 6, pp. 3017–3024, June 1981.

[15] ——, "Applying power system stabilizers. part ii: Performance objectives and tuning concepts," *IEEE Transactions on Power Apparatus and Systems*, vol. PAS-100, no. 6, pp. 3025–3033, June 1981.

[16] ——, "Applying power system stabilizers. part iii: Practical considerations," *IEEE Transactions on Power Apparatus and Systems*, vol. PAS-100, no. 6, pp. 3034–3046, June 1981.

[17] H. Latorre and L. Ängquist, "Analysis of tcsc providing damping in the interconnection colombia-ecuador 230 kv," *Power Engineering Society General Meeting, IEEE*, vol. 4, pp. 2361–2366, July 2003.

[18] J. Machowski and Others, *Power System Dynamics: Stability and Control*. United Kingdom: John Wiley & Sons, Ltd, 2008.

[19] A. Murdoch and Others, "Integral of accelerating power type pss," *IEEE Transactions on Energy Conversion*, vol. 14, no. 4, pp. 1658–1662, December 1999.

[20] K. Ogata, *Modern Control Engineering. Fourth Edition*. New Jersey: Prentice Hall, 2002.

[21] O. Samuelsson, "Power system damping: Structural aspects of controlling active power," Ph.D Thesis, Lund Institute of Technology, Lund, Sweden, 1997.

[22] S. Yee, "Coordinated tuning of power system damping controllers for robust stabilization of the system," Ph.D Thesis, University of Manchester, Faculty of Engineering and Physical Sciences, Manchester, England, October 2005.

Appendix A

System Parameters

The parameters of the synchronous generator and excitation system used for the calculations and simulations in all chapters of this work were provided by VG Power AB and they are listed as follows.

A.1 Synchronous Generator

Table A.1: Synchronous Generator Parameters

Parameter	Value	Unit
Nominal Apparent Power S_n	69	[MVA]
Nominal Voltage V_n	13.8	[kV]
Inertia Constant H	3	[s]
Frequency f	50	[Hz]
Damping Torque Coefficient K_D	0	[p.u/p.u]
Stator Resistance R_s	0.0033	[p.u]
d-axis Stator Inductance L_{sd}	1.177	[p.u]
q-axis Stator Inductance L_{sq}	0.772	[p.u]
Stator Leakage Inductance $L_{s\lambda}$	0.174	[p.u]
d-axis Open Circuit Transient Time Constant T'_{d0}	6.596	[s]
d-axis Stator Transient Reactance X'_{sd}	0.324	[s]
d-axis Damper Winding Leakage Inductance $L_{1d\lambda}$	0.17879	[p.u]
q-axis Damper Winding 1 Leakage Inductance $L_{1q\lambda}$	0.20104661	[p.u]
q-axis Damper Winding 2 Leakage Inductance $L_{2q\lambda}$	0	[p.u]
Field Resistance R_{fd}	0.00056937	[p.u]
d-axis Damper Winding Resistance R_{1d}	0.02462133	[p.u]
q-axis Damper Winding 1 Resistance R_{1q}	0.02768629	[p.u]
q-axis Damper Winding 2 Resistance R_{2q}	0	[p.u]

A.2 Excitation System

Table A.2: AVR and Exciter Parameters

Parameter	Value	Unit
AVR Proportional Gain K_p	20	[p.u]
AVR Integral Gain K_i	0.2	[p.u]
Terminal Voltage Transducer Time Constant T_r	0.01	[s]
Time Constant due to type of AVR T_4	0.004	[s]
Power Converter Positive Ceiling Voltage VR_Max	4	[p.u]
Power Converter Negative Ceiling Voltage VR_Min	-3	[p.u]
Maximum Integral Control Action Voltage Vl_Max	4	[p.u]
Minimum Integral Control Action Voltage Vl_Min	-3	[p.u]
Maximum Proportional Control Action Voltage Vp_Max	10	[p.u]
Minimum Proportional Control Action Voltage Vp_Min	-10	[p.u]

Table A.3: Parameters Depending on the Type of Exciter

	Value		
Parameter	**Rotating**	**Static**	**Unit**
Derivative Gain K_d	-5	0	[p.u/p.u]
Derivative Filter Time Constant T_d	2	0	[s]
Rotating Exciter Gain K_e	1	1	[p.u/p.u]
Rotating Exciter Time Constant T_e	0.9	0	[s]
Saturation Function for Rotating Exciter S_e	0	0	[-]

Appendix B

Transformations Equations for 3-Phase Systems

The transformations from 3-phase system to $\alpha\beta$ system which is a stationary reference frame, and to dq system which is a rotating reference frame, are presented in the following equations. In this case, zero sequence is not considered since the assumption of a symmetric or balanced system is made [8].

B.1 Power Invariant 3-phase to $\alpha\beta$ Transformation

$$\underline{s}(t) = s_\alpha(t) + j s_\beta(t) = \sqrt{\frac{2}{3}}(s_1(t)e^{j0} + s_2(t)e^{j2\pi/3} + s_3(t)e^{j4\pi/3}) \tag{B.1}$$

$$\begin{bmatrix} s_\alpha \\ s_\beta \end{bmatrix} = \sqrt{\frac{2}{3}} \begin{bmatrix} 1 & -\frac{1}{2} & -\frac{1}{2} \\ 0 & \frac{\sqrt{3}}{2} & -\frac{\sqrt{3}}{2} \end{bmatrix} \begin{bmatrix} s_1 \\ s_2 \\ s_3 \end{bmatrix} \tag{B.2}$$

$$\begin{bmatrix} s_1 \\ s_2 \\ s_3 \end{bmatrix} = \sqrt{\frac{2}{3}} \begin{bmatrix} 1 & 0 \\ -\frac{1}{2} & \frac{\sqrt{3}}{2} \\ -\frac{1}{2} & -\frac{\sqrt{3}}{2} \end{bmatrix} \begin{bmatrix} s_\alpha \\ s_\beta \end{bmatrix} \tag{B.3}$$

B.2 $\alpha\beta$ to dq Transformation

From $\alpha\beta$ to dq

$$\underline{v}^{(dq)}(t) = \underline{v}^{(\alpha\beta)}(t)e^{-j\theta(t)} \tag{B.4}$$

$$\begin{bmatrix} v_d(t) \\ v_q(t) \end{bmatrix} = \begin{bmatrix} \cos(\theta) & -\sin(\theta) \\ \sin(\theta) & \cos(\theta) \end{bmatrix} \begin{bmatrix} v_\alpha(t) \\ v_\beta(t) \end{bmatrix} \tag{B.5}$$

Appendix B. Transformations Equations for 3-Phase Systems

From dq **to** $\alpha\beta$

$$\underline{v}^{(\alpha\beta)}(t) = \underline{v}^{(dq)}(t)e^{j\theta(t)} \tag{B.6}$$

$$\begin{bmatrix} v_\alpha(t) \\ v_\beta(t) \end{bmatrix} = \begin{bmatrix} \cos(\theta) & \sin(\theta) \\ -\sin(\theta) & \cos(\theta) \end{bmatrix} \begin{bmatrix} v_d(t) \\ v_q(t) \end{bmatrix} \tag{B.7}$$

Where the angle θ is the transformation angle, which is also presented in Fig. 2.2.